Institute of Cardiovascular Science
University College London

Deep Structural Phenotype of Hypertrophic Cardiomyopathy

from mutation to hypertrophy

PhD Thesis

Dr George Joy
MBBS, MRCP

Supervised by Dr Luis R Lopes, Prof James C Moon

Declaration of Originality

I, George Joy, declare that the work presented in my thesis is my own. Where information has been derived from other sources, I confirm that this has been indicated in the thesis.

Abstract

Hypertrophic Cardiomyopathy (HCM): HCM is characterised clinically by inappropriate left ventricular hypertrophy (LVH) and is the commonest inherited heart muscle disease worldwide. It has a prevalence estimated at 1 in 500. It is a leading cause of sudden cardiac death, arrhythmia and heart failure.

The current paradigm of defining HCM by elevated wall thickness to define disease and target therapy has been inadequate; gene variant carriers without LVH (G+LVH-) undergo interval imaging surveillance, and those with LVH have heterogenous clinical outcomes ranging from asymptomatic disease to sudden death. In recent years myosin inhibitors have demonstrated resolution of left ventricular outflow obstruction, at least some positive cardiac remodelling and improvement in functional and blood biomarkers. Furthermore pre-clinical work has shown correction of sarcomeric mutations with gene editing. These developments have resulted in the need for early disease biomarkers that may respond to therapy.

Whilst HCM is defined histologically by myocyte hypertrophy, it is also characterised by fibrosis, disarray and microvascular disease. Focal fibrosis is measured by cardiac MRI late gadolinium enhancement (LGE) and a high LGE burden is related to adverse clinical outcome, however this tends to occur late. Myocyte disarray and microvascular disease have been less explored. Parameters relating to these characteristics can be obtained through novel CMR techniques; diffusion tensor imaging and quantitative perfusion respectively. I have utilized these techniques to measure *in-vivo* these parametric changes occurring early in HCM, even in the absence of hypertrophy. Recent evidence also suggests that sarcomere variant negative overt disease (genotype negative, G-LVH+) has distinctive morphological and clinical features to G+LVH+. To explore this further, I studied the differing

advanced imaging phenotypes based on presence or absence of sarcomere mutation in overt disease. Ventricular arrhythmia can occur in HCM and is a leading cause of sudden cardiac death in the young. How ventricular arrhythmia forms is poorly understood due to evidence from small invasive and pre-clinical studies. ECG Imaging is a non-invasive high spatiotemporal resolution technique of mapping ventricular activation and repolarization. I integrated this technique into advanced cardiac MRI by co-inventing a fully re-useable ECGI vest [capturECGI vest, US patent approved] to detect early electrophysiological changes in HCM and in overt disease, relate abnormalities to genotype and adverse structural change.

Quantitative Perfusion CMR in physiological and pathological LVH: The presence of ischaemia in HCM has been well described but mechanisms are incompletely understood. Whilst observational studies in HCM commonly compare findings to health, the "grey-zone" patients clinically are often LVH-causing phenocopies such as Athleticism and Hypertension. I therefore explored the relationships between LVH and microvascular function and studied physiological hypertrophy (athleticism), pathological hypertrophy from excessive afterload (hypertension) and subclinical HCM. Quantitative perfusion measures pixel-wise myocardial blood flow under vasodilator stress. The technique is fully-automated, meaning that between-group differences in microvascular function can be more accurately measured. I studied 19 athletes, 10 hypertensives, 20 subclinical HCM and 14 healthy volunteers. Hypertensives and subclinical HCM compared to athletes had significantly impaired stress myocardial blood flow and perfusion reserve suggestive of microvascular disease. Compared to health, athletes had more enhanced perfusion reserve, however this finding was confounded by the requirements for higher doses of vasodilator (adenosine). Using a high-dose adenosine cohort (unmatched for age)

and multivariable regression, the finding of enhanced myocardial perfusion reserve in athletes compared to health persisted. Further work is needed in larger external validation cohorts to confirm this finding. Overall, my data supports the potential use of quantitative perfusion to discriminate between physiological and pathological hypertrophy. To confirm whether quantitative perfusion has discriminatory value, larger cohorts are needed to obtain thresholds when considering potential confounders: primarily age, sex, drugs and comorbidities.

Subclinical HCM and genotyped overt HCM cohorts: In order to detect the earliest manifestations of gene expression in HCM, I studied individuals with pathogenic sarcomeric mutations without hypertrophy and compared findings to healthy volunteers. Overt HCM patients (all genotyped to compare G+ vs G-LVH+) were also studied to understand the compounding effects of LVH and the effects of the presence or absence of sarcomere mutation on the advanced imaging parameters of interest.

Microstructural and microvascular phenotype HCM: Diffusion tensor imaging (DTI) measures the diffusion of water *in-vivo* , which thereby characterizes the myocardial microstructural environment. I performed DTI and quantitative perfusion on all participants and showed that DTI changes suggestive of microstructural alteration (low fractional anisotropy, high mean diffusivity, steeper sheetlet orientation) occur in the absence of LVH in subclinical HCM. Abnormalities in DTI and quantitative perfusion also associated with each other and 12-lead ECG changes, in both subclinical and overt HCM. Furthermore in overt HCM, changes associated with genotype; G+LVH+ had a 100% prevalence of perfusion defects, and G-LVH+ unexpectedly had a more severe microstructural phenotype (steeper sheetlet orientation). Findings show the potential for these novel CMR techniques in early and

disease-specific phenotype detection in the emerging era of disease modifying therapy.

Detection of electrophysiological abnormalities in HCM: Electrocardiographic imaging (ECGI) is a non-invasive technique for detecting electrophysiological abnormalities. It uses body surface potentials obtained from 256 leads across the torso and heart-torso geometry obtained from imaging. Using the inverse solution of electrocardiography, 1000 unipolar electrograms (UEGs) are computed. By analysing the computed UEGS we derive ventricular activation time (AT – defined as the steepest point of the QRS upslope) and repolarization time (RT – defined as the steepest point of the T wave downslope), activation recovery interval (ARI – the difference between AT and RT), markers of spatial conduction and repolarization heterogeneity (gradients of activation G_{AT}, G_{RT}), fractionation and signal amplitudes. I showed that in subclinical HCM, ventricular activation is slowed, and repolarization is more spatially heterogenous. In overt disease, repolarization is prolonged and conduction heterogeneity associated with genotype (more fractionation in G+LVH+), scar and non-sustained VT. These changes are proven to be pro-arrhythmic in multiple other diseases. Findings show that EP abnormalities occur in the absence of LVH in subclinical HCM and in overt disease relate to conventional risk markers. Therefore findings support the use for ECGI in early disease detection and with further longitudinal work, may supplement current conventional risk stratification.

Identification of sub-phenotypes of HCM using unsupervised learning: HCM is characterised by substantial disease heterogeneity in LV morphology and clinical outcomes. Disease is defined by arbitrary maximum wall thickness cutoffs which means the spectrum of adverse changes occurring before these cutoffs are reached goes undetected. Using unsupervised machine learning (agglomerative hierarchical

cluster analysis) we discover that a third of subclinical HCM have microvascular, microstructural EP changes that are comparable to overt HCM, being either intermediate or severe. A half have an abnormal ECG meaning i) this cohort are likely to progress ii) in the absence of ECG changes and LVH, deep phenotyping is the only method of identifying such individuals. Genotype positive vs negative overt disease were balanced between intermediate and severe phenotypes suggesting large overlaps between both. Findings support the use of advanced phenotyping to identify a higher risk category of subclinical HCM that may benefit from more intensive monitoring or early initiation of novel therapy.

Conclusion:

Findings. In left ventricular hypertrophy, quantitative perfusion may supplement current techniques for discrimination of pathological vs physiological LVH. **In HCM,** abnormalities in myocardial microstructure, microvasculature and electrophysiology occur in the absence of LVH. In overt disease, abnormalities associate with important clinical characteristics (adverse structural changes, genotype).

Potential Clinical Application. I have optimised new techniques to visualize *in-vivo* early histological and EP changes occurring in HCM. Whilst we have integrated LVH and scar in cardiac MRI for clinical care, my work has made the measurement of disarray and microvascular disease robust in HCM for future clinical and trial utility. Furthermore early electrophysiological abnormalities can now be detected and related to genotype and structural abnormalities through integration of ECGI with CMR. We found remarkable microstructural, microvascular and EP changes occurring in subclinical disease in the absence of LVH. Curious insights into genotype negative vs positive disease show both overlapping and distinctive phenotypes. These biomarkers may now be tested in longitudinal studies to track whether abnormalities relate to

disease progression and ventricular arrhythmia formation. Overall findings suggest clinical techniques could supplement current care, especially for the detection of early disease but also potentially risk stratification and disease discrimination.

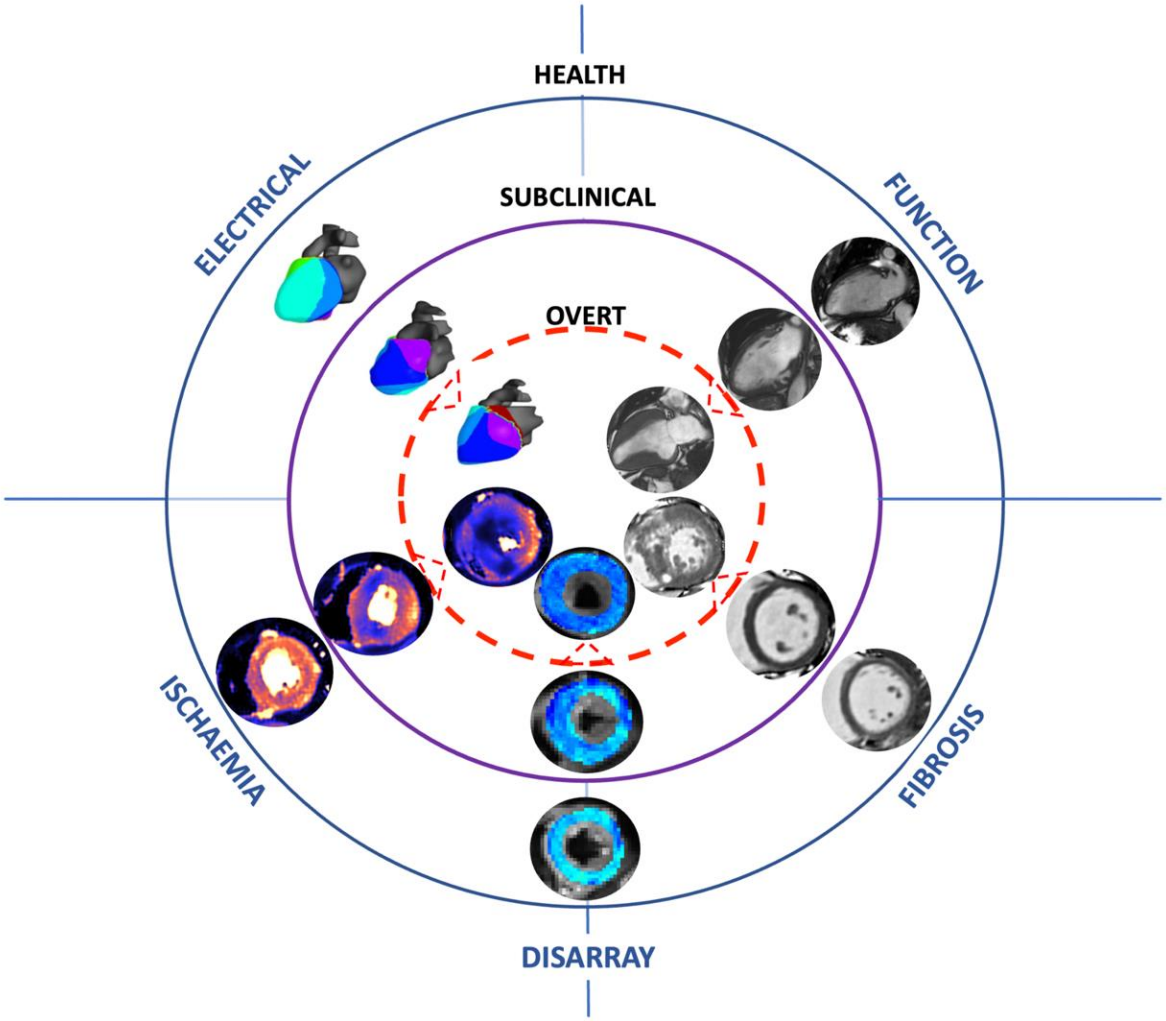

Abstract Figure: Advanced Imaging biomarkers for early (subclinical) HCM

Impact statement

In this thesis I have shown that:

For patients: Diffusion tensor imaging, quantitative perfusion and electrocardiographic imaging are sensitive techniques to detect phenotype development in HCM, even in the absence of hypertrophy. This will help identify patients that have a more severe early expression of pathogenic sarcomeric mutations before the onset of hypertrophy. Current models of care include repeated imaging surveillance which is inefficient and compounded by increasing numbers of individuals with pathogenic mutations identified year-on-year. Further work is needed to relate DTI and quantitative perfusion changes to disease progression. This may then enable early discharge, more accurate monitoring and perhaps even earlier initiation of disease modifying therapy. Current risk stratification relies on often late structural markers of disease (LA dilation/ LVH, scar burden). The use of these novel techniques has shown quantifiable markers of abnormality occurring early, in the absence of LVH and that may be relevant to sudden cardiac death, particularly ECGI changes.

For trials: Disease modifying therapy has shown improvement in left ventricular outflow tract obstruction, biomarkers indicating myocyte death and wall stress and functional limitations in HCM. Here, early-disease biomarkers have been validated and therefore may possibly be used to demonstrate positive deep structural remodelling in response to novel therapy, where macrostructural markers such as LVH and scar, may be less informative.

COVID-19 Impact Statement

I commenced my research Fellowship in October 2019 before the pandemic. My initial research was examining microvascular function in pathological and physiological hypertrophy using quantitative perfusion. The recruitment of hypertensives and athletes and a further comparator cohort of HCM was planned (1.5 Tesla quantitative perfusion). However the pandemic reached the UK in February 2020, and therefore this study had been curtailed. Following this I was unsuccessful in achieving grant funding for this study. Therefore the Chapter "Microvascular function in physiological and pathological hypertrophy" contains only initial exploratory work.

During the pandemic, I was redeployed clinically in ITU and as lead Fellow for COVID research in the COVIDsortium study [COVID-19: Healthcare worker Bioresource: Immune and Pathogenesis IRAS 281884, CI Prof. James Moon]. This study investigated longitudinally the immune response of healthcare workers following COVID-19 infection. There were 700+ healthcare worker participants across St Barts, Royal Free and The Nightingale. The main task was leading a team to facilitate longitudinal serial biological sampling (serum, saliva, nasal swabs), initially weekly collections at 4 months and 6 monthly thereafter (targeted bleeds occurring in-time with vaccinations).

Cardiovascular Research relating to COVID-19

Joy, G,…Moon JC. Prospective Case-Control Study of Cardiovascular Abnormalities 6 Months Following Mild COVID-19 in Healthcare Workers. J Am Coll Cardiol Img. 2021 Nov, 14 (11) 2155–2166.

During the pandemic I led a cardiac MRI study on the cardiovascular effects of mild COVID, comparing seropositive (n=74) and seronegative (n=75) healthcareworkers at 6-months post mild COVID. I scanned and recruited the vast majority of patients (approx. 13 patients recruited by JA at Royal Free and scanning performed by Royal Free Fellows), performed all post-processing, statistical and data analysis, sample collection and most manuscript write-up (overseen by Prof. Moon). Findings showed there was no difference in CMR parameters between seropositives and seronegatives, contrasting initial claims of a deleterious cardiovascular impact of mild COVID from CMR studies (likely as a result of selection bias; those enrolled had worse COVID due to undiscovered pre-existing cardiovascular conditions). As this work was prospective with several quality control steps to ensure the robustness findings and also provided reassurance to initial worrying claims, it received widespread attention [Altmetrics ~700, >130 citations to date, featured in Highlights of JACC 2021, cited in the ACC Consensus for Cardiovascular Sequelae of COVID-19 in Adults].

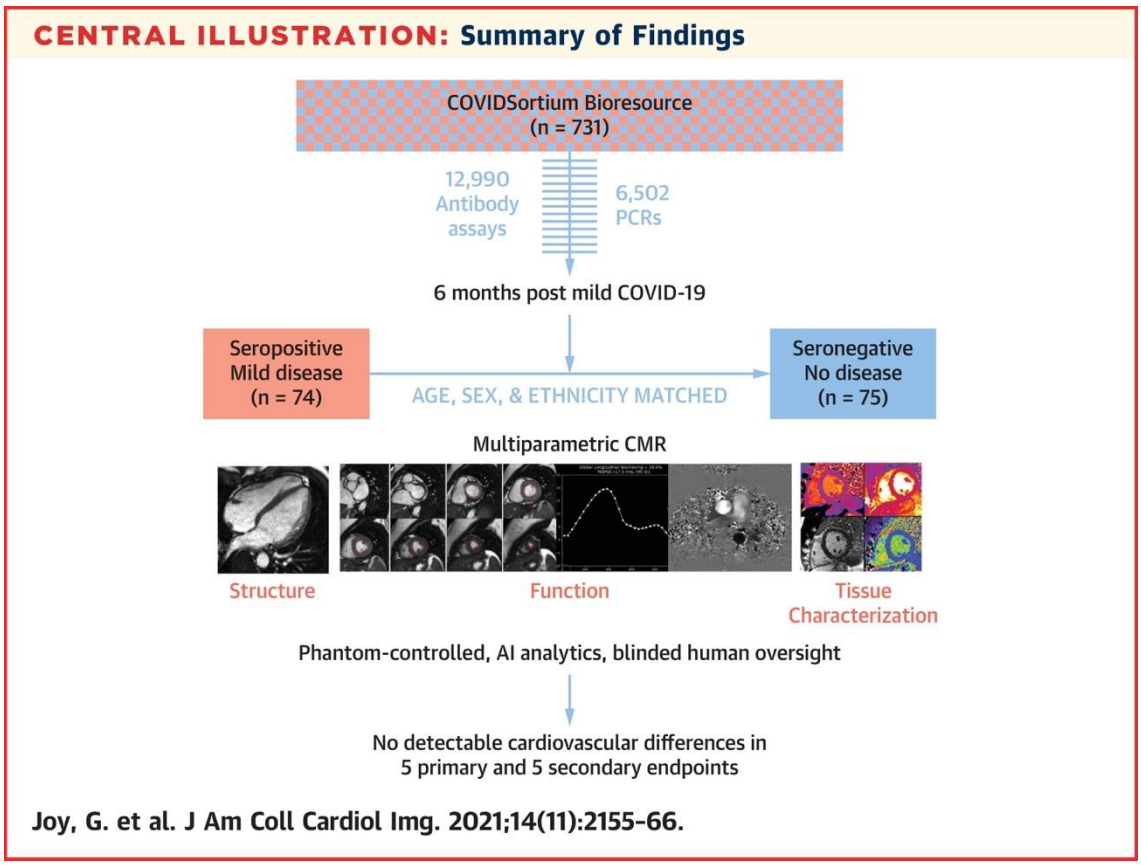

Figure. Cardiovascular Research during the COVID pandemic

Non-cardiovascular research relating to COVID-19

Studying the immune response to COVID-19 in healthcare-workers infection yielded several important insights.

Reynolds CJ .. **Joy G**…Boyton RJ. Discordant neutralizing antibody and T cell responses in asymptomatic and mild SARS-CoV-2 infection. Sci Immunol. 2020 Dec 23;5(54):eabf3698.

Initial work published in Science Immunology 6-months after wave 1 showed that healthcare workers had durability of immunity (T-cell and neutralising antibody responses) long after mild infection. The study suggested that mild or asymptomatic infection immune-response was protective for re-infection and vaccination down-the-line.

Reynolds CJ… **Joy G**…Boyton RJ. Heterologous infection and vaccination shapes immunity against SARS-CoV-2 variants. Science. 2022 Jan 14;375(6577):183-192

Following wave 2 during the Omicron variant outbreak, work form the consortium found immune responses to Omicron depended on prior infection to other variants. For example those with prior Wuhan variant infection had weaker immune responses to Omicron. Findings explained why frequent re-infections often occur.

Reynolds CJ.. **Joy G**… Boyton RJ, Immune boosting by B.1.1.529 (Omicron) depends on previous SARS-CoV-2 exposure. Science. 2022 Jul 15;377(6603):eabq1841.

After vaccines came into effect in the UK, we could track the effect vaccination on the immune response. Findings showed that prior variant type and prior vaccination shaped responses to future vaccination and infection. This meant that there were inter-individual differences in the effectiveness of boost vaccinations.

Swadling L…**Joy G**… Maini MK. Pre-existing polymerase-specific T cells expand in abortive seronegative SARS-CoV-2. Nature. 2022 Jan;601(7891):110-117.

Other work showed some seronegative individuals generated memory T cells that target infected cells expressing replication proteins, meaning they cleared the virus before seropositivity or PCR positivity – termed abortive infection. As these proteins are highly conserved and are unlikely to change or mutate, it served as an attractive target for future vaccination strategy.

Altmann, D.M.. **Joy, G**…Boyton R et al. Persistent symptoms after COVID-19 are not associated with differential SARS-CoV-2 antibody or T cell immunity. Nat Commun 14, 5139 (2023).

Following wave 2 samples and questionnaires were performed allowing ascertainment of individuals with persistent symptoms following initial COVID infection (termed Long COVID). Mixed evidence had suggested that the immune response (either excessive or muted) was responsible for Long COVID. Our granular longitudinal data however had provided evidence against this hypothesis as there was no difference in immunity in those with persistent vs no persistent symptoms.

Acknowledgements

Dr Luis Lopes my primary supervisor was extremely encouraging and helpful in my progression in this work. The study builds on his extensive expertise in genetic heart muscle disease. I am very grateful to my supervisor, Prof James Moon for supporting me throughout the period of my PhD and BHF Clinical Research Training Fellowship. I would not have been able to deliver an ambitious and often pain-staking PhD study without his guidance and support.

Dr Gaby Captur's innovations and commitment to the study allowed me to deliver the scale of the ECGI work. Prof. Charlotte Manisty supported my progression when I was unable to achieve grant funding during the COVID 19 pandemic. Dr Erica Dall'Armellina helped me utilize the diffusion tensor technology which was also greatly assisted by Chris Kelly, Jurgen Schneider, Irvin Teh and Chris Nguyen. Drs Peter Kellman, Rhodri Davies and Iain Pierce provided a tremendous deal of technical support with advance imaging deployment and were extremely patient with their assistance in providing this.

There were several PhD Fellows that trained me when I first arrived at Barts and UCL, particularly Drs Kris Knott, João Augusto, Clement Lau, Katia Menacho, Andreas Seraphim and Rebecca Hughes. My peers Drs Matthew Webber, George Thornton, Andrew Lin, Ronke Abiodun, Hibba Kurdi, Christian Nitsche and Ben Dowsing made the whole experience very enjoyable. I owe the radiographers whom trained me in scanning a great deal, particularly Louise McGrath who helped refine the scanning protocols and supported my work at Chenies Mews. For training me in acquisition I also thank Dan Roberts at Chenies and Cavaan McGurk, Cheelo Simaanya, Nadine Miller, Kevin Konickal and Jane Francis at Barts Heart Centre. Sandy Gardner and Peter Sutton from Chenies Mews were always hugely supportive of me and the work. The teams at Barts Heart Centre, Chenies Mews Imaging Centre and UCL provided excellent care to our research participants. Lastly the knowledge gained from this thesis was only possible thanks to the dedication and sacrifice of the patients from Barts Heart Centre, Royal Free London and St Georges' Hospital.

I dedicate this PhD thesis to my wife, Dr Saira Joy, my children, Jacob and Isabel and my parents, Drs Catherine Joy and Joy Varghese for their relentless support and patience.

Table of Contents

List of Tables

List of Figures

Abbreviations

|E2A| - *Second eigenvector angle*
ACS - *Acute Coronary Syndrome*
AF - *Atrial Fibrillation*
AHA - *American Heart Association*
AI - *Artificial Intelligence*
AIF - *Arterial Input Function*
Amp – *Amplitude*
ARIc - *Activation-Recovery interval corrected*
AT - *Activation Time*
cDTI - cardiac Diffusion Tensor Imaging
CMR - *Cardiovascular Magnetic Resonance*
CVD - *Cardiovascular Disease*
ECV - *Extracellular Volume fraction*
EDV - *End Diastolic Volume*
EF - *Ejection Fraction*
ESC - *European Society of Cardiology*
FA - *Fractional Anisotropy*
G+/G- Genotype positive/negative
G_{AT} - *Activation time gradient*
Gd - *Gadolinium*
G_{RTc} - *corrected repolarization time gradient*
HCM - *Hypertrophic Cardiomyopathy*
HR - *Hazard Ratio*
HV - Healthy volunteer
LGE - *Late Gadolinium Enhancement*
LVH - *Left Ventricle Hypertrophy*
LVH+/LVH- Left ventricular hypertrophy positive/negative
MBF - *Myocardial Blood Flow*
MD - Mean diffusivity
MI - *Myocardial Infarction*
MOLLI - *Modified Look Locker Inversion Recovery*
MPR - *Myocardial Perfusion Reserve*
MVD - *Microvascular disease*
MWT - *Maximum wall thickness*
NSVT - *Non-sustained ventricular tachycardia*
OR - *Odds ratio*
PCI - *Percutaneous Coronary Intervention*
PET - *Positron Emission Tomography*
SSFP - *Steady State Free Precession*
T - *Tesla*

CHAPTER 1 – INTRODUCTION

The following manuscript is based on this chapter:

"Detection of subclinical hypertrophic cardiomyopathy"

Joy G, Moon JC & Lopes LR

***Nat Rev Cardiol* 20**, 369–370 (2023).

1.1. Hypertrophic cardiomyopathy - overview

Hypertrophic cardiomyopathy (HCM) is a genetic heart muscle disease characterized by inappropriate left ventricular hypertrophy (LVH). It has a population prevalence of an estimated 1/200-1/500 and is a leading cause of heart failure and sudden cardiac death (SCD). HCM affects an estimated 20 million people worldwide, but its prevalence is often underestimated due to asymptomatic/benign disease in many individuals (1). Clinical outcomes are however heterogenous; sudden cardiac death (SCD) can occasionally be the first presentation. 70-78% of HCM SCD decedents have SCD as their first presentation (2). The overall incidence of HCM SCD is low at 0.31 per 1000 HCM patient years (2,3). In some patients, LVH can progress and reach a stage where it is then overtaken by scar, left ventricular dilation and heart failure. Overall in HCM, adverse events occur in 30-40% and include SCD, symptoms due to left ventricular outflow tract obstruction (LVOTO) or diastolic dysfunction, atrial fibrillation (AF), thromboembolism and heart failure (defined as symptoms and systolic dysfunction) (4,5). Mortality has improved over time, possibly related to improved medical therapy and increasing use of primary prevention implantable cardioverter-defibrillator (ICD), but still confers a two-fold excess mortality compared to the general population with women experiencing excess mortality compared to men (6). Due to

improvements in risk stratification, mortality due to sudden cardiac death (SCD) is now less common, shifting clinical need to addressing morbidity and mortality from heart failure. While mortality from heart failure in HCM is relatively rare (<0.5% per year), excessive shortness of breath and functional limitation from HCM remains common and can be categorised by the presence or absence of left ventricular outflow obstruction (LVOTO – obstructive: oHCM vs non-obstructive: nHCM). LVOTO can occur at rest or only on provocation through valsalva, exercise or pharmacologically (5,7).

1.2. HCM - Clinical Presentation

HCM can be asymptomatic or can present with shortness of breath, syncope, palpitations and chest pain. Initial assessment involves the exclusion of phenocopies including athleticism, hypertension and renal disease, amyloidosis, metabolic abnormalities including Fabry disease. Screening for a clinical syndrome should also be performed, including assessment of any hearing loss or sensory impairment, cognitive impairment or developmental delay, failure to thrive and ataxia. Physical examination may further reveal features relating to LVOTO including a systolic murmur and prominent apex beat or a late systolic murmur of mitral regurgitation from systolic anterior motion (SAM), both of which become more prominent with squatting or Valsalva (7). A family history of SCD and HCM is an important part of assessment and may be positive in 50%. The ECG can be detected as abnormal as part of routine contact with healthcare, athletic screening or screening of affected family members and commonly these abnormalities include LVH voltage criteria, abnormal Q waves and ST-segment or T-wave changes. In overt disease HCM, the prevalence of an abnormal ECG varies according to prior literature, with most studies quoting 90-95%

abnormal ECG findings (7,8). The mainstay of confirming the diagnosis is with imaging which will be discussed below.

Management of HCM

Conventional Management

Mechanisms of functional limitation in HCM include elevated intracavity pressures with or without LVOTO, systemic or pulmonary hypertension from elevated LA pressures and mitral regurgitation, microvascular dysfunction and diastolic dysfunction (5). Current conventional pharmacological therapy for obstructive HCM includes betablockers, verapamil/diltiazem when betablockers are ineffective or contraindicated, combined with dihydropyridine if the above fails. This strategy targets symptom relief as it has not been shown to improve prognosis (7). For those with refractory symptoms related to LVOTO, myectomy is demonstrated as effective for symptom relief and outcomes in specialist centres. For those deemed high risk candidates for myectomy or with favourable coronary and LV morphology, alcohol septal ablation is preferred (5). For non-obstructive HCM pharmacological therapy is aimed at improving LV filling and congestion, however transplantation may be the only option if this fails (9).

Myosin Inhibitors

Mavacamten, the first-in-class small-molecule inhibitor of Beta Myosin ATP activity, improves LV outflow obstruction, functional class and exercise tolerance in those with obstructive HCM, even reversing the need for septal reduction therapy in the majority of eligible patients (9,10). In the phase 2 trial of non-obstructive HCM, the drug is well tolerated and shows improvements in biomarkers reflecting myocyte death and wall

stress. Patients required 4-weekly monitoring of ejection fraction due to a loss of contractility resulting from its mechanism of action (11).

While initial results showing relief of outflow obstruction are unequivocal and established, the remodelling experienced at 30 weeks in obstructive HCM was more limited, with the CMR sub-study showing on average a reduction of 2mm maximum wall thickness, 15 grams of LV mass and no change in scar (12). Mavacamten has recently been licenced by National Institutes for Health and Care Excellence (NICE) for symptomatic obstructive HCM in patients whom are NYHA II to III as an add-on to standard pharmacological therapy (13).

Aficamten, the second-in-class myosin inhibitor has been announced as having positive results in its phase 3 trial for obstructive HCM, Sequoia HCM. It improved cardiopulmonary exercise tests (CPEX) VO_2 max and symptom score, and there is some suggestion it may have a favourable side effect profile to mavacamten (14)

HCM Genetics and screening

HCM is caused by identifiable sarcomeric protein mutation in 40% of patients. Strong evidence variants for HCM involve genes encoding sarcomeric proteins, including thick filament proteins: *MYBPC3 (the most prevalent, ~25%), MYH7* (second most prevalent, ~20% prevalence*), MYL2, MYL3*, thin filament proteins: *TNNT2 (*the third most prevalent, ~5-10%*), TNNI3, TPM1, ACTC1* and non sarcomeric proteins including *CSRP3* ***(Figure 1)***. Furthermore, HCM genocopy variants, occurring in almost 1-3% of those with clinically suspected HCM can be excluded; this includes *PRKAG2* (glycogen storage), *GLA* (Fabry disease), *LAMP2* (Danon disease) and hereditary *TTR* amyloid. Routine inclusion of these phenocopy variants in genetic panels is recommended (15)(7,16). Genetic testing in the proband is beneficial in

allowing cascade screening of relatives. HCM without a detectable sarcomeric mutation, commonly termed genotype-negative (G-), is hypothesised to result from polygenic causes and/or environmental factors (17). HCM is characterised by heterogenous phenotypic expression, as a consequence of non-linear and stochastic relationships with genetic and non-genetic factors. Determining the pathogenicity of pathogenic variants in large families is more easily established than sporadic variants or small families where a probabilistic approach is preferred (15).

Exact mechanisms leading from mutation to hypertrophy are incompletely understood. The sarcomeric mutation pathogenesis is either initiated through defective “poison” peptides interfering with normal function (or leading to “gain of function”) or haploinsufficiency (18). Detectable molecular abnormalities include altered calcium handing, excessive myofilament binding and ATP binding (energetics). Downstream results of myocyte growth (hypertrophy), fibroblast proliferation and collagen deposition (fibrosis), loss of normal myocyte orientation (disarray) and microvascular disease are thought to relate to adverse events (18). Hypertrophy is hypothesised to result from an increased expression of trophic factors and activation pathways such as MAPK and calcineurin whereas fibrosis results from increased expression of the mitotic factors such as TGF-beta1 from cardiomyocytes and activation of corresponding pro-fibrotic pathways in the myocytes and interstitium (15) The presence of small vessel disease is less understood and will be explored further.

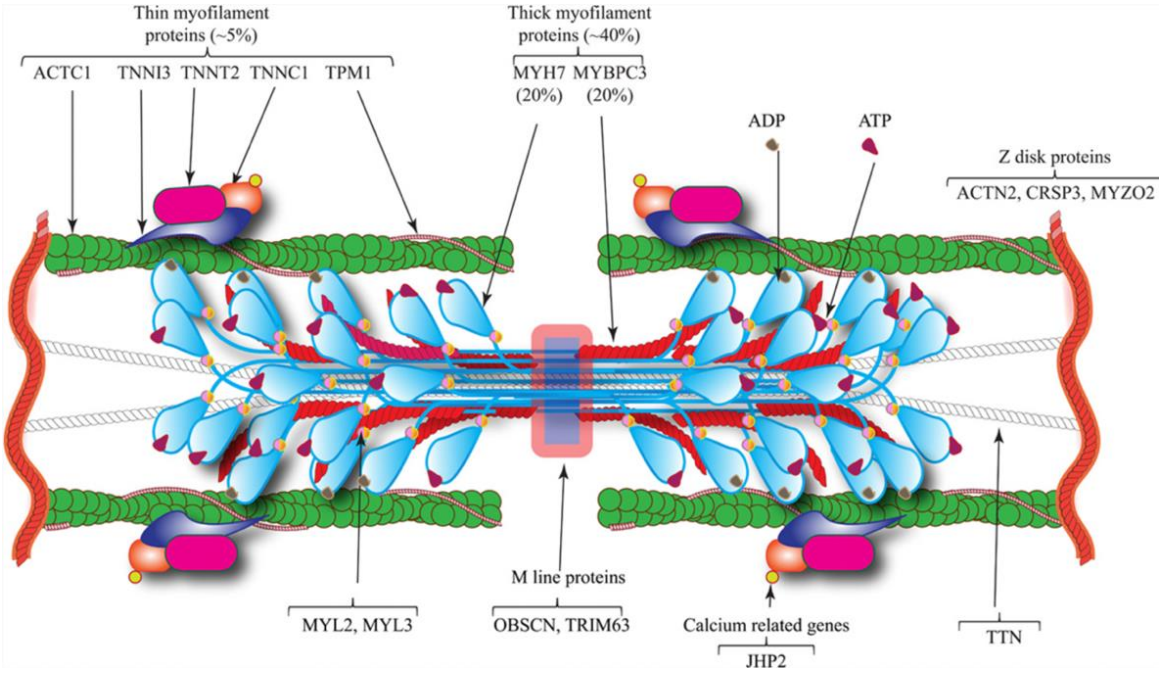

Figure 1. The sarcomere – functional unit of the myocyte – and its protein structure.
From Marian et al (15)

1.3. Clinically measured pathophysiology of HCM

1.3.1. Left ventricular hypertrophy in disease

Heart muscle is responsible for converting chemical energy to the kinetic/potential energy of blood to permit tissue perfusion. It is adaptable, sensing and responding to its environment. At tissue level, this depends on the interplay of cell types (myocyte, myofibroblast), the interstitium (fibrosis) and perfusion (smooth muscle cells, capillaries) with genetic predisposition (susceptibility) and environmental exposure influencing (19–21). A key process is left ventricular hypertrophy (LVH). This may be physiological and adaptive (growth, pregnancy, athleticism, initial responses to disease) or maladaptive (late responses to disease, primary cardiac disease, storage, infiltration). LVH at a population scale is adverse (22) and appears to play a key role in heart failure both with impaired and preserved ejection fraction, an emergent epidemic (23). Multiple processes/pathways are involved in LVH. Current diagnostic

approaches measure a narrow range of these, and their sequence, subtypes and interactions are therefore imperfectly known. This results in uncertainty about aetiology, imprecise therapy and adverse outcomes with adverse consequences for individuals and society.

1.3.2. Left ventricular hypertrophy and HCM

Donald Teare in 1958 described a case series of eight decedents from SCD with asymmetric or focal left ventricular hypertrophy. While he described the findings of septal LVH as a benign hamartoma which we now know to be asymmetrical septal hypertrophy (ASH), it is remarkable how accurately the description of the disease is what we know today, both structurally and histologically: LVH in proximity to the mitral valve, clefts, extensive fibrosis of ischaemic pattern, 'disordered muscle bundles' (disarray) and clinically: systolic murmurs, abnormal ECG and exertional syncope. He had also postulated that the disease could be familial (24). While Teare described mostly asymmetric septal hypertrophy other patterns are well characterised including focal hypertrophy involving 1-2 segments, concentric hypertrophy, reverse septal hypertrophy and apical hypertrophy comprising 10% of HCM (24)(25). Finding of isolated left ventricular hypertrophy is the most common, however occasionally right ventricular and atrial hypertrophy may also be present (26).

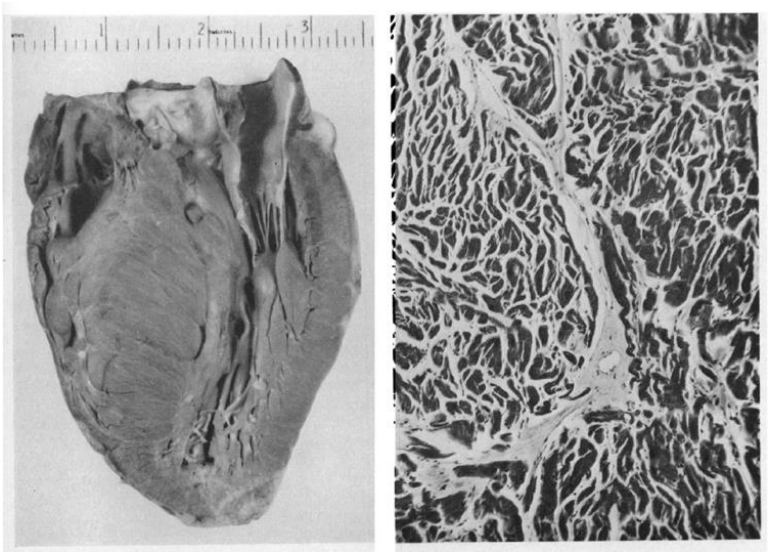

Figure 2. Images taken from Teare's seminal case series in 1958
ASH is shown (Left) with "disordered muscle bundles" (Right), *Teare et al (24)*

The size of myocytes in HCM often exceed that of LVH from other causes; some reported up to 80 micrometers (normal 10-15micrometers) **(Figure 3)**. HCM myocytes also display increased cellular branching, more side-to-side intercellular junctions, widened z-bands and abnormal myocyte nuclei (enlarged, convoluted nuclear walls, binucleated). The relationship of myocytes with the interstitium can also be heterogenous within the same myocardium; some regions may resemble idiopathic LVH with large myocytes and no interstitial expansion with other regions having both large myocytes and highly expanded interstitium with diffuse fibrosis (27,28). Histological studies have also attempted to correlate findings with clinical factors: an inverse relationship between the degree of hypertrophy and age has been found (26,29). Increased myocyte size on histological examination also associated with younger age at ICD implantation. Myocyte size also positively associated with mortality following surgery and atrial fibrillation (29).

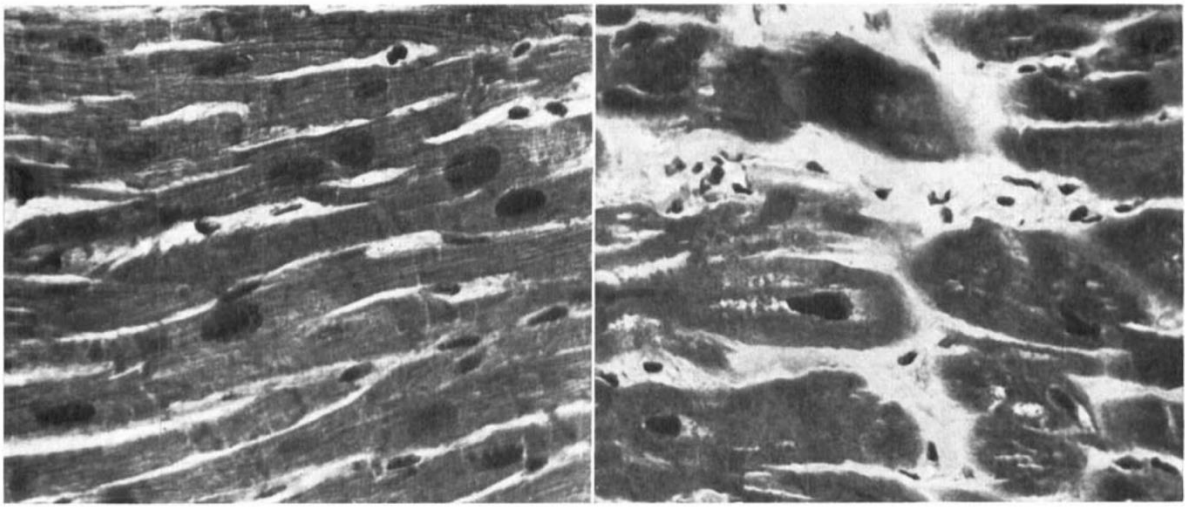

Figure 3. HCM Myocardium.
Left – hypertrophied sub-aortic stenosis myocardium – average fibre diameter 17 micrometres. **Right** – HCM myocardium – short, hypertrophied fibres with expanded connective tissue, average diameter 37 micrometers. *Noorden et al (28)*

1.3.3. Fibrosis in disease and HCM

Fibrosis in disease

Myocardial fibrosis is conceptually associated with thinning, but it is almost always associated initially with hypertrophy. Histological studies have shown fibrosis subtypes classified by composition, distribution and extent, which vary between diseases (26) (30). Advances in clinical imaging such as the late gadolinium enhancement (LGE) technique by cardiovascular magnetic resonance (CMR) have brought the identification and measurement of cardiac fibrosis to healthcare (31). Detected fibrosis *in vivo* also carries disease specific significance: for example a small amount of LGE (eg. 2%) in severe aortic stenosis is highly adverse, whereas scar is found in most HCM and is less adverse (30,31). LGE in early Fabry's disease appears to be mostly inflammation rather than fibrosis which occurs later (32). LGE is therefore a major part of clinical care and under investigation as a key risk stratifier (31). The limitation with fibrosis is that it is a downstream process and there are no treatments available. Similarly, adaptive and pathological LVH is easy to differentiate at advanced

disease stages, but hard in milder LVH, where there are few *in vivo* classifiers. We need pre-fibrotic markers and markers that may define LVH as adaptive or pathological.

Fibrosis in HCM

Surprisingly the description of fibrosis in Teare's seminal paper in 1958 was somewhat muted, with the description of the stark myocyte/myofibril disarray taking precedence in his descriptions- subsequent histological examinations of HCM reported varying degrees of fibrosis in myocardium. Of the few mentions of fibrosis in Teare's paper was its interspersion between muscle fibres leading him to postulate that the myocardium was contracting inefficiently (24). The lack of fibrosis description could be in part due to the fact that his subjects were relatively young decedents of SCD where fibrosis was less extensive.

Predominant types of fibrosis that are observed in HCM are replacement fibrosis (scar), interstitial fibrosis and mixed types. Serum biomarker testing of collagen synthesis and degradation in HCM reveals increased synthesis and turnover (33). LGE imaging has provided substantial insights into the pattern (33), extent and clinical significance of scar in HCM, which will be discussed below. However, the pattern of scarring is important to note – at RV insertion points, the LGE seen represents expanded ECV (focal interstitial fibrosis as opposed to replacement fibrosis) (34). It is well established that when scar becomes significant in quantity (20% of myocardium) the risk of further progression to heart failure is high - LV myocardium undergoes thinning and a dilated phase with depressed ejection fraction (EF) (35). Histological analysis of explanted hearts from patients in this dilated phase showed the scar was mainly replacement type as opposed to interstitial with scar forming

prominently in myocardial midwall as opposed to subendocardial/subepicardial. However, histological findings are likely reflective of patient selection; myectomy samples often show interstitial fibrosis predominates – which may be reflective of hyperdynamic myocardial function, as opposed to reduced EF/dilated heart failure phenotypes (36,37).

1.4. Measurement of LVH and fibrosis: Conventional Imaging

1.4.1. Echocardiography

Echocardiography is the recommended initial evaluation in HCM and is the recommended serial screening measure for identification and monitoring of LVOTO and mitral regurgitation. Transoesophageal echo is recommended to plan septal reduction therapy, exclude subaortic membranes and better characterise mitral regurgitation (7) (38). In those with symptoms but no LVOTO on Valsalva, exercise transthoracic echo (TTE) is recommended to identify exercise-induced LVOTO and MR from SAM. In particular, in those with refractory symptoms, the exclusion of exercise LVOTO can signpost treatment towards heart failure therapies and possible future transplantation (5). Other causes of exercise limitation can also be ascertained such as diastolic function and exercise induced pulmonary hypertension. Severe symptoms can also be corroborated with cardiopulmonary exercise parameters. Such measures including the maximal rate of oxygen consumption during exercise (VO2 max) and submaximal parameters which may provide important prognostic information. Furthermore, severely aberrant CPEX measures can also guide therapies including transplantation and septal reduction therapies (38).

1.4.2. Cardiac MRI – structure and function

Cardiac MRI (CMR) forms the gold standard imaging technique for the measurement of cardiac structure and function, and is enhanced in diagnostic capabilities by tissue characterisation – crucially scar identification, characterisation and quantification. CMR forms a crucial role in the management of HCM. Firstly the identification and quantification of hypertrophy is vastly superior to echocardiography, especially detection in segments easily missed by standard echo views, commonly the anteroseptum (often missing LVH between the 2 chamber and 3 chamber views) and the apex. Furthermore where SCD risk is unclear, the quantification of left atrial size, LVH and scar can guide decisions on risk. Other benefits include the identification of subclinical and 'burnout' features, discrimination of phenocopies and planning of septal reduction therapy (7). While CMR cannot measure LVOTO gradients which is reserved for echocardiography, identification of abnormal attachments to the mitral valve (particular AMVL), papillary muscle abnormalities including bifid papillary muscle and elongated AMVL can be augmented by CMR (39). Advances in CMR scanning in patients with implantable devices has improved access for high-risk HCM in some centres (40).

1.4.3. Cardiac MRI - Late gadolinium enhancement

Gadolinium is an inert tracer that distributes in extracellular water but cannot infiltrate intact cell membranes, and has a late washout period. It therefore accumulates in myocardium with expanded extracellular space in comparison with normal myocardium. Paired LGE CMR and histological study shows a very high agreement with LGE and myocardial collagen content (**Figure 4**) (41). LGE CMR in HCM using gadolinium contrast allows the characterization of scar which in turn helps to support the diagnosis when present or identify alternative diagnoses, particularly amyloidosis

(37). In longitudinal studies, the extent of LGE was related to sudden cardiac death and progression to heart failure, even after correction for conventional risk markers, and even in those with conventionally low or intermediate risk. Extensive LGE is therefore considered in decisions surrounding ICD implantation (34). The significant progression of LGE in HCM is variable with limited study quoting 15-26% over a follow-up period of 4 and 6 years respectively (42,43). Longitudinal follow-up of HCM patients with LGE CMR shows that scar progression is related to baseline LGE mass and predicts future heart failure and the necessity for ICD implantation (42). LGE mass progression in those with a large quantity of scar importantly heralds adverse LV remodelling including LV dilation and wall thinning. Impairment of perfusion and metabolic energetics prior to LGE progression has been demonstrated, however de-novo LGE can also be seen to develop in segments without prior perfusion defects. The robustness of this observation however depends on the frequency of serial imaging (43) (31).

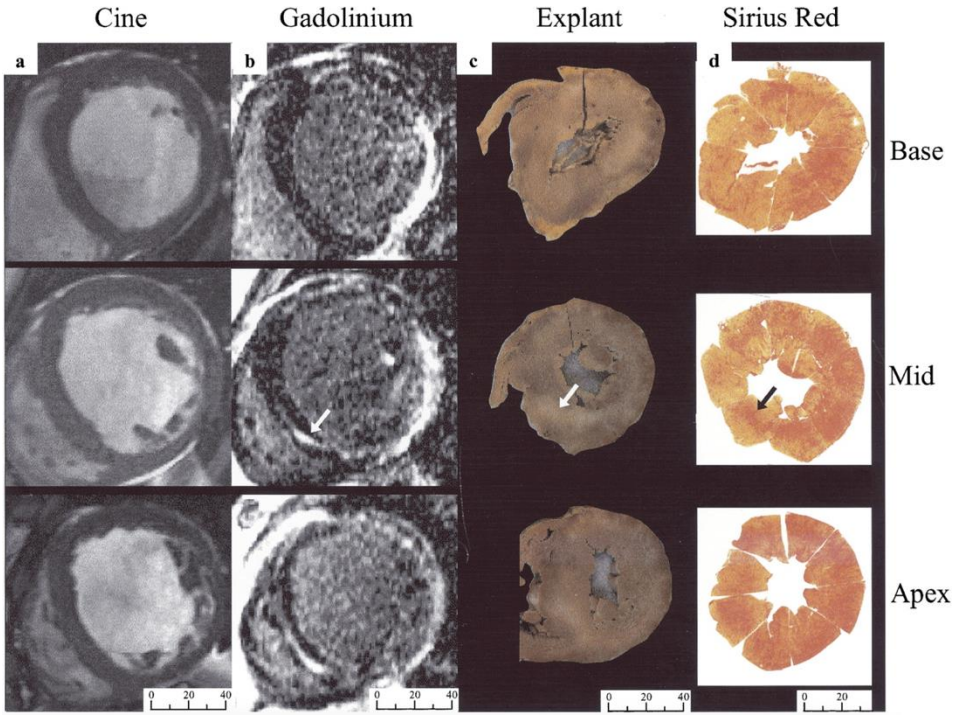

Figure 4. Scaled *in-vivo/ex-vivo* image from an explanted heart peri-transplantation (patient with end-stage cardiomyopathy).
Cine CMR imaging (a), late gadolinium enhancement imaging (b), explanted heart specimens (c) Sirius-red stained sections (d). Arrows show correlation between focal fibrosis (pale on specimens and red on stained sections) and LGE. *Moon et al (41)*

1.5. Missing Pathophysiology in HCM: Disarray

1.5.1. Normal myocardial microstructure

From endocardium to epicardium, cardiomyocytes change orientation starting in a left-handed helical course at the epicardium (+60degrees) to a more circumferential course at the mesocardium (0 degrees) and then a right handed helical course at the endocardium (-60 degrees) **(Figure 5)** (44). The helical arrangement of cardiomyocytes permits myocardial rotation and torsion (clockwise basally, anti-clockwise apically). However as the myocytes are contracting in opposite directions within these layers, the differences in strain are resolved and wall thickening is enhanced by a secondary structure termed sheetlets: these are aggregated units of approximately 4 cardiomyocytes thick which are interspersed with collagenous

perimysium to allow sheer between neighbouring myocytes (45). The re-orientation of myocardial sheetlets have been proposed as a primary facilitator of wall thickening (myocytes themselves only thicken by 8% but the LV wall often by 40%). This has been subject to some debate with some supporting evidence from diffusion tensor imaging (DTI) discussed below (45,46) **Figure 5)**.

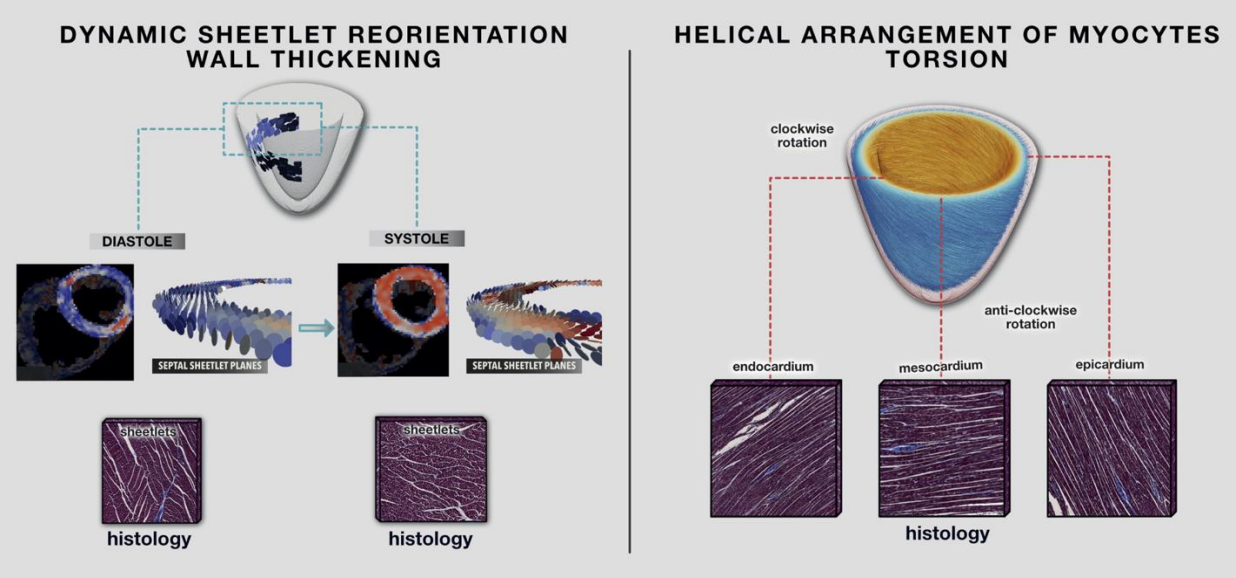

Figure 5. Helical and Sheetlet Orientation.
Left: Sheetlet (functional unit of myocytes) re-orientation facilitates wall-thickening from wall-parallel to perpendicular orientations – reflected by cardiac DTI. **Right:** Individual myocytes arranged in helical orientation – clockwise (endocardium) and anticlockwise (epicardium). *Nielles-Vallespin et al* (46)

1.5.2. Presence of disarray in health and other diseases

Disarray is defined as the loss of normal myocyte organization on histology. The disorganization can be observed at the light microscopy level of individual myocyte spatial relationships including where bundles of myocytes are arranged in a herringbone pattern i.e arranged perpendicularly to each other or whorled in appearance (**Figure 6**) (47).

Disarray can be present in health, particularly in the RV insertion points, around large blood vessels, and in the right ventricle. Disarray is not specific to HCM, having been found in congenital heart disease, infarction, systemic or pulmonary hypertension and other cardiomyopathies (47). Some ultrastructural features overlap with LVH from other causes (excess mitochondria and glycogen), however the extent of disarray enhances specificity for HCM on pathological examination (minimum 5%, typically up to 30% but often >50% of myocardium) (27,28).

1.5.3. Presence of disarray in HCM

The pattern of disarray varies between reports with some suggesting a diffuse pattern, and others describing focal/patchy distributions similar to scar and ischaemia. Extent of disarray has been shown to vary greatly between segments and within segments (26). Disarray appears to be independent to the extent of LVH; normal myocyte arrangement has been observed in the hypertrophied HCM apex despite very enlarged myocytes. Disarray has also been reported to be more marked in young HCM (21, 22,23).

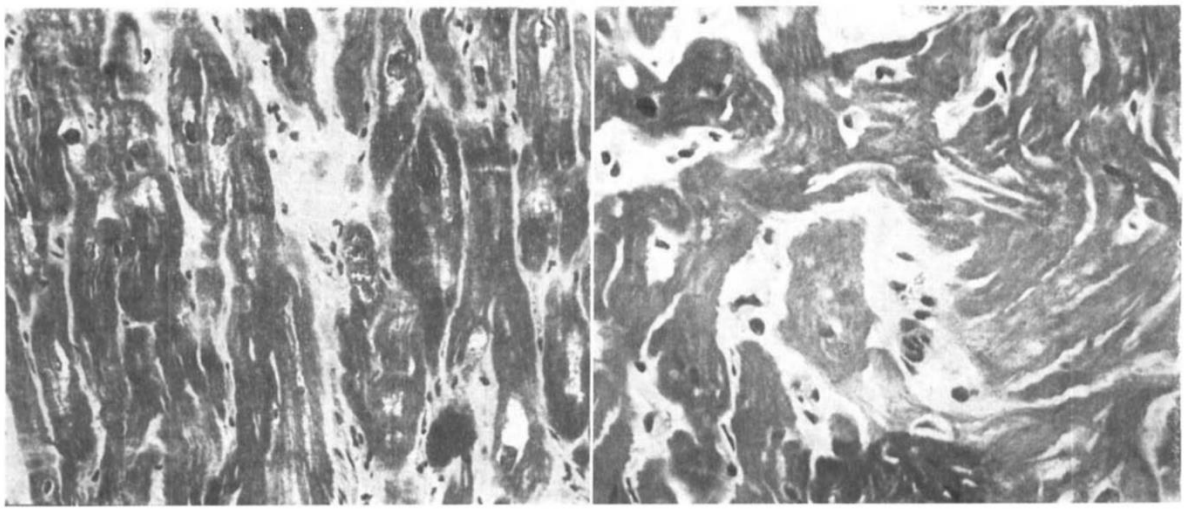

Figure 6. **Microstructural abnormalities in HCM**.
Left –halo around abnormal nuclei, **Right** – whorled myocardial appearance,
Noorden et al (28)

1.5.4. Role of disarray in arrhythmogenesis

The organisation of myocardial microstructure is fundamental to the electromechanical properties of the heart (48). Disarray has been hypothesised to contribute to arrythmia formation through disruption of gap junctions, slowed longitudinal conduction resulting in increased transverse conduction and propagating re-entry (47). Marked disarray being found on autopsy studies of SCD victims led the first hypotheses into its malignant role in ventricular arrhythmia (26) (24). This was further re-enforced by case series reports of SCD with marked disarray on autopsy with no significant LVH, later found to be attributed to a Troponin T mutation (49).

1.6. Technique to investigate disarray - Diffusion tensor imaging

While disarray has been described on autopsy reports at the time of disease discovery, advanced imaging allows us to quantify physical parameters *in-vivo* that are likely related to disarray, avoiding the need for ionising radiation and histological specimens. DTI is currently employed in routine clinical brain imaging to detect microstructural changes and oedema related to neuropathology and its treatment. Recently, advances in cardiac MRI have overcome technical challenges such as bulk motion and susceptibility thereby allowing resolution of fine myocardial structures (the microstructure) (50).

1.6.1. Diffusion CMR Principles

Diffusion CMR maps the diffusion of water within the imaging voxel. Free diffusion occurs when water molecules diffuse in all directions equally (isotropic diffusion). Restriction of diffusion due to the myocardial microstructure, primarily through

cardiomyocytes and connective tissue, results in restricted and less isotropic (anisotropic) diffusion.

Diffusion CMR is performed by measuring the signal loss between the acquisition of 2 images – the reference image and a main image with a diffusion weighting described by the b-value (45). The b-value is a factor that reflects diffusion gradient amplitudes, duration, and temporal separations of the gradient pulses, quoted in units of seconds per square millimetre (typically 0-1000 s/mm^2). The higher the b-value, the stronger the diffusion effects.

$$\mathbf{S = S_o e^{-bD}}$$

S_o: signal at baseline

b: b-value

D: diffusion co-efficient [how fast a substance diffuses in a given medium due to random motion]

S: signal after the diffusion gradient

Low b-values will be confounded by other sources of diffusion-like incoherent motion including perfusion and high b-values will be less easily distinguished from background noise. Diffusion weighting was first discovered in neuro-imaging where more signal loss (resulting in more diffusion or elevated apparent diffusion co-efficient (ADC)) was found when a diffusion gradient was applied in the axonal direction. Information from diffusion weighting is used to compute the direction and magnitude of diffusions in three dimensions – termed the eigenvector (45).

1.6.2. DTI Sequence Anatomy: Second-order motion compensated Spin Echo

A classical diffusion sequence uses a 90 degree excitation pulse followed by a diffusion gradient and a 180 degree refocusing pulse and a second diffusion gradient which realigns spins from static tissue at equal but opposite net magnetization. Therefore, static spins undergo equal dephasing and rephasing, flow spins experience a phase shift, and diffusion undergoes incomplete rephasing, phase dispersion and decreased net magnetization and signal attenuation. Diffusivity is calculated from signal loss and diffusion weighting (see equation above).

Technical challenges in diffusion imaging include magnetic susceptibility in the thoracic region, low signal to noise due to the short T2 of myocardium and bulk motion confounding the diffusion encoding. Two main strategies to overcome bulk motion by minimizing diffusion gradients to be classified as diffusion weighting include spreading diffusion encoding over two neighbouring R-R intervals by Stimulated Echo Acquisition Mode. This splits the 180 degree refocussing pulse into two 90 degree pulses so that the time over which the diffusion is measured is an RR interval and each image is acquired over 2 cardiac cycles. Cardiac motion is minimised by acquiring data so that the heart is in the same position every time the diffusion gradients are applied, minimising the effects of cardiac motion. A consistent RR interval is required, meaning STEAM is more susceptible to error during arrhythmia and due to the longer diffusion time. There is also more confounding with strain (compression and decompression of myocardium will alter diffusion properties) (45). Overcoming these limitations and also bulk motion is the second order motion compensated spin echo sequence (M2SE). As this does not overcome more complex motion occurring in diastole (including jerk motion), M2SE is acquired in systole, and involves a 90 degree excitation and 180 degree refocussing pulse with a relatively short period of time over which the diffusion occurs (diffusion time) (**Figure 7**).

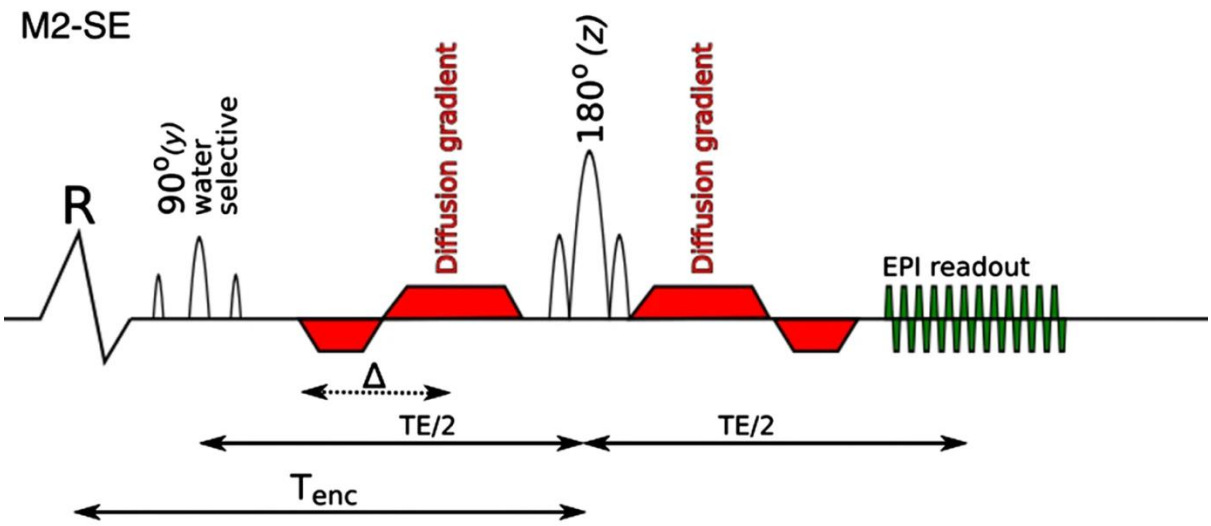

Figure 7. Motion-compensated Spin Echo Sequence anatomy.
Triggered every R wave. ∆is the measured diffusion time. Slice selective gradient is played-out on the y axis. T_{enc} time from R-wave to effective time of diffusion encoding, RR-interval. *Khalique et al, (45)*

The second-order-motion compensated spin echo sequence that was used in the study was designed by Nguyen et al in 2014 based on a balanced steady state free precession approach (50).

1.6.3. The Eigensystem

Perfectly unrestricted diffusion occurs in a sphere whereas restricted diffusion occurs in an ellipsoid with the three dimensional axes of diffusion labelled λ_1, λ_2, λ_3 in order of their diffusion magnitudes (eigenvalues) and diffusion directions: E1, E2, E3 (eigenvectors) (**Figure 8**). The eigenvectors are projected onto the short axis plane and matching several histological studies, the E1 angle represents the cardiomyocyte orientation (E1A commonly referred to as the helix angle) and E2 angle represents the sheetlet orientation (functional units of myocytes that dynamically re-orientate to facilitate wall thickening) (45,46).

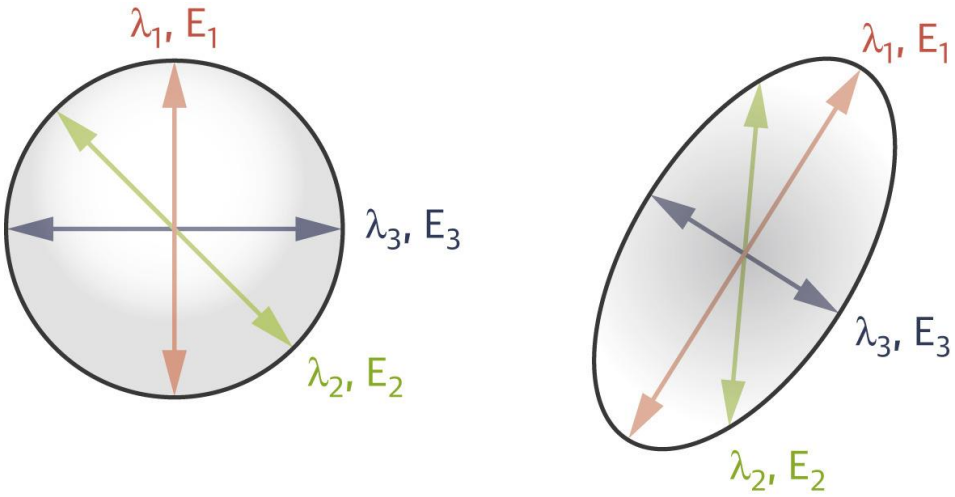

Figure 8. The eigenvectors
Left – isotropic (unrestricted diffusion) occurring in a sphere. **Right** – anisotropic diffusion occurring in an ellipsoid. λ_1, λ_2, λ_3 represent diffusion magnitudes (eigenvalues) and E1, E2, E3 (eigenvectors) are the diffusion directions, *Khalique et al (48):*

1.6.4. Post Processing of cDTI

Diffusion images are co-registered and images with failed co-registration or images and segments with artefact omitted. Diffusion weighted image repetitions per diffusion gradient orientation are then used for tensor reconstruction. Based on registered data, magnitude averaged images are generated according to diffusion direction and b-value; tensors are then calculated using a linear least squares approach (51)

1.6.5. Diffusion Tensor Imaging in HCM

HCM is characterised by i) low fractional anisotropy (FA), a measure of the directional variability of water diffusion with low values suggestive of myocyte disarray and collagen deposition ii) high mean diffusivity (MD) measuring the magnitude of diffusion, thought to reflect myocyte packing with high values reflecting increased interstitial fibrosis and changes in intra-and extra-cellular volume, iii) elevated absolute second eigenvector angle (|E2A|), reflecting sheetlet orientation which conforms to

hypercontracted states (elevated |E2A|) in systole with failure to re-orientate in diastole, implying roles in diastolic failure in HCM and increased cardiomyocyte tension (44,46,52,53). Use of STEAM based techniques also allows assessment of sheetlet mobility (from diastole to systole) and has shown steeper sheetlet orientation in both diastole and systole resulting in reduced sheetlet mobility. Head-to-head comparison of M2SE and STEAM sequences showed that this relationship is not found when using M2SE due to its inherent limitations in imaging during diastole. This comparison also showed that M2SE had higher MD and lower FA values than STEAM, and had greater discrimination in identifying segments with scar and LVH through MD and FA derangement (**Figure 9**) (54). Impaired sheetlet mobility and steeper sheetlet configuration in overt HCM possibly reflects increased ATPase-related myosin calcium sensitivity, increased cardiomyocyte tension and diastolic failure (44). A small pioneering DTI study in HCM (n=10) focussing on sheetlet orientation showed E2A was more severely elevated in hypertrophied segments, with no clear relationships with late gadolinium enhancement (44). Strain effects as a confounder to DTI findings was considered, especially as STEAM sequences were used. In a later study by the same group, animal work comparing *in-vivo* DT CMR at peak systole and arrested contracted hearts using barium chloride showed that strain effects contributed 17% of the E2A value (44,46). This is taking into account the use of the STEAM sequence with more influence of strain on E2A due to long mixing times (44). This study went on to perform DT-CMR in HCM and DCM patients and showed impaired sheetlet mobility in both. The study also correlated E2A findings with impaired mechanical strain in both diseases showing perhaps a functional relationship between myocardial microstructure and mechanics (46) (44,46).

A larger (n=50) study of DT-CMR in HCM sought in particular to correlate fractional anisotropy to non-sustained VT to ascertain its value as a risk marker for ventricular arrhythmia. FA was low in HCM compared to controls even after adjustment for LGE and ECV, leading investigators to propose that lowered FA was detecting disarray incrementally to fibrosis. FA was associated with the development of NSVT supporting the hypothesis that low FA suggestive of disarray was pro-arrhythmic. Importantly investigators only used the FA of maximally hypertrophied segments, as this was the segment consistently with the lowest FA between individuals. The limitation to this approach is that disarray has been shown to vary greatly both between segments and within segments (26). Furthermore, the most hypertrophied segment commonly contains the most expanded ECV and the most scar and may not be the source of ventricular arrhythmia. Some qualitative comparisons were also made with histological findings where investigators described a band of high FA in the myocardial midwall in controls that was disrupted in HCM with low FA. Importantly no difference in mean diffusivity between HCM and controls were found, potentially highlighting the limitations of STEAM based sequences. In studies utilising M2SE, findings of high mean diffusivity suggestive of impaired myocyte packing, expanded ECV and possibly elevated intracellular volume have been found consistently (52,53).

A paired quantitative perfusion and diffusion tensor study has been performed by collaborators seeking to identify relationships between microvascular disease and myocardial disarray. This study utilising M2SE showed that HCM segments with normal wall thickness, normal perfusion and no scar still had more isotropic diffusion (low FA, high MD) than normal control segments suggesting that diffusion parameters indicative of disarray and fibrosis alter early in phenotype development. Both were more impaired in the subendocardium, potentially suggesting a relationship between

local microvascular and microstructural remodelling or possibly both being confounded by subendocardial fibrosis (resulting from elevated intracavity pressures and AMVL contact with the subendocardium) (55).

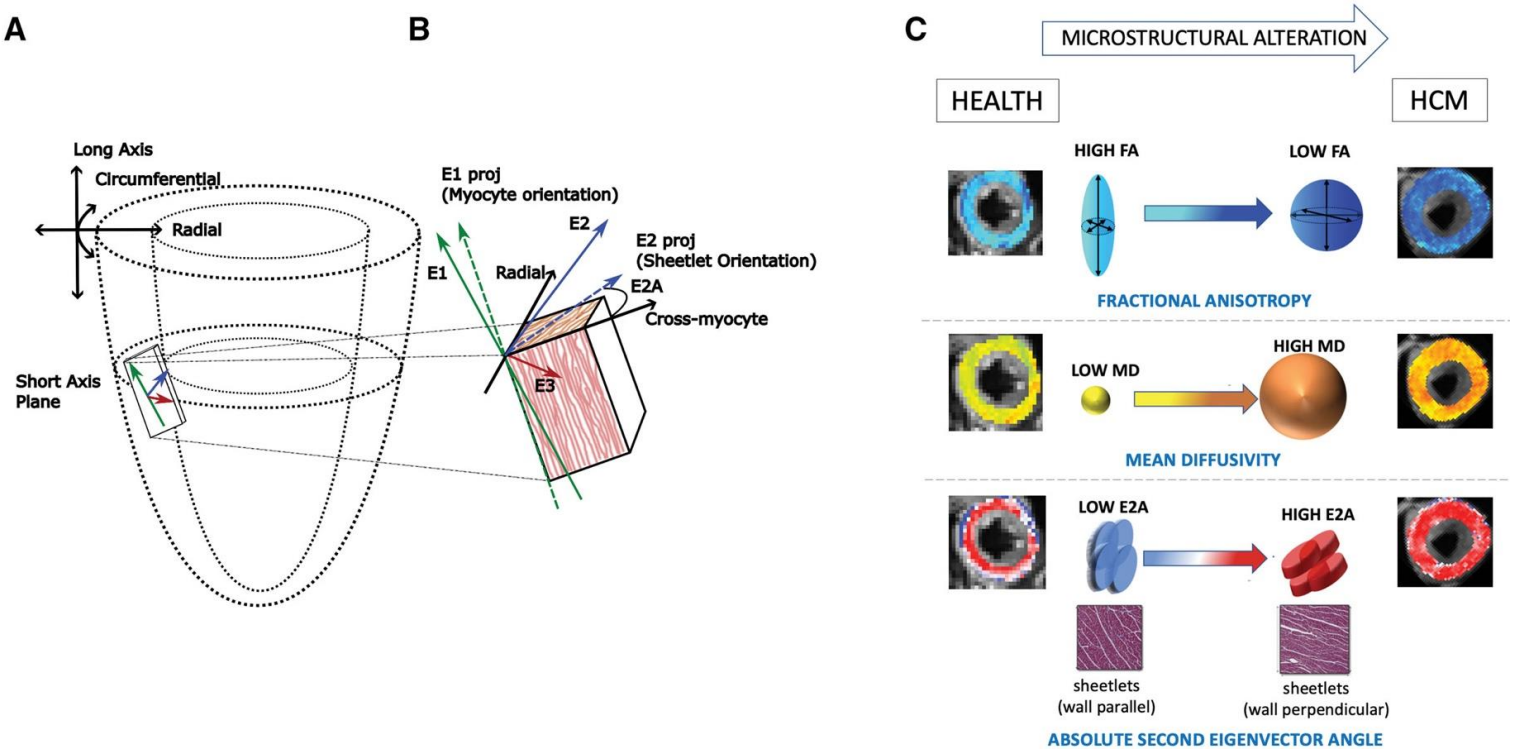

Figure 9. Cardiac diffusion tensor imaging.

A, Representation of the short-axis imaging plane with a magnified imaging voxel containing ≈50 000 myocytes. Diffusion tensor imaging measures magnitudes (eigenvalues λ1, λ2, and λ3) and direction (eigenvectors E1, E2, and E3) of water diffusion. B, Three arrows (green, blue, and red) representing the 3-dimensional directions of diffusion: the 3 principal eigenvectors. E1 (green) is the direction of maximum diffusivity orientated along the myocyte long axis. Myocytes are organized into sheetlets, functional units of myocytes that dynamically reorientate to facilitate wall thickening, reflected by the E2 (blue) angle against the cross-myocyte plane (right angles to E1 projection on the wall tangent plane). C, Sheetlets angled parallel to the wall tangent have a low absolute second eigenvector angle (|E2A|), and sheetlets positioned perpendicular to the wall tangent have a high |E2A|, signifying a more contracted sheetlet configuration. If myocytes were perfectly randomly orientated (isotropic diffusion), fractional anisotropy (FA) would be 0; hence, myocyte disarray causes lower fractional anisotropy (FA) values. Mean diffusivity (MD) is the mean of the eigenvalues, with higher values representing a greater magnitude of diffusion. MD is thought to be sensitive to myocyte packing and intracellular and extracellular volume shifts. HCM indicates hypertrophic cardiomyopathy

1.6.6. DTI in other diseases

Aortic Stenosis

DTI changes in LVH resulting from excessive afterload in AS showed low FA, elevated mean diffusivity and steeper sheetlet orientation (high E2A). Significant changes in ECV were not detected suggesting that DTI changes were in response to increased intracellular volume as opposed to diffuse fibrosis (higher ECV). DTI parameters were noted to resolve after aortic valve replacement suggesting plasticity in DTI changes, but the extent to which the parameters are influenced by elevated myocyte size or disarray is unresolved (56).

Amyloidosis

Infiltration of the interstitium with amyloid resulted in low FA, higher MD and steeper sheetlet orientation. Unsurprisingly, derangement was more severe in amyloid than HCM. There was a strong correlation between MD and ECV showing the strong influence of amyloid burden on DTI parameters (57).

DCM

Contrasting HCM, the failure of sheetlets to reorientate to facilitate wall thickening in DCM results in lower E2A (less steep sheetlet orientation). DCM in remission (previous LV failure which recovered over time and with medical therapy) also showed lower E2A and impaired sheetlet mobility compared to controls despite remission, but more improved DTI parameters than with persistent DCM and reduced LVEF (45).

Myocardial Infarction

Acute infarction had DTI parameters consistent with disarray (low FA, high MD) but unlike in HCM, sheetlet orientation was less steep in infarcted segments. Furthermore E2A and FA derangement were predictive of adverse remodelling even after correction for conventional predictors (infarct size, MVO). Proposed relationships between

adverse microstructural changes caused by infarction and adverse remodelling are plausible, as infarcts with severely disrupted microstructure are more likely to lead to adverse macrostructural changes (58).

1.7. Missing Pathophysiology in HCM: Microvascular Disease

In HCM, the presence of microvascular disease can be seen clinically; patients often present with chest pain, ischaemic changes on ECG and elevated troponin reflecting myocyte death – even in the asymptomatic (59). Some have even hypothesised that ischaemia is the main driver of sudden cardiac death as opposed to a primary ventricular arrhythmia (60).

Subendocardial scar in obstructive HCM is related to impact lesions from anterior mitral valve leaflet (AMVL) contact (26). Otherwise the development of scar in HCM could be related to ischaemic injury; replacement scar histologically colocalizes with severe small coronary vessel disease (26) (36), and ischaemic scar was frequently observed in decedents of SCD. Furthermore ischaemic scar at different stages can be observed: acute – coagulative necrosis and neutrophilic infiltrate, sub-acute-myocytolisis and granulation tissue healing, and post-necrotic replacement-type fibrosis (60). On histological examination, small vessel disease extent also correlates with fibrosis extent and also septal thickness, suggesting there is an interplay between hypertrophy, small vessel disease and hypertrophy (60). Small vessels have been described as structurally abnormal with intimal proliferation, medial hypertrophy and vasomotor limitation to stress (60). However, it is possible that small vessel disease on histology may be a result of and not causative of ischaemic scar. Other proposed mechanisms include extrinsic compression of hypertrophied myocardium on coronary

microvasculature, malignant myocardial bridging and excess myocardial oxygen demand but exact mechanisms remain unresolved. (60).

1.7.1. Possibility of a unifying explanation

While sarcomeric gene mutations may have direct associations with myocyte hypertrophy, other features of the disease are less easily explained by this, namely elongated mitral valve leaflets, crypts and abnormal trabeculation. With observations that disarray and the above features can be observed in newborn babies, and also these structural features occurring in individuals with a sarcomeric mutation (genotype positive) but without hypertrophy (LVH-), led some to propose a developmental origin for HCM from 'cross talk' between abnormally contracting sarcomeres and healthy pluripotent epicardial derived cells. This hypothesis also seeks to explain the presence of abnormal coronary microvasculature, interstitial fibrosis and myocyte disarray (61). Some evidence for an embryological origin for the HCM phenotype can be seen in embryonic murine models studied with high-resolution episcopic microscopy. Here *mybpc3* truncating mutations in embryonic mice resulted in greater myocyte disarray (**Figure 10**), an increased number of crypts and trabecular complexity compared to wild type mice. Anterior mitral valve leaflet prolongation was not observed in the fetal murine models however, raising the possibility this is more related to mechanical stretch after birth. Furthermore, an asymmetry between the septum and lateral wall is observed after septation but reduces in prominence as the fetus develops. It is unknown whether this asymmetry also relates to the presence of sarcomeric mutation in the developing HCM heart (62) (63).

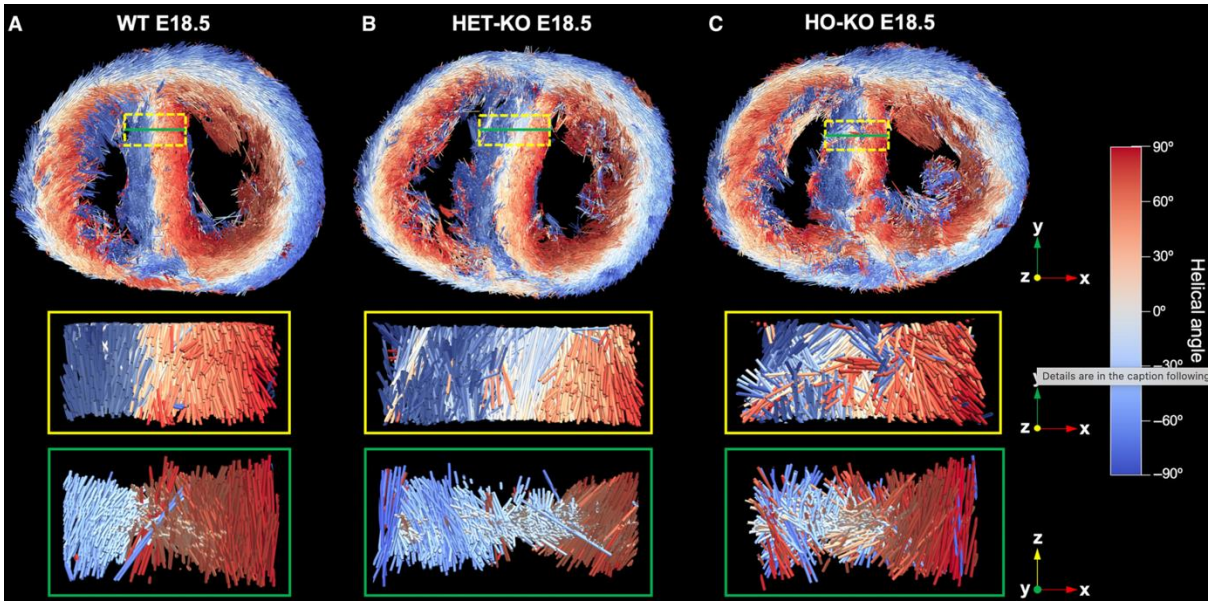

Figure 10. *Ex-vivo* imaging (episcopic microscopy) of MYBPC3 knock-out murine models
3D representations of myocyte tracking (each rod corresponds to the long-axis of myocytes). Increasing myocyte disarray between the wild-type mouse, (Left), heterozygous (Middle) and homozygous (Right) MYBPC3 knock-out mice. *Garcia-Canadilla et al (62)*

1.7.2. Disease discrimination and the potential role of microvascular function assessment

There are phenotypic structural overlaps with HCM and differentiation can be challenging. Exercise has substantial global and cardiovascular health benefits. Cardiac changes with regular, intensive exercise are referred to as ‘athlete’s heart’ with structural, electrical and functional cardiac adaptations. Part of this can be physiological LVH. The degree of LVH is dependent on exercise type (aerobic/isometric), sex, ethnicity, and other factors (performance enhancing drugs). LV structural and electrical changes in response to athleticism can phenotypically overlap with mild cardiomyopathy. Features indicating cardiomyopathy include dynamic LVOTO, the presence of symptoms, family history of cardiomyopathy,

pathological Q waves, lateral T-wave inversion (TWI), left bundle branch block (LBBB) and abnormal scar and suboptimal VO2 max (64). A reduction in wall thickness after a period of deconditioning favours a diagnosis of physiological adaptation, but this is not always easy to achieve. Clinical features discriminating physiological from pathological LVH may be absent or non-specific, resulting in the so-called athletic 'grey-zone'.

Myocardial perfusion impairment suggestive of impaired microvascular function measured by CMR or PET-CT has been well-described in HCM and other cardiomyopathies (61,65,66). While the effect of exercise on positive macrovascular changes in sedentary individuals has been shown (67), the effect of athleticism on microvascular function has been less well explored.

Karamitsos et al studied 11 athletes using perfusion cardiac MRI (CMR) and blood-oxygen dependant signal intensity change (a sequence capitalising on the paramagnetic effect of de-oxygenated haemoglobin to induce signal loss from de-oxygenated tissue). The technique sought to investigate ischaemia in more depth as impaired perfusion may not result in ischaemia in certain scenarios with low metabolic demand (hibernating myocardium) and conversely in HCM with hypercontractile myocardium. Compared to 20 healthy volunteers, there were no differences in perfusion or tissue-oxygenation in athletes compared to controls. As normal perfusion & oxygenation was in the setting of an expected elevation in LV mass, investigators proposed this technique had potential as a discriminator of pathological vs physiological LVH (68).

Heinonen et al used PET-CT and radiolabelled oxygen [^{15}O] to study circulatory alterations in 13 athletes. Findings showed athletes experienced a higher oxygen extraction fraction (the ratio of oxygen consumption to myocardial blood flow) and

lower rest and exercise myocardial blood flow (69). While these findings may contrast those from Karimitsos study, importantly exercise stress is fundamentally different to adenosine with the latter causing large drops in microvascular resistance, lower increases in rate pressure product (systolic blood pressure * heart rate) and being endothelium independent (exercise is endothelium dependent) (70) (69). Laaksonen et al used PET perfusion to study seven endurance-trained subjects at rest and exercise and found that rest perfusion was no different, however submaximal exercise perfusion was enhanced in athletes but not during maximal exercise (71). It is evident that while contrasting findings may relate to differences in cohorts and techniques, further exploration into the microvascular function would add to understanding and would further investigate the potential for this adaptation in disease discrimination.

LVH in hypertension is caused by an increased afterload and consists in initially compensatory, later pathological hypertrophy (72). Hypertensive LVH can be asymmetric (25%) and can result in SAM and LVOTO (73) whilst the degree of hypertrophy can be quite marked (up to 20mm) in some scenarios, for example hypertensive Black patients (74). The grey zone can be large and a recent study by collaborators showed a 4% prevalence of HCM in hypertensive patients - 20x higher than the general population (75). Advanced imaging adds some value - 45% of hypertensive patients have some LGE but at lower volumes than HCM (76). Strain is less reduced in hypertensive vs HCM LVH and endocardial/epicardial ratios may help distinguish, although reproducibility is lower (72). Further assessment of microvascular function in hypertensives and athletes will provide mechanistic insights and determine if there is discriminatory value in this approach.

1.7.3. Techniques to investigate microvascular disease: Quantitative perfusion

The assessment of microvascular disease may address some of the clinical challenges in HCM, namely disease discrimination, subclinical HCM and characterizing genetic substrate in overt disease.

1.7.4. Quantitative Perfusion Sequence

The Kellman fully automated perfusion sequence gained traction as the method of choice for CMR quantitative myocardial perfusion imaging due to distinct technical advantages over other methods summarised as follows: 1) fully-automated workflow 2) pixel-wise flow calculation 3) single contrast bolus 4) complete free breathing acquisition 5) inline deployment (77).

Arterial input function

Quantification of myocardial blood flow requires knowledge of the amount of contrast agent in the myocardial tissue and the arterial input function (AIF) driving the delivery of contrast into the tissue (**Figure 11**). The quantification of tissue-level myocardial blood flow (MBF) would be optimally obtained from input and response curves but there is non-linearity between signal intensity and tissue contrast concentration caused by imperfect magnetisation saturation, T2* decay due to high blood-pool contrast and non-linear response inherent with saturation recovery. A dual sequence protocol was developed (avoiding disadvantages of separate bolus for AIF) which optimised for imaging for AIF and myocardial tissue (77).

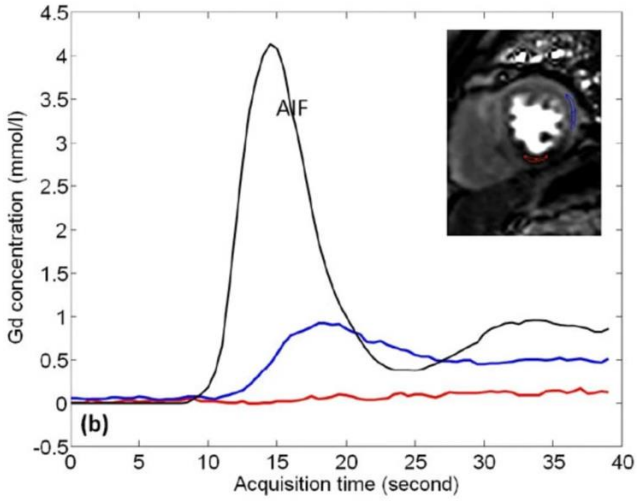

Figure 11. The arterial input function.
AIF curve is plotted in black, and Gd concentration curves of well-perfusion region of interest (ROI) in myocardium (blue) and poorly perfused (red) are shown, *Kellman et al* (77).

The Kellman perfusion sequence

Here follows a summary of the sequence and image reconstruction (77) (**Figure 12**):

1. Multi-slice saturation recovery imaging during a single bolus of Gd during free breathing
2. Low-resolution blood pool image with each heartbeat for the measurement of AIF
3. AIF imaging used a dual-echo FLASH sequence with T2* correction during the first pass
4. FLASH/SSFP for higher resolution myocardial imaging
5. Proton density weighted images required prior to contrast for correction of surface coil intensity correction and conversion to Gd concentration (mmol/L)
6. Motion-correction of both AIF and perfusion images
7. Automated AIF segmentation of LV blood pool signal
8. Surface coil intensity correction

9. Conversion to [Gd] from saturation recovery (SR) and proton density (PD) intensities using Bloch equation calculations including correction of T2* loss in AIF from dual echo signal
10. Calculation of pixel-wise MBF maps by deconvolution processing and display using a custom colourmap (77)

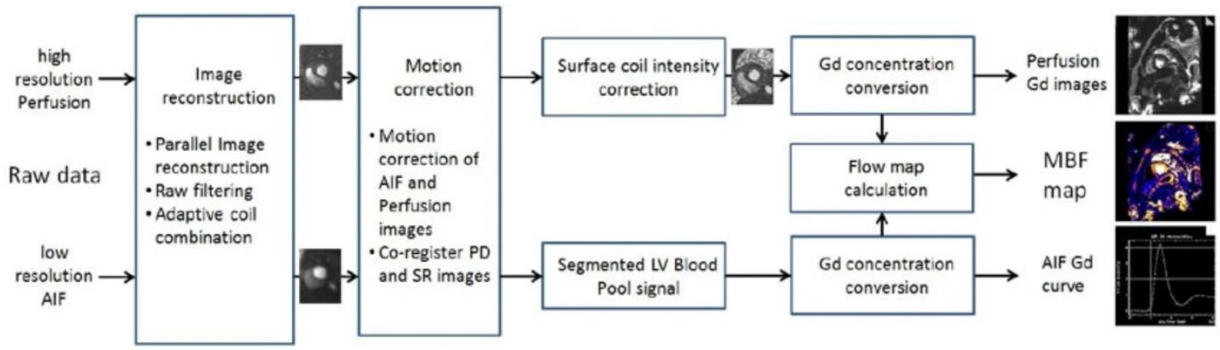

Figure 12. Flow-chart of quantitative perfusion workflow
In-line automated MBF maps from acquisition to reconstruction, *Kellman et al (77).*

1.7.5. Quantitative Perfusion mapping Repeatability

Brown et al has examined the repeatability of the perfusion sequence. Intra-study repeatability was tested by performing three stress perfusion sequences within the same study and on a separate visit, three stress perfusion sequences. Test:re-test repeatability was tested by comparing stress perfusion on different visits at least 7 days apart. Co-efficient of variation was low overall; 11% for stress MBF within studies and 12% between studies (test: re-test). Regional (segmental) repeatability was less robust (repeatability coefficient stress MBF 30-37%, and for MPR, RC 35-43%) (78).

1.7.6. Perfusion mapping findings in HCM

Initial evidence of perfusion impairment suggestive of ischaemia in HCM was shown in PET-CT studies. A reduction in MBF under vasodilator stress and focal reductions

in MBF defined as perfusion defects were found and those with impaired stress MBF had a higher risk of adverse events (79). Impaired perfusion also associates with adverse functional consequences with abnormal blood pressure response to exercise (itself an adverse prognostic indicator) (80).

Insights from tissue characterisation enabled by CMR shows impaired perfusion also associates with both hypertrophy, scar burden and scar progression (65,66). In macroscopically 'normal' segments (no LVH, no scar), perfusion is still impaired in HCM, and its presence can be detected in sarcomere mutation carriers without hypertrophy, with perfusion defects occurring in almost a third (25). This challenges assumptions that ischemia was secondary to hypertrophy and instead occurs early, before hypertrophy and perhaps even developmentally in the disease course.

Perfusion defects and impaired global perfusion have long been detected in overt HCM and hypothesised to relate to compressive forces of hypertrophied myocardium, outflow obstruction, elevated intracavity pressures and abnormal smooth muscle thickening of small vessel walls (59). Long term follow-up of patients with impaired global perfusion on PET showed increased progression to heart failure and sustained VT while regional defects relate to abnormal blood pressure response to exercise and apical aneurysm formation (79,82). The question of whether impaired perfusion results in ischaemia is supported by oxygen-sensitive cardiac MRI studies showing impaired tissue oxygenation which can also be detected in mutation carriers without hypertrophy (83). Alongside supply deficits, a higher energy cost of contraction in the setting of mutated sarcomeres with overt HCM was observed in a phosphorous magnetic resonance spectroscopy study (84). A paired DTI-quantitative perfusion study also showed regional association of DTI parameters and perfusion reserve ((52).

1.8. Missing pathophysiology in HCM: Arrhythmogenesis

SCD in HCM is caused by ventricular arrhythmia but our understanding of mechanisms behind this are poorly understood as we have relied on small invasive studies or *ex-vivo* studies alone (85–87). While the 12-lead ECG has been used to screen for HCM and shown to contain prognostic information in subclinical HCM (an abnormal ECG confers a fourfold increased risk of progression to overt disease) (88), its prognostic value in overt disease has been largely disappointing, potentially due to confounding with comorbidities, ethnicity and athleticism, but also due to variance in the definition of an 'abnormal ECG' (8). Indeed sensitivity is lost as LVH in HCM is very commonly associated with repolarization changes (T-wave inversion/ ST depression). An invasive EP study of 179 HCM patients found that those with fractionation induced through RV pacing had a higher positive predictive value for SCD or equivalent events than conventional risk markers. The study was based around the principle that conduction would be delayed around diseased and fibrotic tissue near their relative refractory period and blocked by areas of prolonged refractoriness resulting in delayed ventricular activation and subsequent fractionated electrogram signals (86). It is likely however that scar would play an important role in this signal, there was low positive predictive value (0.38 – even though this was better than a non-invasive risk strategy) and the invasive approach is not without risk (a few participants had VF induced by the procedure). This would suggest that non-invasive approaches to detect fractionation but also other EP markers that occur early would be desirable. Another invasive EP electroanatomic mapping study of nine overt HCM patients found prolonged stimulus-to-V times, prolonged endocardial action potentials, lowered septal voltages (the investigators postulated as a result of scarring) and fractionation. The lateral wall would often activate before the septum and action potential (AP)

prolongation was worse in the septum that the lateral wall (85). Invasive EP studies provide valuable insights into HCM myocardial electrophysiology but at the cellular and molecular level, mechanisms behind arrhythmia formation are less understood. A study of myectomy samples from 26 patients using patch-clamp methods showed prolonged AP duration and related this to increased late sodium and calcium currents, reduced repolarizing potassium currents, prolonged calcium transients, higher diastolic calcium and a higher prevalence of early and late after depolarizations (87). Other findings such as elevated QTc as a predictor of ICD discharge, QT dispersion and dynamic QT changes on Holter monitoring have been proposed as markers of repolarization abnormalities occurring in the disease but none have been especially successful limited by poor repeatability, technical limitations and a skew towards more advanced disease (89,90).

Pro-arrhythmic substrate is related to adverse cardiac structural change (hypertrophy, fibrosis, disarray, small vessel disease) and those with a sarcomere gene mutation (genotype positive left ventricular hypertrophy positive [G+LVH+] vs G-LVH+) have a higher incidence of SCD (7,91). Abnormalities in ventricular activation and repolarization could be the link between structural changes and SCD (85). In this domain, electrocardiographic imaging (ECGI) provides detailed non-invasive electrophysiological (EP) assessment in intact hearts under physiological conditions and may be more sensitive to early changes (subclinical disease) than structural assessment by macroscopic imaging, i.e. cardiovascular magnetic resonance (CMR) alone.

1.8.1. Techniques to investigate arrhythmogenesis in HCM - Electrocardiographic Imaging

While the presence of ECG abnormalities are established and prognostic in subclinical HCM, it is a binary entity and therefore limited in its ability for quantification and tracking response to novel therapy. In this domain, electrocardiographic imaging (ECGI) could be informative. Unlike the 12-lead ECG which measures the integrated electrical activity over the entire heart, ECGI computes individual unipolar epicardial electrograms for visualisation of the EP substrate; ECG imaging is a non-invasive method of spatiotemporal mapping of epicardial ventricular activation and repolarization and activation-recovery interval (a surrogate for action potential duration) (92). Early *ex-vivo* validation was performed using the Torso-Tank setup. This involved placing a perfused dog heart in a model of a Torso filled with electrolyte solution – 384 rods projected from the body surface to the heart. Signals measured at the torso provided the input for the inverse solution (see below) and signals measured at the epicardium (using an electrode sock containing 64 electrodes) were compared. Results showed that faithful simulation of ventricular activation from pacing and repolarization was achieved (93) (**Figure 13**). Further animal studies validated the technique in normal and abnormal canine hearts (94).

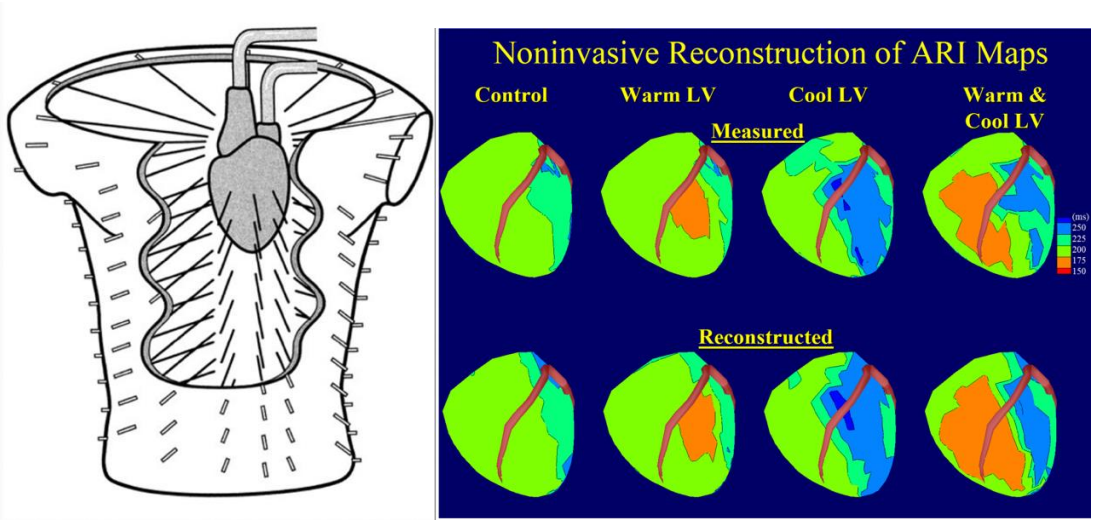

Figure 13. Torso-Tank experiment.
Left: A perfused dog heart is suspended in an electrolyte tank moulded in the shape of a torso – this includes 384 torso surface electrodes and 384 rods projecting radially from the torso surface toward the centre of the tank. Each rod had an electrode at its tip and multiple electrodes along its length within the torso volume, for a total of 918 electrodes. Measured potentials are obtained from an electrode sock wrapped on the epicardial surface and containing 64 electrodes **Right:** Computed vs measured activation-recovery intervals. Warming and cooling of the heart causes regional shortening and prolongation of activation recovery. Computed and measured ARI maps show good agreement, Oster et al (93)

1.8.2. The inverse solution of Electrocardiography

The method of computing epicardial potentials from body surface potentials is referred to as the inverse solution of electrocardiography. In summary, there are two major aspects. The first is the discretization of Laplace's equation ($\nabla^2\phi=0$ where where ∇^2 is the Laplacian (a differential operator) and ϕ represents the potential). Discretization is where the infinite points on the epicardial and body surface are converted to finite points so they can be computed. The method of discretization is Green's second theorem and boundary element method. This results in a matrix relationship which can be solved to obtain potential values from specific points or elements. As small errors in the body surface potential can result in large errors of the computed epicardial

potentials, a Tikhonov zero-order regularization is applied to stabilize the inverse solution (93).

1.8.3. Normal Human Activation and Repolarization measured by ECG Imaging

The advantage of ECGI to reconstruct epicardial activation from body surface potentials is primarily that it can be done non-invasively avoiding complications of invasive EP studies. It is also performed under physiological conditions (no anaesthesia/ other drugs) at rest or exercise and obtains panoramic maps of activation and repolarization. Normal ventricular conduction occurs from the AV node down the left and right bundle branches and from endo to epicardium through the Purkinje system. Epicardial breakthroughs are commonly first located in the RV paraseptal region, subsequently RV and LV breakthroughs and apex to base activation of the posterior LV. The latest activations occur at the LV base and RVOT (**Figure 14**). While this is the general pattern of activation, there are small interindividual differences in activation sequences. Repolarization is slower across the epicardium than activation and repolarization sequences are largely unaffected by the activation sequence supporting the hypothesis that this is dependent on local action potential duration (94).

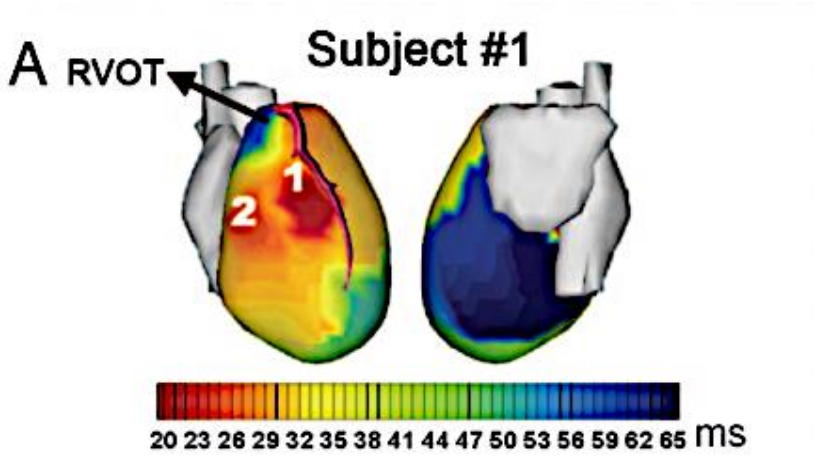

Figure 14. Normal ventricular activation.
Activation isochrones are shown with each colour representing regions of LV activating at the same time. Earliest activation – RV paraseptal region, latest activation, LV basal infero-lateral wall. *Ramanathan et al* (95)

1.8.4. ECG Imaging in disease

Primary Electrical Cardiac Disease

Mechanistic insights into primary electrical cardiac diseases such as Brugada syndrome and long QT syndrome could be obtained using the panoramic EP mapping approach provided by ECGI.

Brugada is an inherited sodium channelopathy resulting from *SCN5A* mutations in 40% and is characterised by an abnormal right bundle branch block appearance with ST elevation in V1 to V3, occurring either at rest or on pharmacological provocation. While previously considered a disease of structurally normal hearts, recent evidence showed subepicardial fibrosis overlying the RVOT. In this domain, ECGI showed multiple EP abnormalities that were visualized exclusively overlying the RVOT: ST elevation and T-wave inversion, prolonged activation and repolarization, low signal amplitude and fractionation. Findings were compared to participants with idiopathic right bundle branch block which showed entire RV delayed repolarization without other

abnormalities, demonstrating the ability of ECGI to differentiate between both. A parameter that is not obtainable by the 12-lead ECG is presence of spatial repolarization heterogeneity which provides a substrate for ventricular arrythmia. In long QT syndrome, an arrhythmogenic disorder causing syncope and SCD, prolonged repolarization and also steep changes in repolarization were observed which were worse in the symptomatic (92). The abnormality of steep repolarization gradients has been demonstrated to result in increased arrhythmogenicity in a preclinical study and also in VF survivors with structurally normal hearts (96).

Infarction

An intuitive application of electrocardiographic imaging is to ascertain the pro-arrhythmic potential of scar as it is a common downstream process in multiple disease states. Scar in the myocardium results in abnormal cellular electrophysiology and microstructure, especially in the border zones where viable tissue and fibrotic tissue are colocalized. In this domain, an ECGI study of 24 individuals following myocardial infarction showed that scar resulted in lower epicardial voltages, signal fractionation and late potentials with ECGI localising scar identified by LGE with high accuracy (97).

Arrhythmogenic Right Ventricular Cardiomyopathy

ARVC is caused by fibrofatty infiltration of the myocardium with epicardial predominance and is mostly caused by desmosomal mutations which are detectable in 30 to 40% and lead to progressive cardiomyocyte death. ECGI showed again slowed and spatially heterogenous ventricular conduction and prolonged repolarization, with abnormalities co-localizing with LGE detected scar (98). Spatially

heterogenous conduction is pro-arrhythmic due to forming asymmetric conduction fronts and supporting conditions for re-entry.

Amyloidosis

In cardiac amyloidosis, multiple EP abnormalities were detected by ECGI and were more severe in AL that ATTR amyloid, in parallel with clinical course. There were also associations between markers of disease severity (T1 & ECV) and epicardial signal amplitude, fractionation and repolarization times, showing that worsening storage was related to a worse EP phenotype.

HCM

There is a small ECGI study in overt HCM (n=10) which showed high activation dispersion, higher signal amplitude and greater voltage dispersion but integration with LVH and scar was not studied (99).

1.8.5. Comparison with invasive EP Mapping and the need for further work

Some effort has been spent on validating ECGI with invasive electroanatomic mapping and here ECGI shows only modest accuracy in measuring activation and repolarization times when using invasive EP mapping as ground truth (100). Furthermore, ECGI was tested against invasive EP mapping to ascertain whether it could be used to guide ablation therapy for VT, however again resolution for identifying the VT source was not sufficient, but it was found that ECGI could guide the segment of interest for invasive EP Mapping (100,101). Another study comparing ECGI activation mapping and contact mapping showed poor agreement and inaccurate visualization of breakthrough sites. The difficulties with the comparisons between invasive EP mapping and ECGI are that the co-registration of mapping from both

techniques are very susceptible to error, and often EP mapping uses bipolar electrodes whereas ECGI is unipolar (102). Taking this into account, further work is needed to ensure accuracy. Perhaps more encouragingly, ECGI has been used successfully clinically in humans to guide radiotherapy for refractory VT [published in NEJM] and for this application it is already emerging into clinical practice (103).

1.9. Clinical Challenges in HCM: Disease stratification

Whilst the 2014 ESC risk prediction tool is effective for identifying high risk patients, some external validation cohorts show it misses SCD in a proportion, suggesting more sensitive prediction is needed (104). Furthermore specificity is also key, with the ICD strategy resulting in disadvantages summarised by the 6 I's: implantation risk (pericardial effusion, tamponade), infection (4% lifelong), inappropriate discharge (1% per year), imperfection (device failure), insufficiency (tricuspid regurgitation), insurance risk – risk device never used – analogous to life insurance (105). A strive for improved accuracy is clearly needed – a knowledge gap where advanced imaging is primed to play an important role.

Current risk stratification involves the imaging quantification of hypertrophy (MWT) and is now supplemented by measures of focal fibrosis (LGE quantification) (74). The limitations to this approach are that risk predominantly occurs at the extremes of hypertrophy and scar burden, with scar only modestly predictive of adverse events and both occurring late in phenotype development (43). Furthermore, arbitrary cut-offs for LV MWT (15mm or 13mm if there is a family history) fails to acknowledge both the influence of body size, ethnicity and the spectrum of phenotypic expression occurring before hypertrophy. This leaves us unable to modify disease before patients

progress to experiencing symptoms, both obstructive and non-obstructive in nature, and events. Risk prediction is also limited in low-intermediate risk and does not predict important clinical complications such as heart failure and atrial fibrillation (31). Clearly biomarkers that more accurately reflect risk (SCD/ heart failure) are needed.

Disarray and microvascular disease have both been implicated in adverse events (29,47,55,79) and therefore it follows that integration of these histological HCM features might supplement current risk stratification. Furthermore, using quantitative imaging markers (quantitative perfusion/ diffusion tensor imaging) may add a more granular and personalised approach to risk as opposed to dichotomous markers.

1.10. Clinical Challenges in HCM: Genotype positive vs negative HCM

New insights into genotype-negative HCM support a polygenic inheritance with several distinct clinical features to genotype-positive HCM: lower incidence of adverse events paralleled by less scar on CMR, higher incidence of LV outflow tract obstruction and apical HCM, greater interaction with diastolic hypertension, obesity and diabetes, older age at presentation, lower mortality and a suggested lower risk to relatives of the proband (17,31)(91). Those with a sarcomeric mutation and overt disease (genotype positive [G+LVH+]) have more ventricular arrythmia events and a younger age at onset compared to genotype negative disease. G+LVH+ have also a stronger family history of HCM, SCD and greater MWT (109). Ventricular arrhythmia events are greater in incidence even after considering a younger age at onset.

Those with variants of uncertain significance (VUS) have an intermediate outcome between G+L VH+ and G-LVH+ suggesting that some of these mutations are indeed pathogenic. (91). The cause of a more deleterious impact of sarcomeric mutation on clinical course is incompletely understood but likely to involve the greater impact of

sarcomeric mutation on protein structure and function. It follows that some mutations would have a greater negative impact on this than others, and in this regard more wide-scale studies are needed (91). Large multi-centre observational studies have reported differences in morphology and tissue characterization with G+LVH+ characterised by less LVOTO, more reverse-septal curvature morphology, less apical HCM, more scar and higher ECV. Demographic differences were also described with G-LVH+ being older, more male and less White ethnicity (31). Genotype-positive HCM has also shown reduced MBF compared to genotype negative with more visual perfusion defects, but with semi-automated techniques (110). Human heart or animal tissue models show limited evidence that disarray is more prevalent in thin-filament mutations and large-scale studies of myectomy samples show a significantly higher prevalence and severity of disarray in those with sarcomeric mutations (29,47). Electrical consequences of the genetic substrate are limited, however it has been shown that lateral T-wave inversion is more prevalent in genotype negative (111).

The relationship between genotype positive vs negative HCM and its differing phenotype, clinical outcomes and prevalence of ventricular arrythmia is incompletely understood. Therefore an exploration of myocardial disarray, microvascular disease and deeper electrical phenotype may lead to further insights. In the emerging era of disease modifying therapy, differing clinical approaches may be required in genotype positive vs negative HCM. Therapeutic approaches may be aided by a more granular understanding of phenotypic differences.

1.11. Clinical Challenges in HCM: Subclinical HCM

Individuals with pathogenic/likely pathogenic sarcomere variants identified on cascade genetic screening are termed to have subclinical HCM. Possibly reflecting a hypercontracted microstructural state as found in overt disease, subclinical HCM display differences in left ventricular structure (lower end diastolic and end-systolic volumes and function (higher ejection fraction)(63,106). Some evidence of increased fibrosis has been shown through blood markers of increased collagen synthesis (33). Adult subclinical HCM also displays phenotypic expression that could be developmental in origin as opposed to related to contractile abnormalities– namely increased myocardial crypts, disarray and trabecular complexity, all of which likely result from abnormal embryological development (63,107)(62)(108). Pathological ECG findings are seen in a third of subclinical HCM and signify a fourfold risk of progression to overt disease (88). Case series autopsy reports have also described young SCD victims displaying significant disarray in the absence of hypertrophy (62). The current models of care for those with subclinical HCM involve surveillance imaging which is inefficient and leads to uncertainty. More accurate biomarkers are needed to facilitate early discharge, more intensive monitoring in those particularly at risk, and earlier initiation of disease modifying therapy. Therefore understanding phenotype development is highly important, as simply knowing the genetic variant is insufficient due to highly variable expressivity.

The structural changes occurring in subclinical HCM have been well-studied though imaging. Elongated anterior and posterior mitral valve leaflets have been described in overt HCM and anterior mitral valve leaflet (AMVL) elongation in subclinical HCM (106). The absence of AMVL elongation in foetal MYBPC3 knock-out mice have led to the hypothesis that elongation is a response to mechanical stretch as opposed to an abnormality in embryogenesis (63). The combination of AMVL elongation and

systolic anterior motion (SAM) of the mitral valve leaflets worsens LVOTO and mitral regurgitation, and therefore both are important to characterize early and accurately. 2D tracking of the mitral valve apparatus using cine CMR post processing has shown abnormal motion of the entire apparatus as opposed to just the AMVL and also AMVL SAM occurs in subclinical HCM in the absence of LVH. Interestingly, prior theories that SAM was due to the Venturi effect of flow acceleration and turbulence at the LVOT have been contested by those showing drag forces and also MVLs may be pushed anteriorly by posterior vortices created by late diastolic inflow could be the predominant causes of SAM. This suggests that further work is needed on the aetiology and monitoring of AMVL abnormalities and SAM considering the significant adverse effects of obstruction (109).

While CMR has the ability to detect structural and functional early expression of sarcomere variants, more thought-provoking is its ability to interrogate tissue in this cohort; scar is uncommon in subclinical HCM and therefore less useful but recent advances have allowed characterization of tissue perfusion and oxygenation. Karamitsos et al showed impaired oxygenation during vasodilator stress which was further reaffirmed by work from the same group using more advanced blood-oxygen techniques. The investigators proposed this to be evidence of an early higher energy-cost of myocardial contraction which is supported by findings of impaired strain and mechanics (68,83). Fully-automated quantitative perfusion has permitted more accurate quantification of myocardial perfusion and has shown impairment of myocardial perfusion and the presence of visual perfusion defects. Taken together there are likely interrelationships between impaired blood oxygenation, perfusion and also inefficient hypercontractile myocardium (81).

1.12. Future Outlook

The first-in-class myosin inhibitor mavacamten suppressed cardiomyocyte disarray in pre-hypertrophic murine models and not in mice with overt hypertrophy (110). With a greater detection and understanding of pathological changes underlying HCM, now detectable at the very earliest manifestations of phenotype expression, it may be possible to monitor effects of novel drugs and target therapies that do not depend on the one-dimensional measurement of hypertrophy alone. Myosin inhibitors are likely to herald an era of disease modification although direct comparison with septal reduction therapy is needed. Examining changes in advanced imaging parameters in patients receiving myosin inhibitors would further support evidence of genuine myocardial pathophysiological modification as opposed to solely improvement resulting from relief of mechanical obstruction. These findings may also help identify individuals that are more likely to respond to myosin inhibitors as well as higher risk subclinical HCM. A further understanding of the processes which are reversible and in what order will help elucidate the relationship among myocyte disarray, fibrosis, increased thickness, and microvascular health.

In subclinical HCM, conferring an increased risk of progression to overt disease are higher ejection fraction, lower E' velocity, higher NT-proBNP, longer posterior mitral leaflets, ECG abnormalities and male sex (106). TNNI3 mutations have been found to have a lower risk of penetrance compared to MYBPC3 (6). However limitations are that the majority of these markers are subject to significant measurement variability, confounding with comorbidity, ethnicity and athleticism, and a dependence on serial follow-up. Advanced imaging in this regard is primed to increase accuracy on how this population is stratified. Before larger longitudinal studies employing these techniques

are carried out, first the abnormalities need to be accurately defined, quantified and related to current conventional markers (genotype, scar, ECG abnormalities) which will be a primary goal of this PhD. As novel sarcomere modulators provide promise for disease modification, early markers of disease are a rapidly emerging research priority (11). Analyzing the effect of sarcomeric mutation on microstructural, microvascular and EP phenotype development will enhance our ability for precision medicine in future (29,55,91).

CHAPTER 2 - HYPOTHESES

1) Microvascular changes detected by quantitative perfusion will differ between physiological hypertrophy (athletes) and pathological hypertrophy (caused by excessive afterload in hypertension)

2) Microstructural and microvascular changes can be detected by DTI and quantitative perfusion and will occur in the absence hypertrophy in subclinical HCM, and in overt disease relate to genotype (G+ vs G-LVH+).

3) Electrophysiological abnormalities can be detected by ECGI and will identify EP abnormalities in subclinical HCM. In overt disease abnormalities will differ with genotype (G+ vs G-LVH+) and associate with adverse structural change.

CHAPTER 3 - METHODS i: TECHNICAL DEVELOPMENT STATEMENT

In order to deliver the following prospective observational studies, we needed to advance existing imaging technology to be optimized to the cohorts under investigation and to be deployed in local academic infrastructure, particularly the scanners at Bloomsbury Centre for Clinical Phenotyping and Barts Heart Centre.

Captur ECGI vest [Patent No. US 18/194 235]

I co-invented the capturECGI vest with my supervisor Dr Gabriella Captur. The two components of data required for ECGI are the recording of body surface electrocardiograms (commonly 128-256 electrograms) from the torso, and heart-torso geometry obtained from imaging. The imaging modality typically used has been computed tomography (CT), which lacks the same abilities for most tissue characterization obtainable from cardiac MRI. Prior to this PhD there were no re-usable and cost-effective technology available for combining ECGI with CMR, and therefore the research community was unable to explore this further.

Two predominant commercially available ECGI vests are produced by Medtronic (Cardioinsight ^{TM}) and Bio-Semi ECGI. Medtronic vests are high cost (£1700 per vest/per person) and single-use. The Bio-Semi solution required fiducial markers consisting of cod-liver oil, with 256 of these individually applied and overall 2.5 hours of preparation time. These markers may sporadically burst and cause discomfort to the patient.

The capturECGI vest is full re-useable and high-throughput, requiring only 10 minutes pre-CMR and 5 minutes of acquisition within the scanner bore. A patent was granted for the vest design – particularly the embedding of the electrodes into the vest, and a

“mirror-vest” which can be kept on the participant once the recording vest is used to allow near-perfect co-registration of fiducial markers and electrodes. It is fully washable after each use and can last for up to >200 recordings.

Academic Outputs

Grants: The ECGI vest was developed from Dr Captur’s special project grant from the BHF (~£500K, SP/20/2/34841). It is also being used to investigate EP changes occurring with DCM and its relation to midwall fibrosis (BHF CRTF).

Publications:

Webber M…**Joy G**…Captur G. Study protocol: MyoFit46-the cardiac sub-study of the MRC National Survey of Health and Development. BMC Cardiovasc Disord. 2022 Apr 1;22(1):140.

Here, the technology is used to characterize EP changes occurring with ageing in a birth cohort (recruited 1946) (112,113). This cohort has had longitudinal data on exposures, risk factors and multimorbidity and this substudy (Myofit46) aims to use cardiac MRI and ECGI better understand the burden of clinical and subclinical cardiovascular disease.

Webber, M., Joy, G., Bennett, J. *et al.* Technical development and feasibility of a reusable vest to integrate cardiovascular magnetic resonance with electrocardiographic imaging. *J Cardiovasc Magn Reson* **25**, 73 (2023).

This study establishes the high repeatability (low test:re-test, inter/intra-observer variability) of our pipeline including the capturECGI vest and also demonstrates some EP changes occurring with the ageing cohort: prolonged repolarization times and steeper activation and repolarization gradients. This publication lays the foundation

for the expanded use of our technique. I had recruited and scanned the healthy volunteers for this study.

Media: Following publication of the prior paper, the DailyMail covered the technique as a potential in future to identify those at risk of SCD, particularly for athletic screening.

Mail Online

After a football collapses on the pitch, scientists unveil a vest that maps the electrical activity of the heart with the potential to save thousands of lives

https://www.dailymail.co.uk/news/article-12875315/Scientists-vest-maps-electrical-activity-heart-save-thousands-lives.html

Media Coverage: Top – extract from Daily Mail article.
Bottom. UCL News coverage. ECGI + Myofit Team: Myself (far left), Middle: Dr Gaby Captur, Dr Michele Orini, Prof. Lambiase

Diffusion Tensor Imaging – Local deployment

While the DTI sequence and post-processing techniques have been established, local deployment was performed in-house at Bloomsbury Centre for Clinical Phenotyping, UCL. This involved forming a consortium with University of Leeds (Erica Dall'Armellina, Jurgen Schneider, Irvin Teh) and Cleveland Clinic (Christopher Nguyen). Phantom calibration was performed by Dr Iain Pierce, Physicist at UCL and collaborator. This involved a temperature-controlled water phantom to cross-check Apparent Diffusion Coefficient (ADC) with that obtained in University of Leeds scanners using the same sequence. Acquisition techniques, initial images and trouble shooting were discussed at two-weekly meetings with Leeds. The acquisition techniques described in the Methods chapter are a result of several weeks of optimisation and trouble-shooting with the consortium. The standard operating procedure (SOP) developed has been used to guide DTI work on a parallel project in DCM (PI Dr Gaby Captur).

Quantitative Perfusion – Local deployment

Initial PhD work was performed on athletes and hypertensives (Chapter 4). The protocol was identical to a clinical workstream, however initial experience with athletes showed that this cohort required a higher adenosine dose to achieve physiological stress. Two cannulas were used to avoid heart block during the contrast infusion (current practice is often one cannula and a Y-connector). This informed the protocol for HCM where careful attention was paid to adenosine dosing. The threshold to increase the dose was changed when commencing work on HCM (from 10bpm HR increase or symptoms to 15bpm HR increase and symptoms). This protected against

under-stressing patients, especially with overt HCM whom were on medication that may alter adenosine effects.

CHAPTER 3 – METHODS ii

3.1. Study Design

3.1.1. Recruitment

In order to understand phenotype development in subclinical HCM (G+LVH-) and the differing response of myocardial microstructure, microvasculature and electrophysiological (EP) substrate to sarcomeric mutation in overt disease (G+LVH+ vs G-LVH+), we needed to recruit sufficiently powered cohorts according to the sample size calculations below. We therefore recruited prospectively from genetics databases at cardiomyopathy clinics in Barts Heart Centre, St George's University Hospital and Royal Free London. Athletes were recruited de-novo from triathlon/cycling clubs. Hypertensives were recruited from hypertension clinics at Barts Heart Centre.

3.1.2. Academic Consortium

For deployment of advanced imaging techniques, we formed an academic consortium consisting of six centres**:** **DTI**: Leeds University, UK; Cleveland Clinic, USA, **Perfusion Mapping**: National Institutes of Health, USA; Barts Heart Centre, UK, **ECG Imaging:** Prof Rudy Lab, Washington University in St Louis, USA; University College London, UK, **Digital 12-lead ECG analysis**: University of Glasgow, UK

3.2. Sample size calculation

ECGI data and micro-structural/vascular changes have not been compared between patients with subclinical HCM and healthy volunteers so we referred to ECGI work on another cardiomyopathy (arrhythmogenic right ventricular cardiomyopathy, ARVC) to derive plausible estimates for effect size (Andrews et al (98)). This study of 20 genotyped ARVC patients vs. 20 controls found a significant difference in activation-recovery intervals (ARI) with an effect size of 0.69 (cohens D). Based on this effect

size we have therefore estimated with 80% power (alpha 0.05) that we would require 63 subclinical HCM (G+LVH-) and 28 (controls) using the Z-statistic and non-centrality parameter. To permit for redundancy (incompletely analysable data (ECGI/DTI/quantitative perfusion)) we have calculated sample sizes of 75 G+LVH and 30 controls. Our secondary analysis was explorative and sought differences in EP and microstructural abnormalities between genotype positive and genotype negative LVH+ HCM. Using equal sample sizes between this group and the same effect size, 35 would be required in each group. We targeted a sample size of 50 in each group to permit for redundancy. The athlete and hypertensive cohorts were exploratory and therefore sample size calculations were not performed.

3.3. Ethical Approval

The study formed a sub-study of "Extended spectrum of apical hypertrophic cardiomyopathy (IRAS 227168)' which contained an identical protocol in terms of investigations. Furthermore, I had applied for a substantial amendment to include the recruitment of individuals with subclinical HCM, healthy volunteers and the use of electrocardiographic imaging and diffusion tensor imaging, which was successfully granted.

3.4. Study Populations

Athlete and Hypertensive cohorts

Only male participants were studied as male athletes tend to mount greater hypertrophic responses to exercise **(64)**. Athletes were defined as adults participating in >10 hours of exercise weekly and in competitions. They had no history of cardiovascular disease and no contraindications to adenosine perfusion CMR. Recruitment was from triathlon and cycling clubs.

Hypertension were defined as individuals undergoing treatment for hypertension defined as clinic BP>140/90mmHg or ambulatory/home BP monitoring >135/85mmHg. To reduce confounding and risk of coronary disease patients with hypertension were excluded if they were current smokers or had diabetes [hyperlipidaemia and FHx of coronary disease was permitted for feasibility].

Healthy volunteers were age matched to athletes and were recruited under the same ethics protocol and did not participate in athleticism, had no cardiovascular risk factors and no contraindications to adenosine perfusion CMR. As athletes required higher adenosine dosing to achieve the same stress response to adenosine (see below), an exploratory cohort of 11 unmatched male healthy volunteers from a prior observational study undergoing high dose adenosine stress were included in a multiple regression analysis (114).

HCM cohorts

We recruited 104 patients with overt HCM (51 G+LVH+ vs 53 G-LVH+), 77 individuals with pathogenic/ likely pathogenic sarcomeric variants without hypertrophy (subclinical HCM// G+LVH-) and 28 healthy volunteers from 3 tertiary referral centres where phenocopies are routinely screened (Barts Heart Centre, St Georges University London and Royal Free London). Pathogenicity was assessed using the American College of Medical Genetics criteria (115). We had screened genetics databases and clinic lists for recruitment for the below inclusion/exclusion criteria. Participant recruitment then involved a phone conversation for pre-consenting and ensuring safety to undergo the protocol (particularly no contraindications to adenosine stress perfusion CMR) with further consenting prior to participation on the day of protocolling the patient.

Inclusion Criteria

- Overt HCM – defined according to ESC & AHA guidelines: increased LV wall thickness that is not solely explained by loading conditions (MWT ≥15mm in any cardiac segment by any imaging modality or MWT ≥13mm if positive family history of HCM) (7,74)
- Subclinical HCM – individuals with a pathogenic/likely pathogenic sarcomeric variants without hypertrophy (MWT ≥13mm) defined as above and identified on cascade screening.
- Healthy volunteers – adults without a known history of cardiac disease or risk-factors and with no contraindications to stress perfusion CMR

Exclusion Criteria

- To optimise imaging conditions (particularly due to artefact on DTI CMR), and reduce risk of confounding causes of LVH, participants with BMI>30kg/m^2 were excluded.
- Poorly controlled hypertension (suboptimal control despite 2 antihypertensives)
- Persistent atrial fibrillation
- High ectopic burden
- Significant valvular disease
- Implantable devices
- Known coronary disease or significant pre-test probability for coronary disease without prior coronary imaging
- Contraindications to adenosine
- Pulmonary hypertension
- Prior alcohol septal ablation or myectomy

- Prior cardiovascular surgery
- Claustrophobia
- Unwilling to consent

3.5. Clinical Variables

Clinical notes were used to record clinical variables including family history of sudden cardiac death, drug history and previous unexplained syncope. Non-sustained VT was defined as 3 beats ≥120bpm occurring on Holter monitoring. LVOTO was defined as peak left ventricular outflow tract gradient ≥30mmHg at rest, provoked or on exercise. The European Society of Cardiology HCM risk calculator was used for every patient for SCD risk scores (116).

3.6. Digital 12-Lead ECG

12-lead ECG was acquired at rest using the Beneheart R3, (Mindray, China) and recordings were sent to University of Glasgow Core-Lab for automated analysis of electrical intervals (PR, QRS, QTc), QT dispersion, amplitudes and the presence of ECG abnormalities (117,118). ECG abnormalities known to be relevant to disease progression in HCM were defined as: abnormal Q-waves (≥2 contiguous leads and with minimum amplitude 0.3mV or ≥25% of the subsequent R wave, or duration >40ms); LVH criteria: Sokolow-Lyon or Cornell criteria and repolarisation abnormalities (T-wave inversion in ≥0.1mV in ≥2 contiguous leads and/or ST-depression ≥0.1mV in ≥2 contiguous leads) (88) (119)

3.7. Conventional CMR Acquisition

HCM and corresponding HV scans were performed on a single 3 Tesla scanner (Siemens Prisma equipped with Gadgetron running on a local external server) at

Chenies Mews Imaging Centre, QS Enterprises. Athletes, hypertensives and their corresponding HV scans were performed on 1.5 Tesla scanners at Barts Heart Centre and Chenies Mews Imaging Centre. Imaging acquired: standard anatomical transaxial dark blood (HASTE) stack, balanced steady state free precession (bSSFP) cine imaging: three long axes and a short axis stack (11-14 slices), 3 short axis pre- & post-contrast T1 mapping (Modified Look Locker Inversion with same-day haematocrit for ECV). 4 long axes and a short axis stack (11-13 slices) of averaged, motion-corrected, bright blood single shot bSSFP late gadolinium enhancement (LGE) imaging were also acquired post-contrast.

3.8. Conventional CMR Analysis

3.8.1. Cine CMR Acquisition and Analysis for LV volumes and wall thickness

Cine acquisition (2 chamber (2ch), 3ch, 4ch and a short axis (SAX) stack (commonly 11-13slices)) were standard using bSSFP. An automated AI algorithm for cine imaging developed by Davies et al (co-author (120)) was used for obtaining LV volumes and maximum wall thickness with trabeculations and papillary muscle included in blood pool (smooth contours) (24,25). The AI algorithm was deployed offline following cine acquisition. The algorithm employed 4 convolutional neural networks (2-chamber, 4-chamber, short-axis stack – endocardial and epicardial borders) and a U-net architecture. Initial training was performed on 1923 scans for several institutions and diseases and shown to have superior precision to expert human segmentation (scan re-scan co-efficient of variation for (LVEF human: 6% vs AI: 4.2%) (120). The algorithm was then tested in HCM for maximum wall thickness measurement (MWT) and was found to exceed test-retest precision (AI: 4.3% vs experts: 5.7-12.1%) (121). The higher precision afforded by the algorithm was therefore highly advantageous due to the ability to detect LVH with greater confidence,

provide between group comparisons (particularly G+LVH+ vs G-LVH+), and correlate DTI findings in particular to LVH (where DTI might be confounded by expanded intracellular volume).

3.8.2. Late Gadolinium Enhancement Quantification

We acquired LGE imaging 5 minutes after administration of gadolinium based contrast agent, Gadoterate meglumine (Dotarem, Guerbet, S.A. France). This was administered in two split boluses at time of stress and rest perfusion. The total dose was 0.1mmol/kg and each 0.05mmol/kg bolus was given through a power injector at a rate of 4ml/s followed by a 25ml saline bolus. The sequence used averaged motion-corrected bright blood single shot bSSFP. Further acquisitions were occasionally required when there was artefact or ambiguous/subendocardial LGE raising the possibility of prior infarction. In these circumstances, changing the phase encoding direction, acquiring cross-cut images and dark-blood LGE images were also used.

In terms of post-processing, the extent of late gadolinium enhancement and scar burden was an important measure in HCM, due to its direct influence on DTI parameters, its pro-arrhythmic potential thereby influencing ECGI measures and prior evidence suggesting LGE differs between G+LVH+ vs G-LVH+ (31). Commonly used techniques include thresholding signal intensity using a reference region of interest (ROI) with LGE defined as pixels with 2,3,4, 5 or 6 standard deviations above the mean intensity of that ROI. Alternatively the full-width half max. technique uses half the max. signal intensity of the LGE as the threshold with some suggestion that this may be the most reproducible (122). With significant variance in measurement techniques, integration with diffusion tensor imaging was successfully conducted by Ariga et al using the 5SD approach (55) and therefore was ultimately adopted. This involved

semi-automated segmentation of endocardial and epicardial borders of the SAX LGE stack using circle CVI software (version 5.14, Calgary, Canada) and applying the 5SD approach using the most appropriate (normal) reference ROI. Regions with erroneously included pixels (commonly LV outflow tract at the most basal slice) and any segments containing signal noise were excluded. Regions of LGE were totalled and expressed in grams. For the athlete/hypertensive cohorts, LGE was qualitatively assessed for significant LGE (non RV-insertion point).

3.8.3. Parametric Mapping

HCM: Modified look-locker inversion recovery 5(3s)3 was used for T1 acquisition. 3 short axis slices pre- and post-contrast for extra-cellular volume (ECV) were acquired according to recommendations from the T1 mapping consensus for diseases with diffuse fibrosis (123). Error maps were used for to detect off-resonance and poor motion correction (MOCO) and were reviewed for every slice and MOCO was checked by reviewing each T1 acquisition. Frequency offset was occasionally required for frequency-artefact (occurring more commonly in 3T). Any segment/image containing artefact or poor MOCO were discarded. Same-day haematocrit (Hct) was also sampled and measured for ECV. Semi-automated contour detection of endo- and epicardial borders with manual adjustment where required were performed using the software to apply the formula ($ECV = 1 - Hct*(\Delta R1_{myocardium}/\Delta R1_{blood})$ where $\Delta R1_{myocardium} = 1/\Delta (T1_{myocardium}$ pre - post-contrast) and $\Delta R1_{blood} = 1/\Delta (T1_{blood}$ pre -post contrast) for ECV. Septal measurements were preferred in line with consensus guidelines due to the relative resistance to susceptibility from lung, liver and veins and less off-resonance (123). Septal ECV was used for primary endpoints and regression analyses and referred to as ECV.

Athletes & Hypertensives: Due to less heterogenous myocardium in these cohorts a single septal ROI was used in the 4chamber for ECV.

3.8.4. Quantitative Perfusion

Fully-automated quantitative vasodilator stress perfusion was performed using a validated dual sequence approach (77,124). In brief, adenosine was given intravenously at 140-210mcg/kg/min for a minimum of 4 minutes. A test-image was used for identification of artefacts, particularly frequency artefacts. Images were planned for co-registration to DTI and parametric mapping as far as possible. Physiological stress response to adenosine was carefully considered due to variable responses in the athlete cohort (see below). Prior work assessed the non-invasive indicators of adenosine stress and found that HR response >15bpm had area under receiver operator curve of 0.87 for a genuine stress response (gold standard – invasive coronary angiography vasodilator testing - this was superior to splenic switch-off 0.62) and therefore this heart rate (HR) cut-off including convincing symptoms of adenosine stress was used for final dosing of the adenosine infusion (125). Rarely, two concatenations were required when HR increased above 100bpm to avoid mis-triggering. Gadolinium-based contrast (Dotarem, Gadoteric Acid, Guerbet, UK) was then administered intravenously at 0.05mmol/kg. Due to the higher adenosine dosage frequently used, a gap of 7 minutes from the first gadolinium injection was used as a minimum prior to rest perfusion to ensure no residual pharmacodynamic adenosine effects. All automated segmentation were reviewed for errors. No manual post-processing was required, and quantitative MBF values were extracted directly from Digital Imaging and Communication in Medicine (DICOM) files. Automated in-line adenosine stress perfusion maps were acquired to obtain stress and rest myocardial blood flow (MBF, ml/g/min), and myocardial perfusion reserve (MPR - ratio of stress

and rest MBF), and visual perfusion defects (defined according to clinically recommended Task-force criteria (126)) assessed separately by two experienced operators (GJ & JM) from conventional images and perfusion maps.

3.8.5. Diffusion Tensor Imaging

A second order motion compensated single shot spin-echo echo-planar imaging DTI sequence was performed for 3 short axis slices at peak systole using previously described protocols (**Figure 15a)** (52). This was acquired free-breathing without respiratory navigation and has been validated both *ex-vivo, in-vivo* and shown to detect microstructural changes in HCM (83 ,121). Acquisition parameters are as follows: TE/TR 77 ms/3 RR intervals, field of view 320x121 mm^2, matrix size 138x52, in-plane resolution 2.3 x 2.3 mm^2, 8mm slice thickness, 8mm inter-slice gap, and partial Fourier= 7/8. Scout diffusion-weighted (DW) data were acquired with diffusion-weighting applied in three orthogonal directions to ensure data quality. Each full data set comprised b-values of 100 s/mm^2 (3 DW directions, 12 repetitions), and 450 s/mm^2 (30 DW directions, 6 repetitions). Cine imaging was used to define the time from R peak to maximum systole. The trigger delay was set at 30% of maximum systole.

Acquisition of DTI was technically challenging due to susceptibility artefact (commonly from lung in the inferolateral wall) **(Figure 15b)**, ghosting artefact (caused by signal instability between cardiac cycles due to cardiac motion) and wrap artefact due to the limited FOV employed. Efforts to reduce frequent susceptibility artefact include a tight shim around the LV and for other artefacts including wrap, 30 degree rotations were acquired around the SAX slice. This resulted in the use of 6-10 test scans (3 diff directions, 2 Weights, 1 Average) with adjustments of 30ms in trigger delay if any signal drop-out during MOCO. Once optimal test-acquisition was acquired the patient

was counselled prior to a long acquisition which was 10-minutes, free beathing. To reduce susceptibility artefacts further, patients were asked to have a small meal prior to the scan to avoid field inhomogeneity from an empty/full stomach.

Average magnitude images were generated from registered data by averaging cross repetitions and diffusion tensors were calculated. Contouring was performed onto cDTI maps with tensor eigenvalues, MD, FA and absolute |E2A| obtained globally and segmentally. Segments containing artefacts were omitted from analysis (12,13). Overall 18% of segments were discarded – these were predominantly from the inferolateral wall.

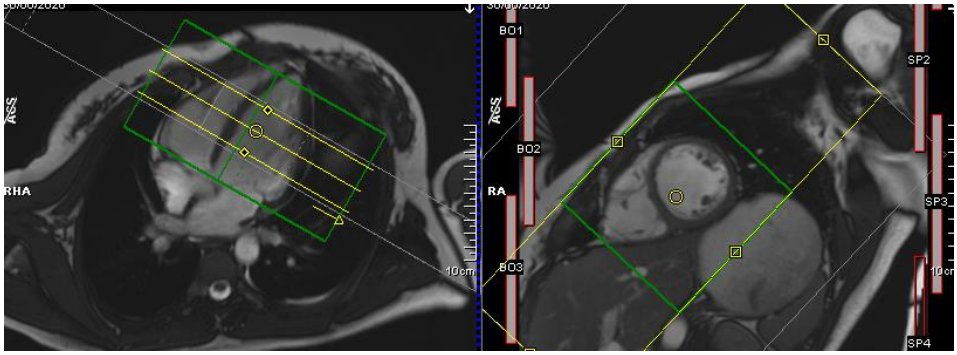

Figure 15a. DTI planning.
Three short axis slices are acquired in the same base to apex plane as perfusion and T1 mapping. Rotations around the mid-SAX slice are employed for optimal avoidance of artefact. A tight-shim was attempted to reduce susceptibility artefact.

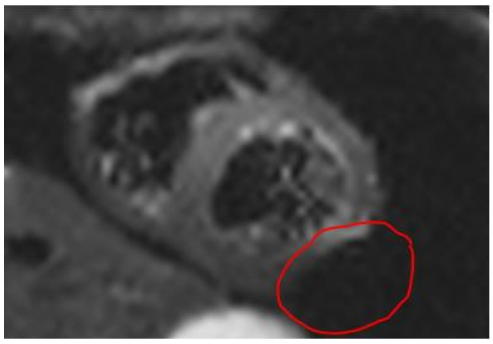

Figure 15b. Exemplar of susceptibility artefact in the basal inferolateral wall

3.8.6. DTI repeatability testing

Inter-observer variability in post-processing techniques for the same sequence has been tested by Das et al post STEMI showing good agreement in all parameters (**Figure 16a**) (51). Further local test:re-test acquisitions have been performed on 5 participants showing demonstrating good repeatability of the sequence (**Figure 16b**).

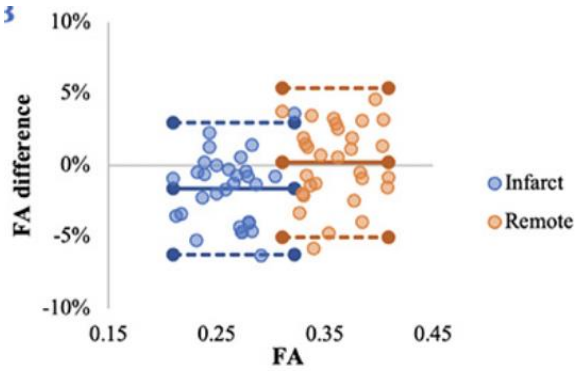

	Bias	Limits of agreement	
		Upper	Lower
Infarct	-0.02	0.030	-0.063
Remote	<0.01	0.054	-0.051

Figure 16a. Bland-Altman plot for inter-observer variability of infarct and remote segments for fractional anisotropy demonstrating good repeatability for both
Das et al (51)

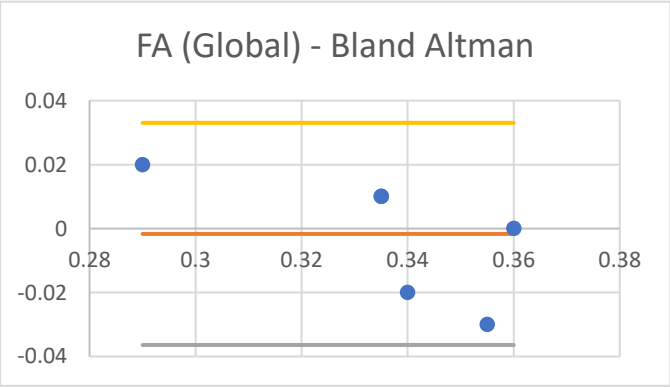

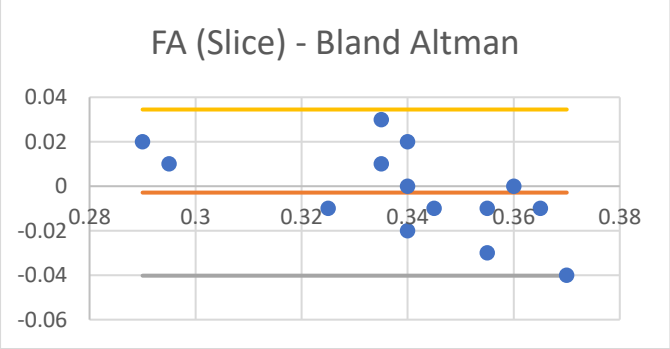

Figure 16b. Bland Altman for test:re-test acquisitions.

5 participants (3 healthy volunteers, 2 subclinical HCM), Fractional anisotropy: above – global FA agreement, below slice FA agreement (1 apical slice discarded due to artefact). Overall good agreement between test-retest

3.9. Electrocardiographic Imaging

3.9.1. The ECGI vest

In collaboration with Dr Gaby Captur, we co-invented the capturECGI vest – a re-useable washable vest for collecting ECGI body-surface potentials [patent approved Application No. US 18/194 235] (**Figure 17a**). This contains 256 uniformly distributed electrodes (128 electrodes front and back) that are sewed into a fabric with a single ground lead attached to the patient's right shoulder via a sticker. Velcro strapping allows optimal apposition onto the participants torso and through experience with healthy volunteers, sufficient tightness is required for good quality signals. Signals were measured from leads connected to a g.Hlamp (gtec, Austria). This a high-performance biosignal amplifier (FDA cleared, CE approved) which can also be utilised for brain electro-encephalography/ electro-myography. The high-resolution signals (2400 Hz – high pass filtered, acquired for 5 minutes) are processed by g-tec software.

Figure 17a. capturECGI vest (patent approved - US 18/194 235)

Webber et al (112)

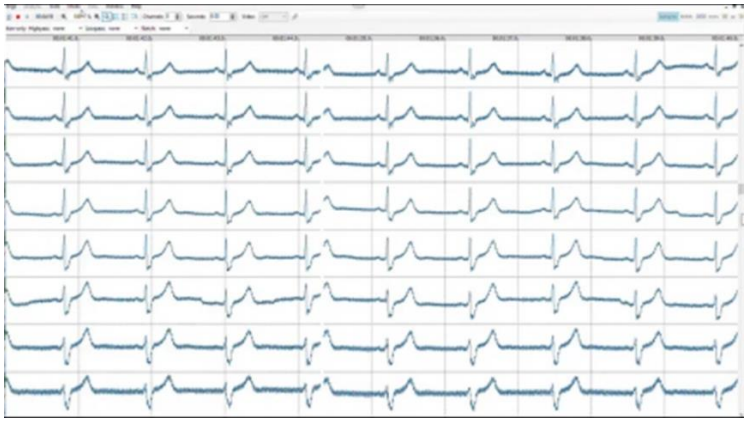

Figure 17b. Signals from the vest are checked for noise at the point of acquisition.

Signals are checked for noise and signal-loss (**Figure 17b**). If this was encountered, we occasionally would reapply the vest from scratch. After successful donning, markers were placed on the 8 corners of the vest using washable ink on the participants skin, which were used when replacing the ECGI vest with the 'mirror vest' containing 256 fiducial markers that were imaging opaque to allow segmentation of the electrode positions during post-processing. Co-registration of electrodes and fiducial markers were important due to the theoretical risk of small variations in electrode positions resulting in large differences in computed UEGs (93). However test: re-test repeatability was strong despite this theoretical risk (112). Due to the high sensitivity of the amplifier to electrical noise, all electronic equipment including the laptop charger the amplifier was connected to was removed from the room. The operator stood outside the recording room to minimise interference, and the participant was asked to breathe gently and stay stationary for the 5 minutes. Due to the position and number of electrodes on the vest, occasionally high-quality recordings were not possible with very low-BMI individuals (overall 7 recordings unusable).

3.9.2. Signal Pre-processing

Prior to the inverse solution computation performed by Prof. Rudy lab, raw signals acquired from participants (body-surface potentials) needed to be pre-processed using custom-built MATLAB software. This involved removing poor-quality beats and annotating the QRS, T wave and R-R interval. The software automatedly averages the signals and excludes low-quality channels (of 256 channels) (**Figure 18**). A loss of 56 cannels were permitted for the inverse-solution.

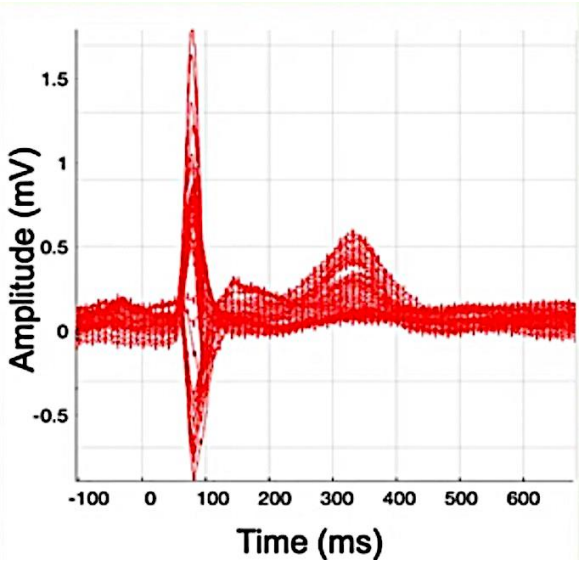

Figure 18. Signal averaging and quality control from 256 leads.
Signals are checked for correlation, signal to noise ratio, and number of useable channels. Low quality signals are excluded, Webber et al (113)

3.9.3. Anatomical & fiducial marker imaging

Acquisition of heart-torso geometry

A 110 thin-slice (4mm) dark-blood HASTE anatomical stack was acquired (5 minutes free-breathing) for heart-torso geometry whilst the participant was wearing the mirror vest within the scanner bore. This was removed after the anatomical stack (participant had to lean forwards slightly to remove medical tape used to attach the mirror vest whilst not losing localization within the scanner). This permitted further DTI acquisition

without artefact appearing from the ECGI dots and improved participant comfort within the bore.

Heart-Torso segmentation

The anatomical stack was used for heart-torso segmentation through the use of Amira-Avizo software. Imaging was performed immediately after donning the 'mirror-vest'. Fiducial markers appearing on the torso were manually annotated and the epicardial heart surface from the aortic root to the LV apex was also segmented (**Figure 19**).

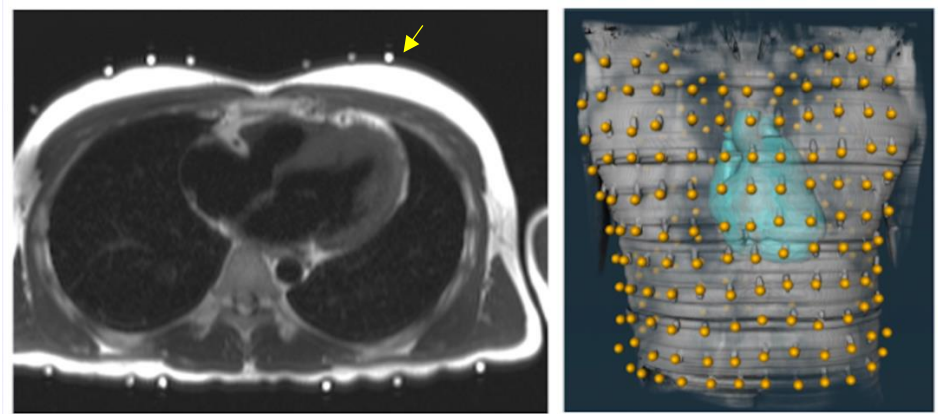

Figure 19. Heart-Torso acquisition & post-processing.
Left – 110 thin slice anatomical stack with patient wearing 'mirror-vest' containing fiducial markers (yellow arrow). **Right** – heart torso geometry segmentation with annotation of fiducial markers (yellow dots)

3.9.4. Post- inverse solution

Epicardial maps containing 1000 computed unipolar electrograms (UEGS) were generated from Prof. Rudy Lab. Each UEG was automatedly annotated for activation-defined as the steepest point of QRS signal downslope and repolarization time - defined as the steepest point of the T-wave upslope (128). Occasionally this was erroneously annotated due to noise and in these cases, these were manually corrected. UEGS positioned on the valve plane were manually excluded. One-

thousand UEGs (**Figure 20**) were computed per heart to obtain activation time (AT - the time from the earliest activation in the epicardium to steepest point of the QRS downslope), repolarization time corrected for heart rate (RTc - the steepest point of the T-wave upslope (128)), and activation-recovery interval (ARIc - the difference of AT and RTc) (92). Heart rate correction used the Fridericia formula (129). Dispersions of AT and ARIc (ΔAT, ΔARIc) were measured as the maximum-minimum of AT & ARIc respectively across the entire myocardium. Spatial gradients (G_{AT}, G_{RTc}) were computed for each epicardial site as the absolute value of the difference between neighbouring sites (within 15mm) divided by their distance, averaged across all neighbours. Signal amplitudes were defined as the peak to peak (maximum to minimum) of the QRS complexes, and signal fractionation defined as number of UEGs with ≥2 negative deflections within the QRS complex (including Q, R', r', S notching, R notching).

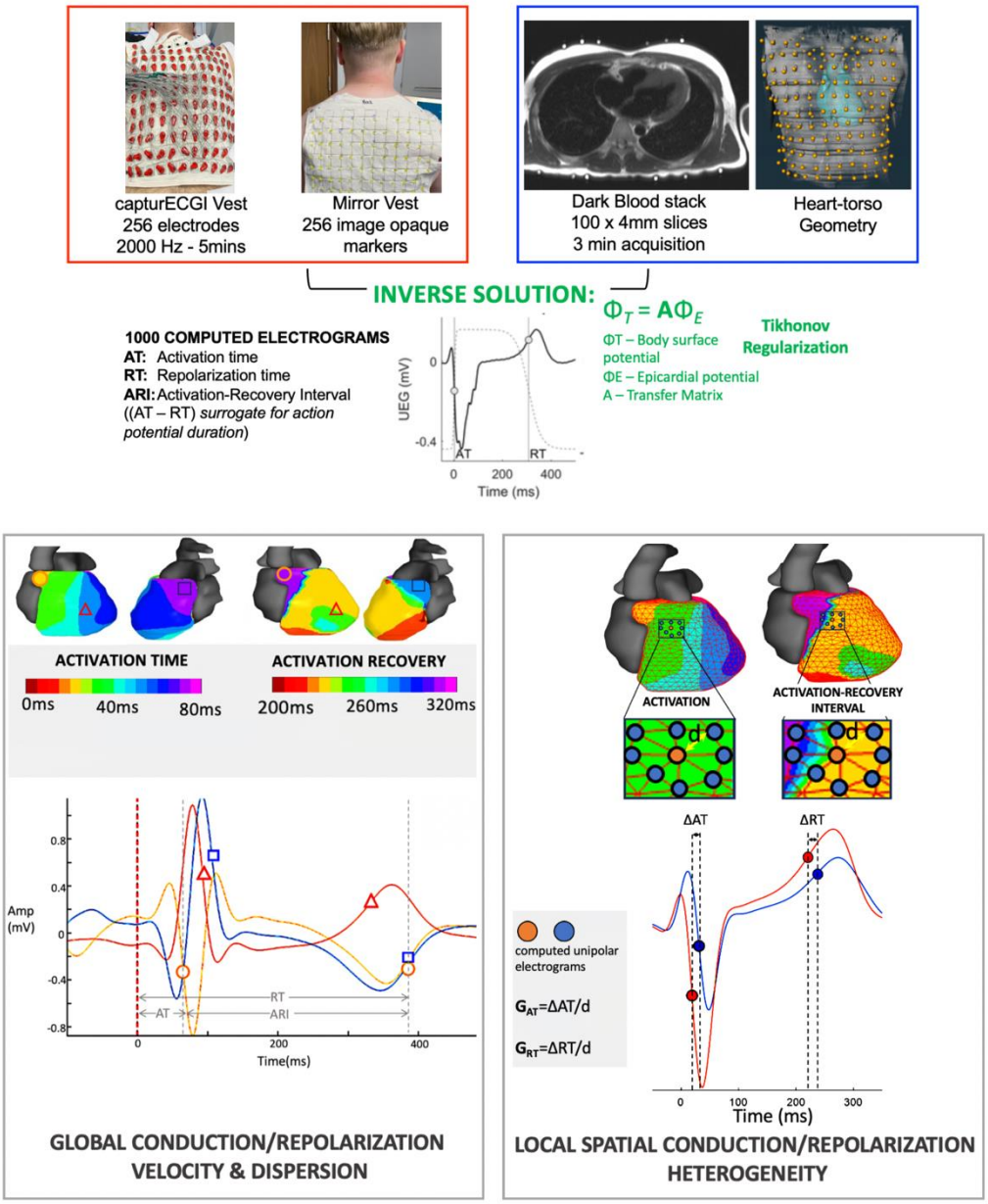

Figure 20. ECGI acquisition and post-processing.
Top: A 256-lead ECG is recorded using the fully re-useable CapturECGI vest. The mirror vest is positioned to match the electrode-vest and the participant wears this during the Dark blood (HASTE) anatomical stack acquisition. Heart-torso geometry is obtained using segmentation of the epicardium and the markers on the mirror vest using Amira-Avizo software (Thermofischer, USA). The inverse solution is performed according to previously described protocols thereby obtaining 1000 computed unipolar electrograms. **Left**: Activation Time (AT) is defined from the point of earliest activation on the epicardium to the steepest QRS downslope. Repolarization Time (RT) is defined by the steepest part of QRS upslope. Both are referenced to earliest epicardial activation. Activation Recovery Interval (ARI) is the difference between RT and AT. Three points (circle, triangle, square) on AT and ARIc maps are shown and their corresponding AT, RT, ARI are indicated on their computed unipolar electrograms (grey arrows show ECGI intervals of the 'circle' UEG). RT (and ARI) are corrected for heart rate. **Right:** AT/RT gradients: (ΔAT/ ΔRT) between unipolar electrograms (UEGs) orange and blue electrograms are shown. Gradients are measured as the difference in AT/RT (ΔAT/ΔRT) between neighbouring electrograms divided by their inter-electrode distance (d).

3.9.6. ECGI Repeatability Testing

Repeatability testing was performed by myself in collaboration with Webber et al (published in JCMR) (112) whom performed ECGI on a birth cohort (National Survey of Health and Development (113) aged 76-77 at the time of the study. Intra- and inter-observer variability was performed on 20 participant acquisitions. Both intra- and inter-observer variability were low (intra-class correlations r_s=0.99 and 0.98 respectively). Seven test:re-test acquisitions were also performed and UEGS were co-registered geometrically demonstrating good test:re-test repeatability (**Figure 21**) (r_s between 0.81 – 0.93).

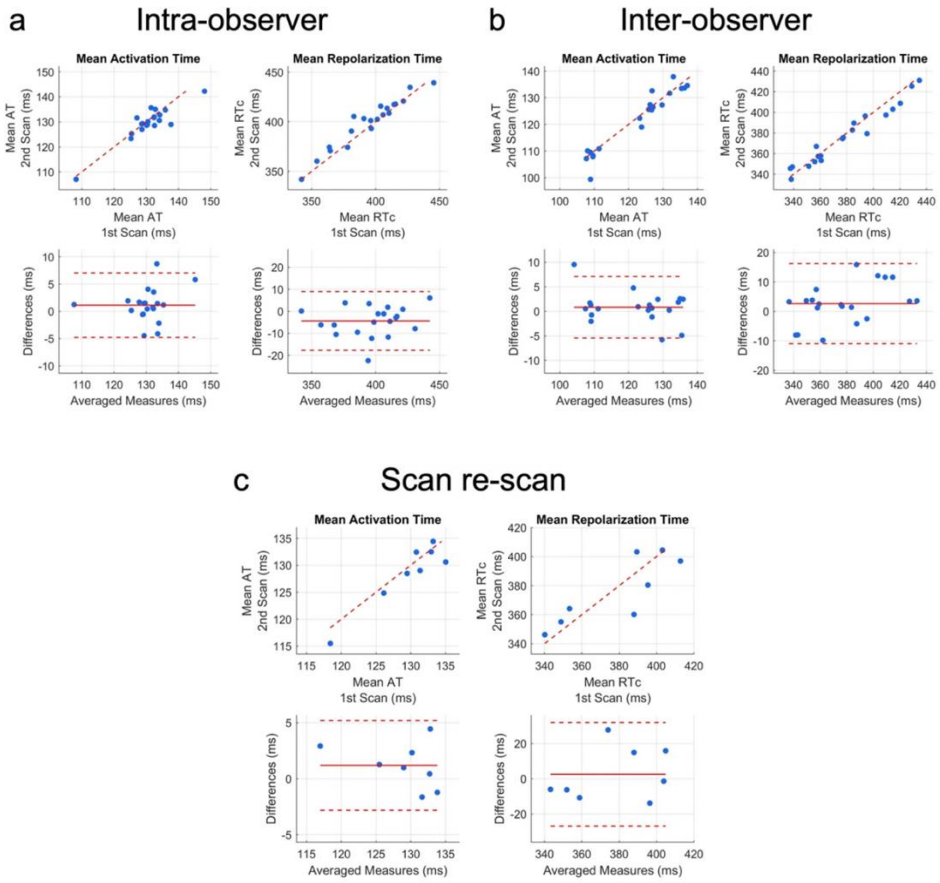

Figure 21. Intra-inter observer and test:re-test variability
Intraclass correlations and Bland-Altmann plots show good overall repeatability, Webber et al, (112)

3.10. Statistical Analysis

Statistical analysis was performed using SPSS (IBM SPSS Statistic, version 28). The distribution of data was examined using Shapiro-Wilk tests. Normally distributed continuous variables were summarised as mean ± SD and compared using independent samples *t*-tests; non-normally distributed variables as median (interquartile range) and compared using Mann-Whitney U-tests. Categorical/binomial variables were expressed as absolute counts and percentages and compared using Chi-squared/Fisher's exact test as appropriate.

3.10.1. Regression Analyses

Microvascular function in physiological and pathological hypertrophy

Multiple linear regression models were used to explore independent between-group differences by including *a priori* defined confounders such as age and adenosine dose. Variance inflation factor <3 excluded collinearity. Due to the lack of physiological response to standard clinical dose adenosine, we included data from 11 healthy volunteers undergoing higher-dose adenosine stress and included age and adenosine dose in a multiple regression model to explore whether there was independently higher stress MBF and MPR in athletes vs healthy volunteers. This was carefully considered due to the relatively low sample size; work from Austin et al showed using Monte-Carlo simulations that the number of subjects per variable (SPV) needed for accurate regression models was 2 SPV so we decided to proceed with multiple regression modelling (130). Assumptions of multiple regression were tested as below.

Microstructural and microvascular phenotype in subclinical and overt Hypertrophic Cardiomyopathy.

Univariable and multivariable linear regression models were used to determine associations of diffusion tensor, perfusion, fibrosis and hypertrophy parameters. Between-group comparisons involving DTI were adjusted for age (see below), fibrosis and hypertrophy (septal ECV, LGE mass, MWT) and expressed as standardized beta (β) coefficients and 95% confidence intervals (CI). A variance inflation factor of <3 excluded multicollinearity. Logistic regression models with inclusion of fibrosis (ECV, LGE) and hypertrophy (MWT) variables as covariates were used to test for odds ratios for independent risk of ECG abnormalities and NSVT. Continuous predictors were normalised before entering the logistic regression and odds ratio (OR) are expressed per 1 standard deviation (SD) increase in MD and |E2A| and 1SD decrease for FA, stress MBF and MPR. A 2-sided p-value of (<0.05) was considered significant. Multiple testing correction with Bonferroni was done for primary endpoints (perfusion and DTI in G+LVH- vs HV, G+LVH+ vs G-LVH+) in a table-by-table basis (adjusted P value threshold = 0.05/ (number of parameters analysed multiplied by number of comparisons)). Age, sex, ethnicity and BMI were tested for associations with DTI parameters in pooled healthy volunteers (n=41), subclinical and overt HCM. MD was found to associate with age in overt HCM, and therefore age was included in all between-group regression analysis involving DTI. Assumptions of multiple regression were tested as below.

Detection of electrophysiological abnormalities in subclinical and overt hypertrophic cardiomyopathy

Multiple testing with Bonferroni was performed on a 3 comparisons per variable basis (P<0.05/3). Spearman's correlations were used to examine simple linear/monotonic relationships between structural variables, risk markers (NSVT/LVOTO) and ECG/ECGI parameters. Multiple linear regression models were used to explore

independent between-group differences by including *a priori* defined confounders as covariates, namely age, sex and QRS duration for AT comparisons or QTc for ARIc comparisons. Additionally, differences in G+LVH- were adjusted for the presence versus absence of an abnormal resting 12-lead ECG. The normality of model residuals was validated using visual inspection of histogram and Q-Q plots. Multiple linear regression modelling involving fractionation required log-transformation, however other ECGI variables showed no need for transformation. Variance inflation factors ≤3 excluded significant multicollinearity. Homoscedasticity and independence of residuals were verified through scatterplots and the Durbin-Watson statistic, respectively, both yielding satisfactory results.

Machine learning classification of ECGI HCM subtypes

Optimal cutoff values to discriminate between subclinical HCM and healthy volunteers for each ECGI parameter separately were initially obtained using R package 'cutpointr' maximize metric function. Next, supervised machine learning (ML) with the support vector machine (SVM) classification was used to build an ECGI biomarker panel for HCM as previously described (131). SVMs are a set of effective, supervised non-parametric ML techniques that recognize patterns in data, and are especially suited to two-group separation challenges (132) (133). Another advantage of SVMs, is their relative resistance to over-fitting given that they use regularization (134). The goal of our exploratory SVM model was to combine all the available ECGI features to predict which phenotypic category (subclinical HCM or control) a participant belonged to. The SVM was trained using 80% of the cohort (split 4:1) with a polynomial kernel tuned to cost 10 and gamma 0.1. SVM performance was then tested on the remaining 20% hold-out dataset for validation. For the model, area under the receiver operating

characteristics curve (AUC, ROC) was calculated using package ‘ROCR’. A similar SVM and ROC approach explored whether the ECGI electrotype in patients with overt HCM could discriminate low risk from high/intermediate risk patients (from the ESC Risk score), including those with prior documented NSVT. For the latter SVM with radial kernel tuned to cost 1 and gamma 0.6, a hold-out dataset for validation was not feasible due to the limited sample size so 10-fold cross-validation was undertaken instead.

CHAPTER 4: RESULTS i. Microvascular function in physiological and pathological LVH

We used fully-automated quantitative perfusion CMR to explore microvascular function in athletes and hypertensives, two conditions that result in physiological and pathological LVH respectively. We also compared findings to 20 participants with subclinical HCM, due to prior evidence of impaired microvascular function in this cohort (81). 63 participants completed the protocol, of these 19 were athletes, 14 were healthy volunteers, 10 had hypertension and 20 had subclinical HCM.

4.1. Hypertension vs Healthy Volunteers

Hypertensives were older but had a low prevalence of other comorbidities (1 patient was obese – BM>30kg/m^2, 1 patient had high cholesterol, none had diabetes). LV cavity size, EF, stroke volumes and mass:volume ratios were similar to healthy volunteers. Hypertensives had higher LV mass, MWT and ECV. Hypertensives had similar stress /rest MBF and MPR. (**Table 1**, **Figure 22**). All LGE was non-significant (n=2, RV insertion point only)

4.2. Athletes vs Healthy volunteers

There were no cardiovascular medication use in either athletes or healthy volunteers. Athletes were similar in age, BSA and BMI. Athletes had larger cavity sizes, higher stroke volume, lower ejection fraction, higher LV mass, higher maximum wall thickness, lower mass:volume ratio and higher ECV. All LGE was non-significant (n=4, RV insertion point only). Athletes had lower rest and stress heart rates, similar stress and rest myocardial blood flow but a higher myocardial perfusion reserve. Athletes however required a higher dose of adenosine to achieve physiological stress (9 required 175mcg/kg/min and 3 required 210mcg/kg/min vs all HV stressed at

140mcg/kg/min p<0.001 [McNemar's test]). Therefore 11 unmatched male healthy volunteers (younger age 23(23-24) years p<0.001) whom received the maximum dose of adenosine (210mcg/kg/min) for stress testing were included in an additional analysis. When adjusting for age and adenosine dose, athletes showed a higher stress MBF (β=0.51, 95% CI: 0.1,0.9, p=0.015) and higher MPR (β=0.43, 95% CI: 0.005, 0.9, p=0.048) (**Table 1, Figure 22**). There were no correlations between stress MBF/ MPR and adenosine dose. There were no correlations between stress MBF/MPR and markers of fibrosis or hypertrophy in either athletes or healthy volunteers.

4.3. Subclinical HCM vs Healthy volunteers

Subclinical HCM were similar in age, BSA and BMI. Subclinical HCM had similar cavity sizes and more hyperdynamic function (higher EF and SV), higher MWT but similar LV mass, higher ECV and lower mass/volume ratio. Rest HR was lower and stress HR was higher. Stress and rest MBF were similar but there was lower MPR **(Table 1, Figure 22)**. 3(15%) had visual perfusion defects. 2(10%) had LGE, both were RV insertion point.

4.4. Athletes vs Hypertensives

Hypertensives had a higher BMI than athletes but were similar in age. Hypertensives had smaller LV cavity sizes, lower stroke volumes, similar LV mass, MWT and ECV. Hypertensives had a higher mass: volume ratio. Hypertensives had a higher rest and stress HR, lower stress myocardial blood flow (MBF) and perfusion reserve (MPR) but similar rest MBF **(Table 1, Figure 22)**.

4.5. Subclinical HCM vs Athletes

Subclinical HCM were younger than athletes, had small cavity sizes, lower stroke volume but higher ejection fraction, lower LV mass but similar MWT, mass:volume ratio and ECV. Rest and stress HR were higher with no difference in resting blood pressures. Subclinical HCM had lower stress MBF and MPR, and similar rest MBF **(Table 1, Figure 22)**.

4.6. Subclinical HCM vs HTN

Compared to HTN, subclinical HCM were similar in age, had lower BMI and higher EF. Other volumetric parameters, MWT and ECV were similar. Subclinical HCM had lower rest HR but higher stress HR. There was no difference in stress/rest MBF or MPR **(Table 1, Figure 22)**. Medication use is shown in **Table 2**.

	Healthy Volunteers (n=14)	Athletes (n=19)	Hypertensives (n=10)	Subclinical HCM (n=20)	P value					
					HV vs Athletes	HV vs HTN	Subclinical HCM vs HV	Athletes vs HTN	Subclinical HCM vs HTN	Subclinical HCM vs Athletes
Demographics										
Age	39(32-46)	47(31-61)	57(53-66)	39(26-42)	0.24	**0.001**	0.52	0.056	**<0.001**	**0.041**
BSA, m^2	2.03±0.2	1.99±0.2	2.04±0.3	1.98±0.1	0.48	0.93	0.32	0.51	0.37	0.83
BMI, kg/m^2	25±2	26±4	29±6	25±4	0.18	0.14	0.48	**0.038**	**0.04**	0.65
LV Volumes, Mass & ECV										
LVEDV, ml	150(129-176)	222(240-270)	184(167-219)	189(149-192)	**<0.001**	**0.048**	0.11	**0.014**	0.45	**<0.001**
LVEDV index, ml/m^2	80±21	119±18	93±11	89±16	**<0.001**	0.056	0.13	**<0.001**	0.45	**<0.001**
SV, ml	96(84-112)	135(114-160)	111(87-134)	123(107-137)	**<0.001**	0.21	**0.042**	**0.045**	0.27	0.11
SV index, ml/m^2	51±14	70±13	57±12	62±8	**<0.001**	0.25	**0.004**	**0.012**	0.17	**0.024**
EF, %	63±4	59±4	60±8	70±8	**0.002**	0.23	**0.002**	0.57	**0.004**	**<0.001**
LV Mass, g	120±29	148±18	141±29	121±33	**<0.001**	0.08	0.91	0.43	0.12	**0.004**
LV Mass index, g/m^2	55(53-64)	72(70-78)	67(62-77)	58(52-67)	**<0.001**	**0.026**	0.56	0.12	0.061	**<0.001**
MWT	8±1	10±1	10±1	10±1	**<0.001**	**<0.001**	**<0.001**	0.48	>0.9	0.97
ECV, %	22±2	24±2	25±2	26±3	**0.004**	**0.004**	**<0.001**	0.85	0.16	0.062
Mass/Volume Ratio	0.75±0.11	0.64±0.1	0.74±0.09	0.70±0.22	**0.01**	0.84	**0.025**	**0.016**	0.061	0.59
Haemodynamics										
Rest HR, bpm	63(55-79)	52(49-60)	63(58-71)	59(52-72)	**0.002**	0.87	<0.001	**0.003**	**<0.001**	**<0.001**
Stress HR, bpm	89(78-98)	78(70-81)	91(80-93)	98(82-107)	**0.032**	0.77	<0.001	**0.006**	**<0.001**	**<0.001**
Rest sBP, mmHg*	-	129±15	-	123±16	-	-	-	-	**0.046**	0.06
Rest dBP, mmHg*	-	74±7	-	77±14	-	-	-	-	0.16	0.95

Perfusion										
Stress MBF, ml/g/min	2.62±0.7	2.81±0.5	2.26±0.5	2.3±0.5	0.23	0.27	0.11	**0.032**	0.87	**0.002**
Rest MBF, ml/g/min	0.77(0.5-0.8)	0.63(0.5-0.8)	0.75(0.6-1.0)	0.73(0.61-0.84)	0.28	0.75	0.67	0.21	>0.9	0.072
MPR	3.7±0.9	4.54±1.2	2.94±0.9	3.11±0.7	**0.042**	0.06	**0.043**	**<0.001**	0.58	**<0.001**

Table 1. Demographics, CMR and perfusion variables between HV, athletes, subclinical HCM and hypertensives.

*Blood pressure only measured in Athletes and subclinical HCM. HV – healthy volunteer, HTN, hypertension, BSA, body-surface area, BMI, body-mass index, ECV – extracellular volume, LV, left ventricle, EDV, end-diastolic volume, SV, stroke volume, MWT, max. wall thickness, HR, heart rate, MBF, myocardial blood flow, MPR, myocardial perfusion reserve.

	Study ID	Drugs List
Hypertensives	HTN001	bisoprolol 1.25mg od, atorvastatin 80mg od, aspirin 75mg od, omeprazole 20mg od, tamsulosin 400mcg/ od finasteride 5mg od
	HTN002	ramipril 10mg OD, amlodipine 10mg OD
	HTN004	Indapamide 1.5mg OD, irbesartan 300mg OD, amiloride 20mg OD, amlodipine 10mg OD
	HTN005	bendroflumethiazide 2.5mg od, amlodipine 10mg od, candesartan 32mg od
	HTN006	olmesartan 40mg od, amlodipine 5mg od, indapamide 1.5mg od, levothyroxine 150mcg od, omeprazole 20mg od, ropinerole 0.75mg od, paroxetine 30mg od
	HTN008	losartan 100mg od, amlodipine 10mg od
	HTN009	bisoprolol 2.5mg od, bendroflumethiazide 2.5mg od, amlodipine 10mg od
	HTN010	lisinopril/ hydrochlorothiazide 20/12.5mg od, felodipine MR 10mg od, bisoprolol 5mg od, antihistamines
	HTN011	felodipine 12.5mg od, catapres tts11 patch OW
	htn012	missing data
Subclinical HCM	dsgp058	ramipril 2.5mg od
	dsgp087	bisoprolol 2.5mg od, ramipril 2.5mg od

Table 2. Medication usage in hypertensives and subclinical HCM

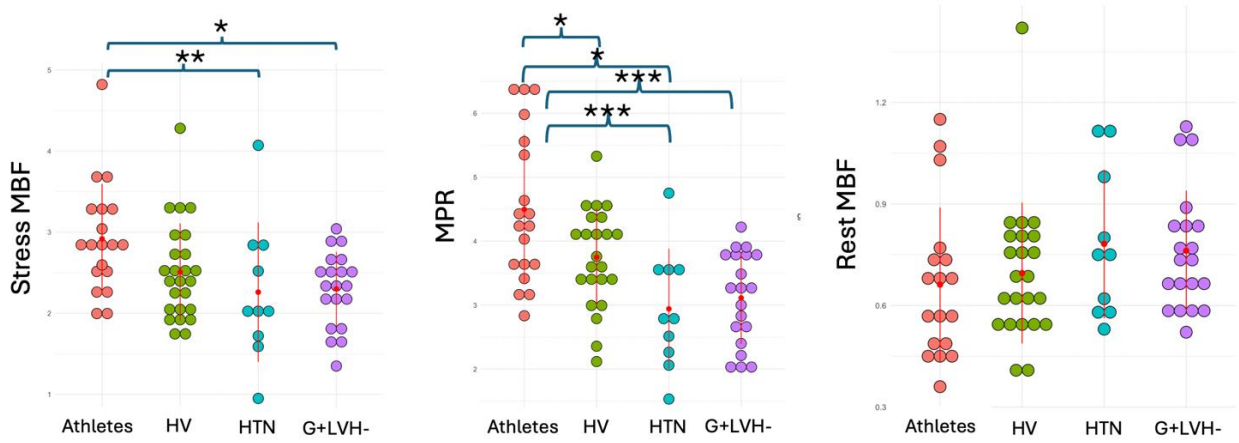

Figure 22a. Differences in stress MBF, MPR and rest MBF between Athletes, healthy volunteers, hypertension and subclinical HCM
Athletes show preserved microvascular function compared to HTN and subclinical HCM. Significant differences are shown in brackets. *, p<0.05, **, p<0.01, ***, p<0.001. HV – healthy volunteers, HTN – hypertension, MBF – myocardial blood flow, MPR – myocardial perfusion reserve

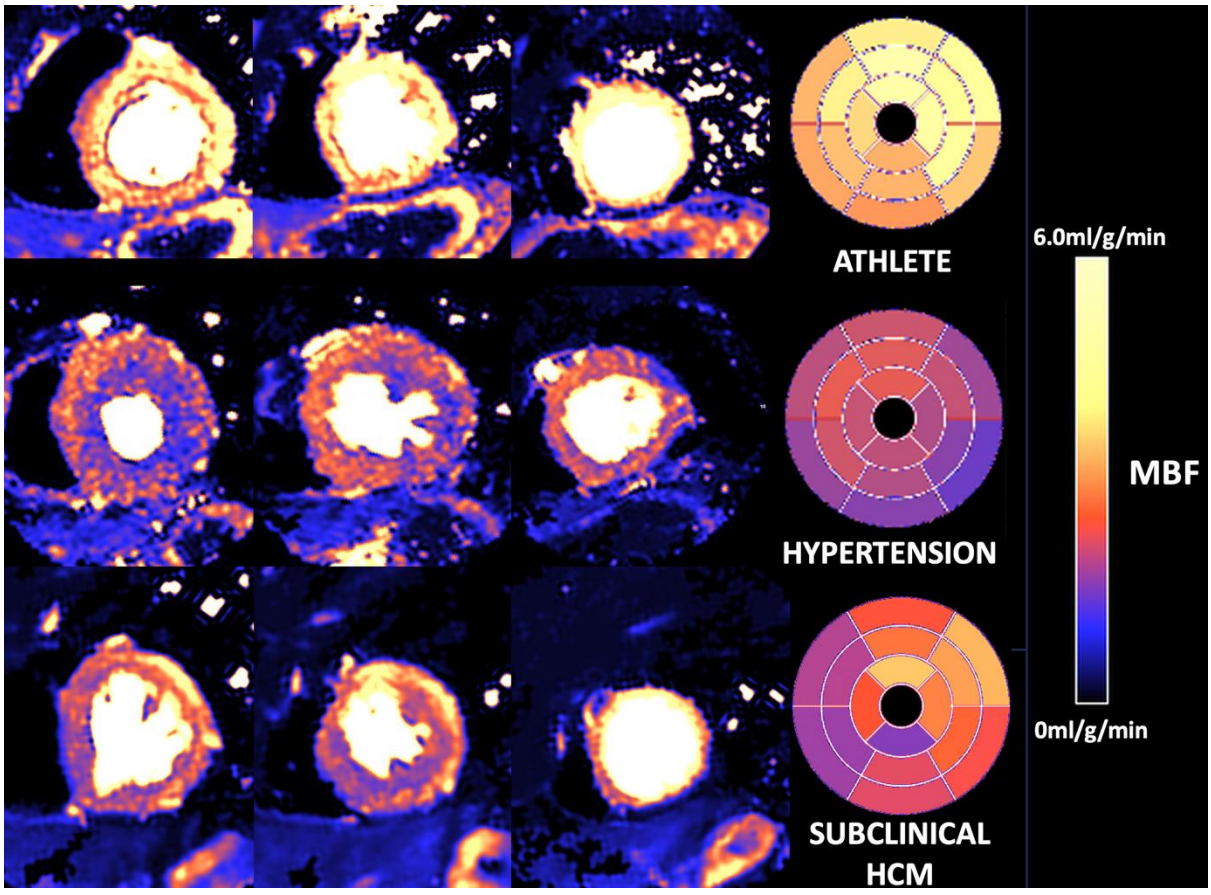

Figure 22b. Exemplar quantitative perfusion stress myocardial flow maps in an athlete, hypertensive and individual with subclinical HCM

CHAPTER 5. RESULTS ii. Microstructural and microvascular phenotype of subclinical and overt HCM

This manuscript is based on the following chapter:

Joy G…Moon JC, Lopes LR, Microstructural and Microvascular Phenotype of Sarcomere Mutation Carriers and Overt Hypertrophic Cardiomyopathy.

Circulation 2023 Sep 5;148(10):808-818.

We aimed to investigate the extent and interrelationships of microstructural alteration (measured by diffusion tensor imaging) and microvascular disease (MVD – measured by quantitative perfusion) in both overt and subclinical HCM. We then studied the associations between these biomarkers and pathological ECG findings and genetic substrate (genotype positive (G+LVH+) and genotype negative (G-LVH+)).

5.1. Clinical characteristics

Overall 206 participants were studied: 101 overt disease (51 G+LVH+, 50 G-LVH+), 77 subclinical HCM (G+LVH-) and 28 healthy volunteers (HV). Of 77 G+LVH-, pathogenic/likely pathogenic variants were 60%(46) *MYBPC3*, 23%(18) *MYH7*, 6%(5) *TNNI3*, 6%(5) *TNNT2*, 1%(1) *MYL2*, 1%(1) *TPM1*, 1%(1) *CSRP3*. Of 51 genotype positive overt HCM (G+LVH+), pathogenic/likely pathogenic variants were 55%(28) *MYBPC3*, 25%(13) *MYH7*, 8%(4) *TNNI3*, 8%(4) *TNNT2*, 2%(1) *CSRP3*, 2%(1) *TNNC1.* Demographics and conventional CMR parameters are summarised in **Table 3**. Comparisons between overt HCM (all LVH+ n=101) and healthy volunteers are provided in **Table 4**. 23%(23) of the overt HCM cohort had a peak left ventricular

outflow tract gradient ≥30mmHg and these patients average gradient at rest was 27(18-60)mmHg and on provocation was 56(38-85)mmHg.

Overt HCM: (All LVH+) vs HV: Overt HCM was characterised by higher ejection fraction (EF), and more severe markers of hypertrophy (higher MWT and higher LV mass) and fibrosis (higher ECV and higher burden of LGE) (**Table 4**).

Overt HCM: G+LVH+ vs G-LVH+: There was no difference in EF and MWT. G-LVH+ had higher LV mass. G-LVH+ had similar LGE burden and lower ECV (but not after correcting for multiple comparisons) (**Table 3**).

Subclinical HCM: G+LVH- vs HV Compared to healthy volunteers, G+LVH- had a lower indexed end-diastolic volume (EDVi), higher EF but no difference in markers of hypertrophy (MWT or LV mass) and no difference in markers of fibrosis (ECV, LGE) (**Table 3**).

5.2. Myocardial perfusion

Overt HCM (All LVH+) vs HV: Patients with HCM had evidence of MVD (lower stress MBF and MPR) with a higher prevalence of perfusion defects (91% (92/101) vs 0% p<0.001) (**Figure 23, Table 4**).

Overt HCM: G+LVH+ vs G-LVH+ (**Table 5, Figures 24 & 25b**): There was no difference in global perfusion parameters (stress MBF or MPR) but all 51 G+LVH+ patients had perfusion defects compared to 82% (41/50) G-LVH+ (p=0.001).

Subclinical HCM (G+LVH-) vs HV (**Table 5, Figures 24 & 25b**)**:** G+LVH- had reduced stress MBF but not after correcting for multiple comparisons. Subclinical HCM had a higher prevalence of perfusion defects (28% vs 0% p=0.002) but no difference in MPR (**Table 5, Figure 23-25**).

5.3. Demographics relationships of DTI

Age

In pooled healthy volunteers (n=41), there was no association between DTI parameters and age (FA: p=0.71, MD: p=0.99 |E2A|: p=0.95). In subclinical HCM, there was no relationship with age (FA: p=0.22, MD: p=0.93, |E2A|: p=0.10). In overt HCM, there was a positive association between MD with age (β=0.22 p=0.027), but not FA (p=0.89), or |E2A| (p=0.11).

Sex

Pooled Healthy Volunteers: DTI parameters were not different between male and female sex (FA: p=0.27, MD: p=0.97, |E2A|: p=0.32) In subclinical HCM, there was no relationship with sex: (FA p=0.34, MD: p=0.43, |E2A|: p=0.064). In overt HCM, there was no DTI relationship with sex (FA p=0.35, MD p=0.26, |E2A| p=0.52).

Ethnicity

Pooled Healthy Volunteers: DTI parameters were not associated with ethnicity: (FA: p=0.6, MD: p=0.6, and |E2A|: p=0.75). In subclinical HCM, there was no relationship with ethnicity (FA: p=0.90, MD: p=0.90, |E2A|: p=0.50). In overt HCM, there was no relationship with ethnicity (FA: p=0.28, MD: p=0.57, |E2A|: p=0.08).

Body Mass Index

There was no association between any DTI parameter and BMI in pooled healthy volunteers (FA: p=0.53, MD: p=0.47, |E2A|: p=0.82), subclinical HCM (FA: p=0.18, MD: p=0.42, |E2A|: p=0.84) or overt HCM (FA: p=0.12, MD: p=0.58, |E2A|: p=0.38).

5.4. Microstructural indices measured by DTI

Overt HCM (All LVH+) vs HV: (**Table 4**): Compared to healthy volunteers, overt HCM had evidence of microstructural alteration: lower FA suggestive of disarray, higher MD and higher |E2A| suggestive of a more hypercontracted sheetlet configuration.

Differences remained when adjusting for fibrosis and hypertrophy. (FA: β=-0.52, 95% CI: -0.32,-0.68 p<0.001, MD: β=0.26 95% CI: 0.05, 0.45 p<0.015, |E2A|: β=0.64 95% CI: 0.48, 0.80, p<0.001).

Overt HCM vs older age-matched HV: The overt HCM group were age sex and ethnicity matched to 24 healthy volunteers (11 overlapped with the younger HV group described above). This was to detect if any DTI differences with the older HCM group and health remained when accounting for age. All 24 HV underwent DTI contrast CMR but 3 did not have ECV mapping.

Compared to overt HCM, healthy volunteers were well matched for age, sex and ethnicity (Age: HCM: 57(47-62) vs 51(42-61) years p=0.32, Female Sex: 24(24%) vs 7(29%) p=0.62, White: 77(76%) vs 20 (83%) p=0.43. As expected, overt HCM had lower LVEDVI (74±13 vs 84±23 ml/m^2 p=0.009), greater LVMi, (86(74-114) vs 60(49-75)g/m^2 p<0.001), higher MWT (17.2(15.4-21.1) vs 10.3(9.0-11.2)mm p<0.001), higher EF (79(74-83) vs 69(65-72)% p<0.001), higher ECV (28.7(26.4-32.6) vs 25.6(23.9-27.8)% p<0.001) and a higher prevalence of LGE (95(94%) vs 5(21%) p<0.001).

Compared to age, sex and ethnicity matched healthy volunteers, overt HCM had lower FA (0.28(0.25 vs 0.30) vs 0.34(0.33-0.36) p<0.001), higher MD 1.57 (1.53, 1.62) vs 1.48(1.44,1.54) $10^{-3}mm^2/s$ p<0.001) and higher |E2A| (61.9(56.5, 65.8) vs 43.4(37.9, 47.3)° p<0.001). Differences remained when correcting for fibrosis and hypertrophy (FA: β=-0.46, 95% CI:-0.31, -0.69 p<0.001, MD β=0.26, 95% CI: 0.07, 0.50 p=0.011, |E2A| β=0.52, 95% CI: 0.32, 0.63 p<0.001).

Overt HCM: G+LVH+ vs G-LVH+ (**Figure 25a, Table 5**)**:** Whilst MD and FA were similar, |E2A| was elevated in G-LVH+ compared to G+LVH+ (p=0.011 – before

correction for multiple comparisons). Differences remained after adjusting for fibrosis and hypertrophy (β=0.35, 95% CI: 0.15, 0.55 p<0.001).

G+LVH+ vs G+LVH-; Compared to G+LVH-, G+LVH+ were older, had lower prevalence of female sex, lower EDV (both absolute and indexed), higher EF and more severe markers of LVH and fibrosis. G+LVH+ was characterised by more severe microvascular disease (lower stress MBF and MPR) and more severe microstructural alteration (lower FA, higher MD, higher |E2A|). Differences remained for FA and |E2A| but not MD after adjusting for MWT, LGE and ECV (FA: β=-0.34, 95% CI: -0.07, -0.52 p=0.012 and |E2A| β=0.42, 95% CI: 0.14,0.58 p=0.002) (**Table 6**).

Subclinical HCM (G+LVH-) vs HV (**Figure 24, 25a**, **Table 5**): Compared to healthy volunteers, G+LVH- had evidence of microstructural alteration (lower FA, higher MD, higher |E2A|) although this was less severe when compared to overt HCM. Differences remained after adjusting for fibrosis and hypertrophy (FA: β=-0.45, 95% CI: -0.28, -0.62 p<0.001, MD: β=0.39, 95% CI: 0.19, 0.56, p<0.001, |E2A|: β=0.35, 95% CI: 0.17, 0.52 p<0.001).

5.5. Gene specific analyses

Subclinical HCM. There was no significant difference in DTI parameters between thick vs thin filament mutations (FA p=0.70, MD p=0.94, |E2A| p=0.67). There was no significant difference in DTI parameters between MYH7 and MYBPC3 (FA p=0.11, MD p=0.77, |E2A| p=0.98). **Overt HCM**: In overt disease, thin filament mutations (n=10) were associated with a more elevated absolute |E2A| (62.8 (60.7, 64.6) vs 58.7 (55.5, 62.9)° p=0.029), but there was no difference in FA (p=0.84) or MD (p=0.74). There was no significant difference in DTI parameters between MYH7 vs MYBPC3 (FA

p=0.09, MD p=0.31, |E2A| p=0.24). All genes and variants affected for genotype positive participants are provided in **Table 7**.

5.6. Relationships of microstructural indices with myocardial perfusion

Overt HCM (All LVH+): All three DTI parameters were associated with stress MBF (all p<0.02) but when accounting for fibrosis and hypertrophy, only |E2A| was independently associated (β=-0.30, 95%CI: -0.11, -0.47, p=0.002).

Subclinical HCM (G+LVH-):

Perfusion defects G+LVH- with (n=21) vs without (n=54) focal perfusion defects were similar in age (p=0.60), sex (p=0.46), maximum wall thickness (p=0.43), ECV (p=0.85), but had a higher prevalence of LGE (5(7%) vs 1(1%) p=0.006), similar global stress MBF (p=0.053), lower global MPR (2.58(2.31-3.05) vs 3.15 (2.62-3.91) p=0.011) and no difference in ECG abnormalities (p=0.62).

G+LVH- with defects had evidence of more severe microstructural alteration (lower FA (0.30(0.29-0.32) vs 0.32(0.31-0.33 p=0.002), higher |E2A| (53.4(47.1-59.8) vs 46.1(41.3-53.0)° p=0.009) but similar MD (p=0.47), (**Figure 23, 25c**).

Global perfusion: MPR but not stress MBF associated with FA & |E2A| and relationships remained after adjustment for fibrosis and hypertrophy (FA: β=0.33 95% CI: 0.08,0.57, p=0.01 and |E2A|: β=-0.32, 95% CI: -0.07,-0.57, p=0.013).

5.7. Associations of DTI, perfusion and fibrosis parameters

Pooled HV (n=41): There was no relationship between any DTI parameter and ECV (FA: p=0.61, MD: p=0.60, |E2A| p=0.48) or MWT (FA: p=0.32, MD: p=0.23, |E2A|

p=0.24). 12%(5) pooled HV had LGE and there was no association with any DTI parameter (FA: p=0.58, MD: p=0.46, |E2A|: p=0.88).

G+LVH- & markers of fibrosis and LVH:

LGE: There were significant associations with |E2A| but not MD or FA (|E2A|: β=0.27, p=0.016). There were no associations between any DTI parameter and ECV or MWT.

Overt HCM - correlations of markers of fibrosis and LVH:

LGE: There were significant associations with all 3 DTI parameters (FA: β=-0.54, p<0.001, MD: β=-0.47 p<0.001 |E2A| β=0.29, p=0.003). **ECV:** There were significant associations with FA and MD but not |E2A| (FA: β=-0.34, p<0.001, MD: β=0.27 p=0.008). **MWT:** There were significant associations with FA, MD and |E2A| (FA: β =-0.33, p<0.001, MD: β =0.33, p<0.001, |E2A|: β=0.34, p<0.001). **Multivariable:** There were no interaction relationships between predictor variables and all associations with DTI parameters. When including LGE, ECV and MWT as covariates, only LGE was independently predictive of FA and MD but not |E2A| (FA: β=-0.26, 95%CI: -0.02,-0.50 p=0.033, MD: β=0.26, 95%CI:0.03,0.50 p=0.028). Only MWT was independently predictive of |E2A| (β=0.36, 95%CI 0.15, 0.58 p=0.001). There were no independent relationships between DTI parameters and ECV.

5.8. Relationships of microstructural indices with ECG abnormalities

Overt disease (All LVH+) ECG: Overall: 84% (85/101) of overt HCM had an abnormal ECG. Abnormal ECG was associated with all three DTI parameters (all p<0.001), stress MBF and MPR (both p<0.016). When accounting for fibrosis, hypertrophy and stress MBF, independent predictors of abnormal ECG were FA (OR=3.3 95% CI 1.3, 8.3 p=0.01) and |E2A| (OR=2.7 95% CI: 1.2, 6.0 p=0.015). Stress MBF was also an independent predictor (OR=2.8 95% CI: 1.2, 6.4 p=0.015

when adjusting for FA, fibrosis and hypertrophy). **Individual ECG abnormalities:** 28% (28) had abnormal Q waves, 71% (72) had T-wave inversion, 49% (49) had ST-depression and 50% (50) met LVH voltage criteria.

5.9 Relationships of microstructural indices with individual ECG abnormalities in overt HCM

Overt HCM: Q-waves were present in 28% (28). TWI was present in 71% (72). ST-Depression was present in 49% (49). 50% (50) met LVH voltage criteria. 34% (34) had LVH with ST depression, 43% (43) had LVH criteria with T-wave inversion. **Q-waves:** No DTI parameter or markers of perfusion, fibrosis or hypertrophy were related to the presence of Q-waves. **T-Wave Inversion (TWI)**: TWI was associated with FA and MD (both $p<0.003$), stress MBF and MPR (both $p<0.033$), MWT ($p<0.001$) and LGE ($p<0.001$). When including markers of perfusion, fibrosis and hypertrophy, no DTI parameter was independently predictive of TWI, however stress MBF was independently predictive (OR=2.6, 95% CI 1.4, 5.0 p=0.003, (FA included in the model)). **ST-Depression.** ST-depression was associated all three DTI parameters (all $p<0.026$), stress MBF and MPR (both $p<0.029$), MWT ($p<0.001$) and LGE ($p<0.001$). When including stress MBF, MWT, ECV and LGE as co-variates, MD (OR=2.3, 95% CI: 1.2, 4.2, p=0.008) and stress MBF were independently predictive (OR=2.0, 95% CI 1.1, 3.8 p=0.033). **LVH Voltage criteria:** LVH by voltage criteria was associated with |E2A| and FA (both p=0.007) and MWT ($p<0.001$). No DTI parameter or stress MBF was independently predictive.

NSVT: 13% (13) of patients had NSVT. NSVT was associated with lower stress MBF (p=0.026), higher MWT (p=0.002), higher LGE mass ($p<0.001$) and higher ECV

(p=0.023). No DTI parameter associated with NSVT (FA: p=0.08). No DTI or quantitative perfusion parameter was independently predictive of NSVT.

Subclinical HCM (G+LVH-) ECG: Overall: 34% (26) of subclinical HCM had an abnormal ECG. An abnormal ECG was associated with all three DTI parameters (all p<0.001) and MPR (p<0.003). When adjusting for MPR, fibrosis and hypertrophy, all three DTI parameters remained independently predictive of abnormal ECG: (FA: OR=4.0, 95% CI: 1.7, 9.1 p=0.001, |E2A|: OR=2.8, 95% CI: 1.4, 5.7 p=0.006, MD: OR 4.8, 95% CI: 2.0, 11.4, p<0.001, MPR: OR=2.2, 95% CI: 1.0, 4.9 p=0.049 (FA included as a covariate)). **Individual ECG abnormalities:** 21% (16) had abnormal Q-waves, 9% (7) had T-wave inversion, 12% (9) met voltage criteria for LVH and no participant had ST-depression. When considering associations with individual ECG abnormalities in isolation, only FA and MD were predictive of abnormal Q waves after adjusting for MPR, fibrosis and hypertrophy (FA: OR=5.2, 95% CI: 1.6,16.0 p=0.006, MD: OR=2.3, 95%CI: 1, 5.3, p=0.049). There were no independent predictors of T-wave inversion/ST depression/LVH criteria.

	Healthy Volunteers	Subclinical HCM (G+LVH-)	G+LVH+	G-LVH+	p-values	
					HV vs G+LVH-	G+LVH+ vs G-LVH+
	n=28	n=77	n=51	n=50		
Demographics						
Age, years	34(32-39)	31(23-40)	52(37-59)	59(51-65)	0.13	**0.005**
Female, n(%)	15(54)	46(60)	16(31)	8(16)	0.57	0.07
BSA, m^2	1.8±0.3	1.9±0.2	1.9±0.2	2.0±0.2	0.34	0.37
BMI (kg/m^2)	24(22-26)	25(22-28)	25(24-28)	26(24-28)	0.23	0.68
White, n(%)	20(71)	64(83)	43(84)	34(68)	0.29	0.054
Asian, n(%)	7(25)	8(10)	7(14)	11(22)	0.11	0.28
Black, n(%)	1(4)	5(6)	1(2)	5(10)	0.99	0.098
Volumes & Mass						
LVEDV index, ml/m^2	94±21	83±14	72±11	76±15	**0.009**	0.15
LVEF, %	66(63-68)	71(67-74)	79(74-83)	79(75-82)	**<0.001***	0.53
MWT, mm	9.3(8.2-10.2)	9.6(8.6-10.6)	17.2(15.4-21.1)	17.2(15.9-21.7)	0.22	0.41
LV Mass index g/m^2	53(45-68)	51(43-60)	77(67-92)	96(81-126)	0.31	**<0.001***
Fibrosis markers						
ECV septum, %	26.2(23.8-28.4)	27.2(25.3-29.7)	30.0(27.1-33.8)	27.1(25.4-30.5)	0.18	**0.009**
LGE, present (%)	0	6(8%)	47(92%)	48(96%)	0.19	0.68
LGE mass, g	0	0(range: 0-3.8)	7.7(2.4-14.9)	6.5(3.1-14.1)	0.13	0.67

Table 3. Demographics and CMR variables across the four groups.

A Bonferroni correction would require a p-value of 0.0036 to declare statistical significance at a nominal type 1 error rate of 0.05 (0.05/14) – CMR and demographics variables are considered separately. * - remains significant after Bonferroni correction.

	Healthy Volunteers	Overt HCM (All LVH+)	p-value HV vs HCM
	n=28	n=101	
Demographics			
Age, years	34(32-39)	57(47-62)	**<0.001**
Female, n(%)	15(54)	24(24)	**0.002**
BSA, m^2	1.8±0.3	2.0±0.2	**0.009**
BMI (kg/m^2)	24(22-26)	25(24-28)	**0.013**
White, n(%)	20(71)	77(76)	0.89
Asian, n(%)	7(25)	18(18)	0.4
Black, n(%)	1(4)	6(6)	0.99
Volumes & Mass			
LVEDV index, ml/m^2	94±21	74±13	**<0.001**
LVEF, %	66(63-68)	79(74-83)	**<0.001**
MWT, mm	9.3(8.2-10.2)	17.2(15.4-21.1)	**<0.001**
LV Mass index g/m^2	53(45-68)	86(74-114)	**<0.001**
Fibrosis markers			
ECV septum, %	26.2(23.8-28.4)	28.7(26.4-32.6)	**<0.001**
LGE, present (%)	0	95(94%)	**<0.001**
LGE mass, g	0	7.1(3.0-15.1)	**<0.001**
Microvascular disease			
Stress MBF ml/g/min	2.77±0.62	1.69±0.51	**<0.001**
Rest MBF ml/g/min	0.77(0.68-0.86)	0.67(0.57-0.79)	**0.012**
MPR	3.47(2.90-3.75)	2.43(2.00-3.08)	**<0.001**
Visual perfusion defects n(%)	0	92/101(91%)	**<0.001**
Diffusion Tensor			
FA	0.34(0.33-0.36)	0.28(0.25-0.30)	**<0.001**
MD, $10^{-3}mm^2/s$	1.46(1.44-1.49)	1.57(1.53-1.61)	**<0.001**
|E2A|, °	41.6(34.9-47.2)	61.9(56.5-65.8)	**<0.001**

Table 4. Demographics, volumetric and CMR parameters between Overt HCM and healthy volunteers

	Healthy Volunteers		Subclinical HCM (G+LVH-)		G+LVH+		G-LVH+	p-values	
	n=28		n=77		**n=51**		**n=50**	HV vs G+LVH-	G+LVH+ vs G-LVH+
Microvascular disease									
Stress MBF ml/g/min	2.77±0.62	↓	2.46±0.54	↓↓	1.77±0.52	↓↓	1.59±0.48	**0.015**	0.067
Rest MBF ml/g/min	0.77(0.68-0.86)	↔	0.80(0.66-0.93)	↓	0.69(0.59-0.83)	↓	0.64(0.55-0.79)	0.76	0.13
MPR	3.47(2.90-3.75)	↔	3.03(2.52-3.75)	↓↓	2.59(1.96-3.19)	↓↓	2.30(2.01-2.96)	0.072	0.42
Visual perfusion defects n(%)	0		21/75(28%)		51(100%)		41(82%)	**0.002***	**0.001***
Diffusion Tensor									
FA	0.34(0.33-0.36)	↓	0.32(0.30-0.33)	↓↓	0.28(0.25-0.30)	↓↓	0.28(0.26-0.29)	**<0.001***	0.93
MD, $10^{-3}mm^2/s$	1.46(1.44-1.49)	↑	1.50(1.47-1.54)	↑↑	1.55(1.52-1.59)	↑↑	1.58(1.55-1.63)	**<0.001***	0.057
|E2A|, °	41.6(34.9-47.2)	↑	49.5(43.7-54.4)	↑↑	60.3(56.0-64.1)	↑↑	64.4(58.7–66.5)	**<0.001***	**0.011**

Table 5. Diffusion tensor and quantitative perfusion parameters compared between the four cohorts

A Bonferroni correction would require a p-value of 0.0036 to declare statistical significance at a nominal type 1 error rate of 0.05 (0.05/14* - remains significant after Bonferroni correction. Arrows indicate comparison with healthy volunteers.

	Subclinical HCM (G+LVH-) (G+LVH-) n=77		Genotype Positive HCM (G+LVH+) (n=51)	p-value
Demographics				
Age, years	31(23-40)	↑	52(37-59)	**<0.001**
Female n(%)	46(60)	↓	16(31)	**0.002**
BSA, m^2	1.9±0.2		1.9±0.2	0.1
BMI kg/m2	25(22-28)		25(24-28)	0.29
White, n(%)	64(83)		43(84)	0.95
Volumes & Mass				
LVEDV index, ml/m^2	83±14	↓	72±11	**<0.001**
LVEF, %	71(67-74)	↑	79(74-83)	**<0.001**
MWT, mm	9.6(8.6-10.6)	↑	17.2(15.4-21.1)	**<0.001**
LV Mass index g/m^2	51(43-60)	↑	77(67-92)	**<0.001**
Tissue Characterization				
ECV septum, %	27.2(25.3-29.7)	↑	30.0(27.1-33.8)	**<0.001**
LGE, present	6(8%)	↑	47(92%)	**<0.001**
LGE mass, g	0(range: 0-3.8)	↑	7.7(2.4-14.9)	**<0.001**
Microvascular disease				
Stress MBF ml/g/min	2.46±0.54	↓	1.77±0.52	**<0.001**
Rest MBF ml/g/min	0.80(0.66-0.93)	↓	0.69(0.59-0.83)	**0.036**
MPR	3.03(2.52-3.75)	↓	2.59(1.96-3.19)	**0.003**
Visual perfusion defects n(%)	21/75(28%)	↑	51(100)	**<0.001**
Diffusion Tensor				
FA	0.32(0.30-0.33)	↓	0.28(0.25-0.30)	**<0.001**
MD, $10^{-3}mm^2/s$	1.50(1.47-1.54)	↑	1.55(1.52-1.59)	**<0.001**
|E2A|, °	49.5(43.7-54.4)	↑	60.3(56.0-64.1)	**<0.001**

Table 6. Comparison of Demographics and CMR, quantitative perfusion & diffusion tensor parameters between G+LVH- vs G+LVH+

PARTICIPANT NO.	SUBGROUP	GENE	NUCLEOTIDE SUBSTITUTION	AMINOACID SUBSTITUTION	ACMG (23) CLASSIFICATION
1	G+LVH-	TNNT2	304C>T	Arg102Trp	P
2	G+LVH-	MYH7	2167C>T	Arg723Cys	P
3	G+LVH-	MYH7	1207C>T	Arg403Trp	P
4	G+LVH-	MYBPC3	1405C>T	Gln469Ter	P
5	G+LVH-	MYBPC3	3163A>T	Lys1055*	LP
6	G+LVH-	MYBPC3	3330+5G>C	N/A	P
7	G+LVH-	MYBPC3	1898-23A>G	N/A	LP
8	G+LVH-	MYBPC3	1898-23A>G	N/A	LP
9	G+LVH-	MYBPC3	2373dupG	Trp792ValfsX41	P
10	G+LVH-	MYBPC3	2373dupG	Trp792ValfsX41	P
11	G+LVH-	MYBPC3	1504C>T	Arg502Trp	P
12	G+LVH-	MYBPC3	1227-13G>A	N/A	P
13	G+LVH-	MYBPC3	2827C>T	Arg943Ter	P
14	G+LVH-	MYBPC3	1624G>C	Glu542Gln	P
15	G+LVH-	MYBPC3	927-2A>G	N/A	LP
16	G+LVH-	TNNT2	304C>T	Arg102Trp	P
17	G+LVH-	MYBPC3	3491-2A>T	N/A	P
18	G+LVH-	MYBPC3	2371C>T	Gln791Ter	P
19	G+LVH-	MYBPC3	1224-19G>A	N/A	P
20	G+LVH-	MYBPC3	c.2950C>T	Gln984*	LP
21	G+LVH-	MYBPC3	305delCinsTGAGG	Pro102Leufs*12	LP
22	G+LVH-	MYBPC3	3476_3479dup	Pro1161Tyrfs*9	LP
23	G+LVH-	MYH7	2162G>A	Arg721Lys	P
24	G+LVH-	MYH7	1231G>A	Val411Ile	P
25	G+LVH-	MYBPC3	2864_2865delCT	Pro955Argfs*95	P
26	G+LVH-	MYH7	1988G>A	Arg663His	P
27	G+LVH-	MYBPC3	1624+4A>T	N/A	P
28	G+LVH-	MYBPC3	772G>A	Glu258Lys	P
29	G+LVH-	MYBPC3	1227-13G>A	N/A	P
30	G+LVH-	MYBPC3	927-2A>G	N/A	LP
31	G+LVH-	MYH7	1750G>A	Gly584Ser	P
32	G+LVH-	MYBPC3	1628delA	Lys543Argfs*12	LP
33	G+LVH-	TNNI3	433C>T	Arg145Trp	P
34	G+LVH-	TNNI3	470C>T	Ala157Val	LP
35	G+LVH-	MYBPC3	3330+5G>C	N/A	P
36	G+LVH-	MYH7	1207C>T	Arg403Trp	P
37	G+LVH-	TNNI3	433C>T	Arg145Trp	P
38	G+LVH-	MYH7	1816G>A	Val606Met	P
39	G+LVH-	TNNT2	304C>T	Arg102Trp	P
40	G+LVH-	MYL2	260G>C	Gly87Ala	LP
41	G+LVH-	MYBPC3	3181C>T	Gln1061*	P
42	G+LVH-	MYBPC3	2373dupG	Trp792ValfsX41	P
43	G+LVH-	MYH7	2389G>A	Ala797Thr	LP
44	G+LVH-	MYBPC3	1504C>T	Arg502Trp	P
45	G+LVH-	MYH7	2539A>G	Lys847Glu	P
46	G+LVH-	MYH7	2717A>G	Asp906Gly	P
47	G+LVH-	MYH7	1711G>A	Gly571Arg	LP
48	G+LVH-	MYBPC3	1504C>T	Arg502Trp	P
49	G+LVH-	MYH7	4259G>A	Arg1420Gln	LP
50	G+LVH-	MYBPC3	3163a>t	Lus1055*	P
51	G+LVH-	TNNT2	853C>T	Arg278Cys	LP
52	G+LVH-	MYBPC3	3163a>t	Lus1055*	P
53	G+LVH-	TNNI3	586G>A	Asp196Asn	P

54	G+LVH-	MYBPC3	3163a>t	Lus1055*	P
55	G+LVH-	MYBPC3	497delIT	Val166fs	P
56	G+LVH-	TNNI3	485G>A	Arg162Gln	P
57	G+LVH-	MYBPC3	3293G>A	Trp1098*	P
58	G+LVH-	MYH7	2162G>A	Arg721Lys	P
59	G+LVH-	MYBPC3	578A>G	Gln193Arg	P
60	G+LVH-	MYBPC3	2373dupG	Trp792ValfsX41	P
61	G+LVH-	MYH7	1063G>T	Ala355Ser	P
62	G+LVH-	MYH7	427C>T	Arg143Trp	P
63	G+LVH-	CSRP3	131T>C	Leu44Pro	LP
64	G+LVH-	MYBPC3	1484G>A	Arg495Gln	P
65	G+LVH-	MYH7	221G>C	Gly741Arg	P
66	G+LVH-	MYBPC3	1624G>C	Glu542Gln	P
67	G+LVH-	MYBPC3	2905+1G>A	N/A	P
68	G+LVH-	MYBPC3	1624G>C	Glu542Gln	P
69	G+LVH-	MYH7	2609G>A	Arg870His	P
70	G+LVH-	TNNT2	311C>T	Ala104Val	P
71	G+LVH-	TPM1	574G>A	Glu192Lys	P
72	G+LVH-	MYBPC3	772G>A	Glu258Lys	P
73	G+LVH-	MYBPC3	655G>C	Val219Leu	P
74	G+LVH-	MYBPC3	821+3G>T	N/A	LP
75	G+LVH-	MYBPC3	1504C>T	Arg502Trp	P
76	G+LVH-	MYBPC3	772G>A	Glu258Lys	P
77	G+LVH-	MYBPC3	Deletion exon 1 to 12	N/A	P

78	G+LVH+	MYBPC3	1224-52G>A	N/A	P
79	G+LVH+	TNNI3	c.485>C	Arg162Pro	P
80	G+LVH+	MYBPC3	1624+4A>T	N/A	P
81	G+LVH+	MYH7	427C>T	Arg143Trp	P
82	G+LVH+	MYH7	1207C>T	Arg403Trp	P
83	G+LVH+	MYH7	4130C>T	Thr1377Met	P
84	G+LVH+	MYBPC3	2373_2374insG	Trp792Valfs*41	P
85	G+LVH+	MYBPC3	2780_2781delCA	Thr927Ilefs*123	P
86	G+LVH+	MYBPC3	927-2A>G	N/A	LP
87	G+LVH+	TNNI3	470C>T	Ala157Val	P
88	G+LVH+	TNNI3	592C>G	Leu198Val	P
89	G+LVH+	MYH7	2080C>T	Arg694Cys	LP
90	G+LVH+	MYH7	2606G>A	Arg869His	P
91	G+LVH+	MYBPC3	1624G>C	Glu542Gln	P
92	G+LVH+	MYBPC3	2905+1G>A	N/A	P
93	G+LVH+	MYH7	2389G>A	Ala797Thr	P
94	G+LVH+	TNNT2	487_489delGAG	Glu163del	P
95	G+LVH+	TNNI3	407G>A	Arg136Gln	P
96	G+LVH+	MYBPC3	126G>A	Trp42*	LP
97	G+LVH+	MYBPC3	1236dup	Glu413Ter	P
98	G+LVH+	TNNC1	c.23C>T	Ala8Val	P
99	G+LVH+	MYH7	2302G>A	Gly768Arg	P
100	G+LVH+	MYBPC3	c.3697C>T	Gln1233*	P
101	G+LVH+	MYBPC3	1927+600C>T	N/A	LP
102	G+LVH+	MYBPC3	772G>A	Glu258Lys	P
103	G+LVH+	MYBPC3	1504C>T	Arg502Trp	P
104	G+LVH+	MYH7	4066G>A	Glu1356Lys	P
105	G+LVH+	MYH7	1063G>T	Ala355Ser	P
106	G+LVH+	MYH7	2681A>G	Glu894Gly	LP

107	G+LVH+	TNNT2	862C>T	Arg278Cys	P
108	G+LVH+	MYBPC3	1224-52G>A	N/A	P
109	G+LVH+	MYBPC3	2221G>C	Gly741Arg	P
110	G+LVH+	MYBPC3	1224-52G>A	N/A	P
111	G+LVH+	MYBPC3	2827C>T	Arg943Ter	P
112	G+LVH+	TNNT2	517G>A	Glu173Lys	P
113	G+LVH+	MYBPC3	1227-13G>A	N/A	LP
114	G+LVH+	MYH7	2389G>A	Ala797Thr	P
115	G+LVH+	MYBPC3	215delG	Gly72Alafs*24	LP
116	G+LVH+	TNNT2	275G>A	Arg92Gln	P
117	G+LVH+	MYBPC3	1224-19G>A	N/A	P
118	G+LVH+	MYBPC3	772G>A	Glu258Lys	P
119	G+LVH+	MYH7	1544T>C	Met515Thr	LP
120	G+LVH+	MYBPC3	1224-52G>A	N/A	P
121	G+LVH+	MYBPC3	3751T>C	Tyr1251His	LP
122	G+LVH+	MYBPC3	2373dupG	Trp792ValfsX41	P
123	G+LVH+	MYBPC3	747C>A	Cys249*	P
124	G+LVH+	CSRP3	449G>A	Cys150Tyr	LP
125	G+LVH+	MYBPC3	c.1504C>T	Arg502Trp	P
126	G+LVH+	MYH7	2609G>A	Arg870His	P
127	G+LVH+	MYBPC3	1224-52G>A	N/A	LP
128	G+LVH+	MYBPC3	1484G>A	Arg495Gln	LP

Table 7. List of pathogenic/likely pathogenic variants in genotype positive participants, ACMG- American College of Medical Genetics

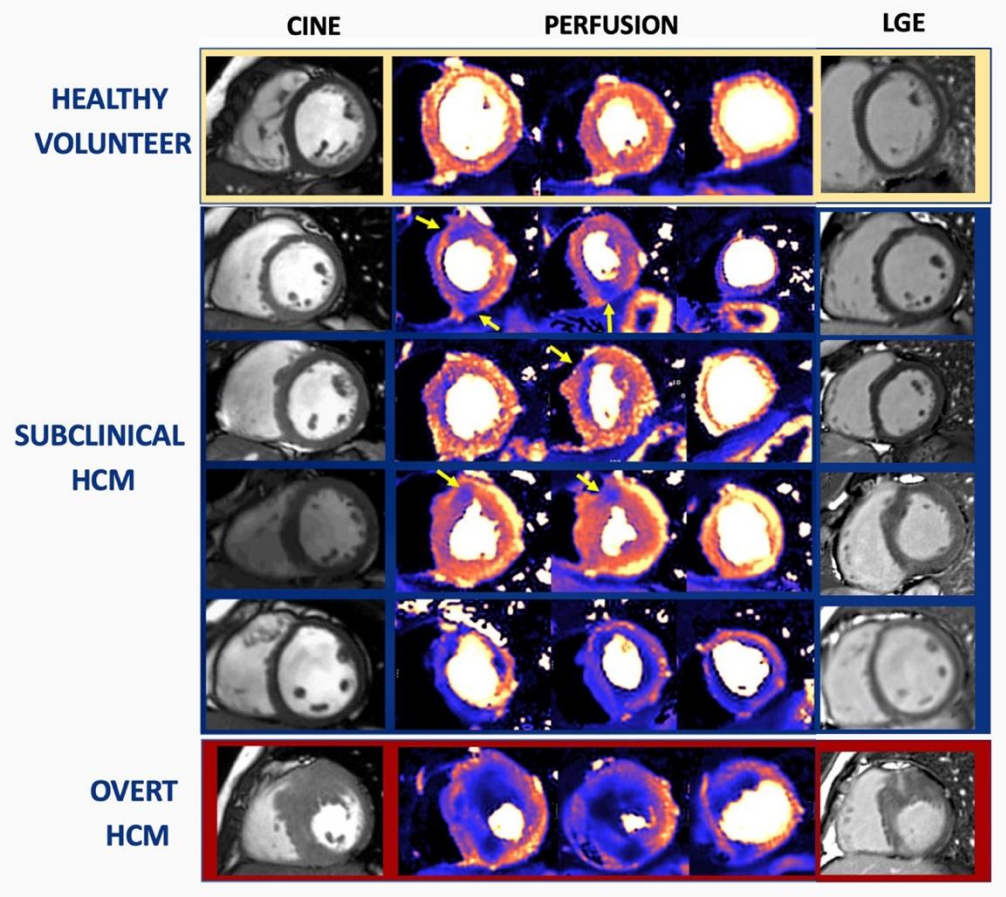

Figure 23: Perfusion defects in HCM
Perfusion defects (indicated by yellow arrows) detected by quantitative perfusion as phenotype develops: subclinical HCM (sarcomere mutation carriers without hypertrophy): 28% prevalence of perfusion defect. Note the absence of scar (and when present, scar is minimal). In overt disease, ischaemia extends beyond scar (inducible ischaemia) and in G+LVH+, there is 100% prevalence. LGE – late gadolinium enhancement, HCM – hypertrophic cardiomyopathy

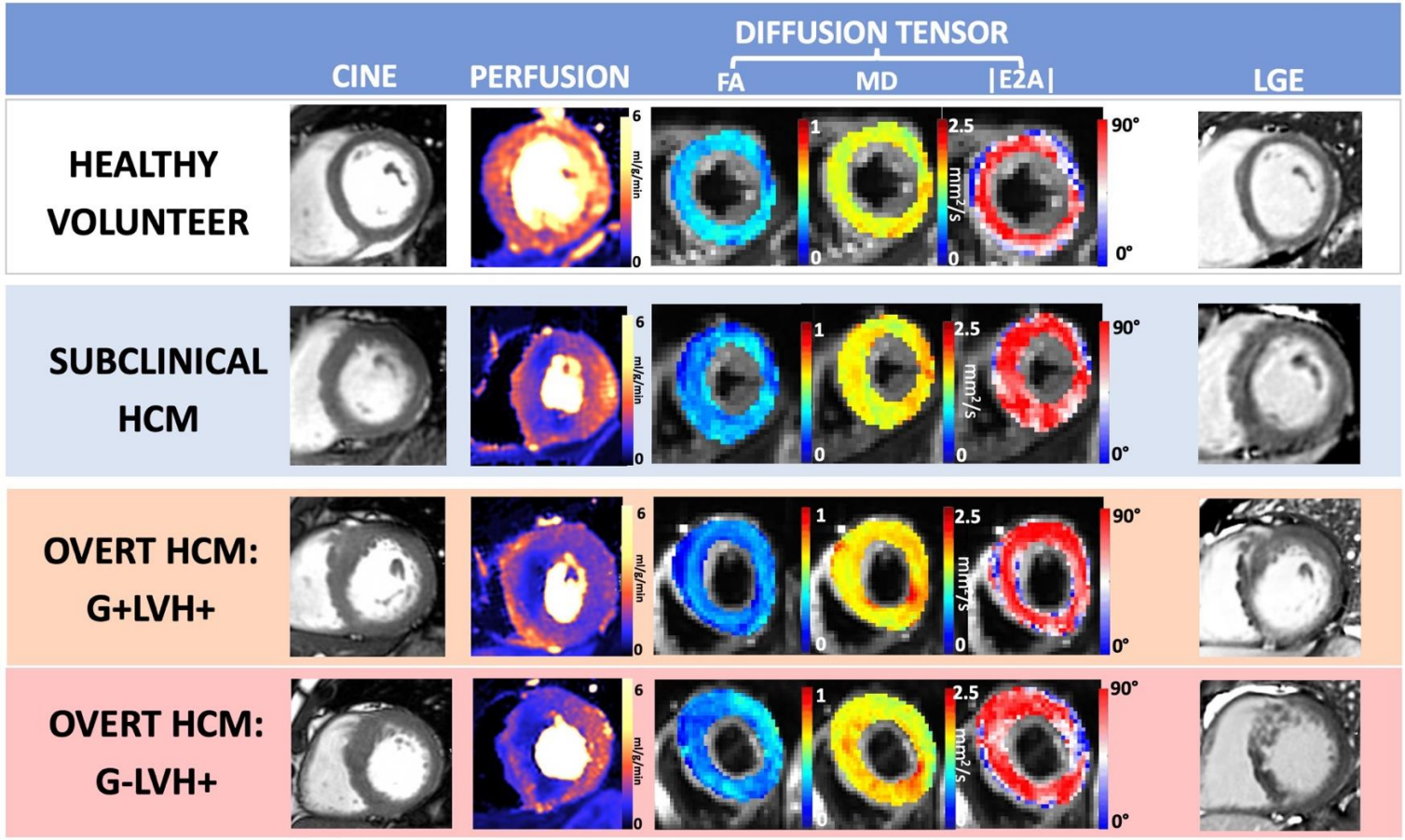

Figure 24. Abnormalities in perfusion and diffusion tensor parameters (low FA, high MD, high |E2A|) occurring in the absence of hypertrophy in subclinical HCM (G+LVH-) and more severely in overt disease (G+LVH+ & G-LVH+)
FA – Fractional Anisotropy, MD – Mean Diffusivity, |E2A| – Second Eigenvector Angle, LGE – late gadolinium enhancement, G+/-, genotype positive/negative, LVH+/- left ventricular hypertrophy positive/negative

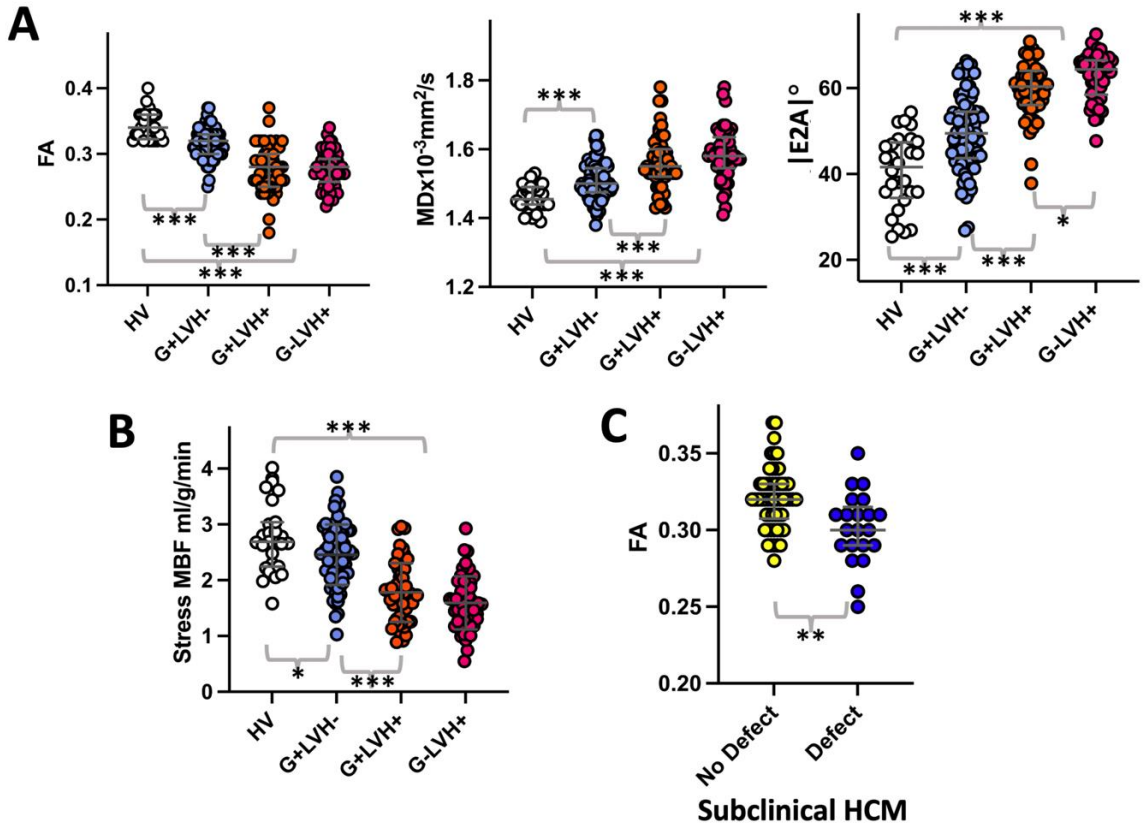

Figure 25. Global quantitative perfusion and DTI parameters between the four cohorts and those with and without perfusion defects in subclinical HCM.

A) Diffusion tensor parameter changes are detectable in subclinical HCM (G+LVH-) and measure more severely in overt disease. Genotype negative HCM (G-LVH+) is characterised by elevated |E2A| compared to genotype positive HCM (G+LVH+). **B)** Stress MBF, reflecting MVD, is reduced in subclinical HCM and more severely in overt disease **C)** Subclinical HCM with perfusion defects had lower FA (suggestive of more disarray) compared to subclinical HCM without perfusion defects. HV – healthy volunteers, G, genotype, LVH, left ventricular hypertrophy, FA, fractional anisotropy, MD, mean diffusivity, |E2A|, second eigenvector angle, MPR, myocardial perfusion reserve. *p<0.05, **p<0.01, ***p<0.001

CHAPTER 6. RESULTS iii. Detection of electrophysiological abnormalities in HCM

The manuscript "Joy, G, Lopes, L, …Captur G. Electrophysiological Characterization of Subclinical and Overt Hypertrophic Cardiomyopathy by Magnetic Resonance Imaging-Guided Electrocardiography. *J Am Coll Cardiol.* 2024" is based on the following chapter.

We hypothesized that ECGI would detect i) subtle EP abnormalities in subclinical HCM and ii) EP abnormalities in overt disease relate to genetic status (G+ vs G-LVH+) and structural changes (maximal wall thickness [MWT], late gadolinium enhancement [LGE]). We compared findings to 12-lead ECG changes and conventional risk markers (NSVT and sudden cardiac death risk).

200 participants were prospectively studied: 70 G+LVH- subjects, 104 LVH+ patients (51 G+LVH+, 53 G-LVH+) and 26 healthy volunteers (HV). Likely pathogenic/pathogenic variants for **G+LVH-** were present in the following genes: 41(59%) *MYBPC3*, 16(23%) *MYH7*, 5(7%) *TNNI3*, 4(6%) *TNNT2*, 1(1%) *MYL2*, 1(1%) *CSRP3*, 1(1%) *ACTC1*, 1(1%) *TPM1* and for **G+LVH+:** 28(55%) *MYBPC3*, 13(25%) *MYH7*, 4(8%) *TNNI3*, 4(8%) *TNNT2*, 1(2%) *TNNC1*, 1(2%) *CSRP3*.

6.1. Clinical Characteristics

***Subclinical HCM (G+LVH-) vs HV**:* Compared to HV, G+LVH- had similar age, sex, ethnicity and body surface area (BSA). G+LVH- had similar LV cavity size and myocardium (MWT, LV mass, ECV and LGE) but more hyperdynamic function.

G+LVH+ vs G+LVH-: Compared to G+LVH-, G+LVH+ had similar BSA but were older, more male and with smaller cavity sizes, more abnormal myocardium (higher MWT, LV mass, ECV and LGE) and higher ejection fraction.

G-LVH+ vs G+LVH+: Compared to G+LVH+, G-LVH+ had similar sex and BSA but were older with similar LV cavity sizes, function, MWT but greater LV mass, lower ECV but similar LGE (**Table 8**).

6.2. 12-Lead ECG

Subclinical HCM (G+LVH-) vs HV: Compared to HV, G+LVH- had shorter QRS intervals but otherwise similar electrical intervals, QRS amplitudes and QT dispersion. G+LVH- had a higher prevalence of ECG abnormalities (30%[21] vs 4%[1] p=0.014).

G+LVH+ vs G+LVH-: Compared to G+LVH-, G+LVH+ had similar heart rates, longer QRS and QTc intervals, greater QT dispersion and greater Cornell amplitude (but similar Sokolow-Lyon). G+LVH+ also had a higher prevalence of ECG abnormalities including T-wave inversion (TWI), LVH by either ECG voltage criteria and ST depression.

G-LVH+ vs G+LVH+: Compared to G+LVH+, G-LVH+ had longer QTc intervals, higher average QRS amplitudes and a higher prevalence of LVH by either ECG voltage criteria. Other 12-lead ECG intervals and prevalence of ECG abnormalities were similar (QRS duration was longer but not after correction for multiple comparisons) (**Table 8).**

6.3. ECGI

G+LVH- vs HV: Compared to HV, G+LVH- had slower ventricular conduction (more prolonged AT). Differences persisted after adjusting for age, sex, QRS duration and the presence of abnormal ECG (β=0.43, 95% confidence interval 0.22, 0.64, p<0.001).

Compared to HV, G+LVH- with a normal 12-lead ECG (*n*=49) also had slower ventricular conduction (prolonged AT (39(35-45) vs 35(31-41)ms, *p*=0.007). There were no differences in repolarization duration (RTc/ARIc) or activation/repolarization dispersion (ΔAT/ΔRTc). G+LVH- had more spatially heterogenous repolarization (steeper G_{RTc}: **Figure 27**, **Table 9**) but ventricular conduction was not different in spatial heterogeneity (similar G_{AT}). There were no differences in signal amplitudes or fractionation.

G+LVH+ vs G+LVH-: Compared to G+LVH-, G+LVH+ had prolonged ventricular repolarization (elevated ARIc and RTc) and differences persisted after adjusting for age, sex and QTc (ARIc: *β*=0.32, 95% confidence interval [CI]: 0.18-0.46, *p*<0.001; RTc: *β*=0.33 95%, CI: 0.19-0.47, *p*<0.001) (**Figure 26**). All other ECGI parameters were similar.

G-LVH+ vs G+LVH+: Compared to G-LVH+, G+LVH+ had more signal fractionation (**Figure 28**) but all other global and local ECGI parameters were similar.

G+LVH+ vs matched healthy volunteers: To compare ECGI changes in G+LVH+ to health-, age-, sex- and ethnicity-matched controls, an older HV cohort was studied (n=23). Compared to older HV, G+LVH+ were similar in age (G+LVH+ vs HV respectively: 52(37-59) vs 44(37-55) years, *p*=0.48), sex (35 males (69%) vs 15(65%), *p*=0.77) and ethnicity (43 White (84%) vs 19(83%), *p*=0.85). G+LVH+ had similar AT but greater AT dispersion, more fractionation, prolonged ventricular repolarization (elevated ARIc and RTc) and more spatially heterogenous repolarization (elevated G_{RTc}) (**Table 10**).

ECGI relationships in pooled HV (including older controls, n=37)

Age was associated with mean AT (r_S=0.37 [95% confidence interval: 0.04, 0.6] p=0.025) and inversely associated with mean G_{AT} (r_S=-0.37 [-0.05, -0.6] p=0.023). Age inversely associated with repolarization duration (ARIc: r_S=-0.32 [-0.009,-0.6] p=0.05; RTc: r_S=-0.35 [-0.01, -0.6] p=0.039) and inversely associated with G_{RTc} (r_S=-0.39 [-0.07, -0.6] p=0.017).

Male sex was associated with mean AT (r_S=0.35 [0.02, 0.6] p=0.033), and inversely with repolarization duration (ARIc: r_S=-0.44 [-0.1, -0.7] p=0.007; RTc: r_S=-0.50 [-0.2, -0.7] p=0.002). Male sex was inversely associated with mean G_{RTc} (r_S=-0.38 [-0.05, -0.6] p=0.022).

Ethnicity, BSA and BMI were not associated with any ECGI parameter.

Drugs and ECGI parameters.

68% (71) of participants with overt HCM were on at least one medication (including non-cardiac). Compared to those without medication, patients with overt HCM on medication were older (58(50-60) vs 48(32-48) years p<0.001) but were similar in terms of sex (p=0.81), BMI (p=0.13), ethnicity, MWT (p=0.09), LGE burden (p=0.71) and presence of LVOTO (p=0.46).

In order to explore whether overt HCM had ECGI changes without medication usage, we compared this group (n=33) to age-, sex- and ethnicity-matched healthy volunteers (n=22). Compared to matched HVs, overt HCM patients without medication were of similar age (overt HCM vs HV respectively: 48(32-58) vs 41(36-53) years p=0.34), sex distribution (21% female (7) vs 32% (7) p=0.38) and ethnicity (85% White (28) vs 82%(18) p=0.77). Compared to healthy volunteers, drug-free overt HCM had prolonged repolarization (longer ARIc and RTc) and greater maximal repolarization gradients. All other ECGI parameters were similar **(Table 11)**. Multiple linear

regression analyses were performed to ascertain whether any drug class (beta-blocker, calcium-channel blocker, disopyramide, amiodarone) had independent effects on ECGI parameters – no independent associations could be found.

LV Morphology and ECGI relationships

Compared to isolated basal LVH, reverse septal morphology had higher signal amplitude and more prolonged repolarization. Compared to Other morphology (defined as concentric or mixed apical LVH), reverse septal curvature had lower signal amplitude. Other morphology had higher signal amplitude, more prolonged activation and repolarization times compared to isolated basal septal LVH (**Table 12**).

Gene Specific Analysis: There were no differences in ECGI parameters between carriers of *MYH7* vs *MYBPC3* variants in both subclinical and overt disease. However, across all genotype positive participants (LVH+/LVH-), *MYBPC3* variant carriers had less fractionation than non-*MYBPC3* variants (p=0.007). Differences persisted after adjusting for age, sex, LGE volume and MWT (p=0.003). *MYBPC3* carriers also had significantly lower RTc (p=0.02) and G_{ATmax} (p=0.046) compared to non-*MYBPC3* variant carriers on univariate analysis, but these were attenuated in fully adjusted models.

6.4. ECG vs ECGI

Across all participants (n=200), AT was associated with QRS duration (r_s=0.28, p<0.001). ARIc and RTc were both associated with QTc (ARIc mean: r_s=0.72, p<0.001; RTc mean: r_s=0.73, p<0.001) and QT dispersion (ARIc: r_s=0.16, p=0.03; RTc: r_s=0.2, p=0.008). ΔRTc associated with QT dispersion (r_s=0.17, p=0.03).

6.5. ECG Structural Relationships

12-Lead ECG: In HV, MWT associated with QRS duration (r_S=0.56 p=0.006). In G+LVH-**,** MWT associated with QRS duration (r_S=0.42 p<0.001), PR interval (r_S=0.31 p=0.012) and Cornell but not Sokolow-Lyon amplitude (r_S=0.38 p=0.002). In overt HCM (all LVH+)**,** MWT associated with Cornell amplitude (r_S=0.34 p<0.001), presence of an abnormal ECG (r_S=0.39 p<0.001) and TWI (r_S=0.40 p<0.001). Also, LGE associated with PR interval (r_S=0.26 p=0.009), the presence of an abnormal ECG (r_S=0.39 p<0.001) and TWI (r_S=0.40 p<0.001).

6.6. ECGI Relationships to Risk Stratifiers

MWT: MWT associated with signal amplitude in HV (r_S=0.42 p=0.032), G+LVH- (r_S=0.26 p=0.028) and overt HCM (r_S=0.33 p<0.001). In G+LVH-, MWT associated with mean ARIc (r_S=0.24 p=0.046), and RTc (r_S=0.28, p=0.019). In Overt HCM, MWT associated with mean AT (r_S=0.25 p=0.011), ΔAT (r_S=0.32 p=0.001), ΔARIc (r_S=0.36 p<0.001) and mean RTc (r_S=0.26 p=0.007).

Scar burden: In overt HCM, LGE volume associated with fractionation (r_S=0.21 p=0.032) and local AT gradients ($G_{ATmean:}$ r_S=0.27 p=0.005).

LVOTO: 24(23%) of overt HCM patients had LVOTO. No ECGI changes were associated with LVOTO.

SCD Risk: To determine the relationship between ECGI abnormalities and surrogate markers of ventricular arrhythmia and risk in overt HCM, we describe a subgroup of 19 participants (18% of overt HCM) whom had an intermediate/high SCD risk score or NSVT. Compared to overt HCM not meeting such criteria, these patients were similar in age (p=0.29), sex (p=0.74) and ethnicity (White: p=0.8), but had a higher MWT (19.6 [17-23]mm vs 17.0 [15-21]mm, p=0.005), more LGE (15.1[8-28]g vs 5.5 [2-13]g, p<0.001) and more spatially heterogenous conduction (G_{Atmax} p=0.007). Other ECGI

parameters were similar. After adjustment for MWT and LGE volume, those with NSVT/intermediate-or-high risk score continued to exhibit more spatially heterogenous conduction (ß=0.29 95%CI: 0.1,0.5 p=0.006).

NSVT: 16(15%) of patients with overt HCM had NSVT. Compared to those without NSVT, these patients were similar in terms of age (*p*=0.07), sex (*p*=0.46) and ethnicity (*p*=0.46), but they had higher MWT (19.0(17-24)mm vs 13.5(10-18)mm *p*=0.01) and LGE volume (16.6(9-32)g vs 1.6(0-13)g, *p*<0.001) and more spatially heterogenous conduction (G_{ATmax}: *p*=0.012). Differences remained after adjustment for MWT and LGE volume (ß=0.026 [0.1, 0.5] *p*=0.016). **(Figure 29)**.

6.7 Machine Learning Classification of ECGI HCM subtypes

As expected, diagnostic cut-points for individual ECGI biomarkers tasked with discriminating subclinical HCM from controls were not sufficiently accurate, with the exception of max G_{RTc} and mean AT with accuracies of 73% [63–82%] and 79% [69–86%] respectively (**Table 13**). Therefore, we explored the use of supervised machine learning applied to the combined 12-biomarker ECGI electrotype in subclinical HCM and HV. This SVM differentiated subclinical HCM from HV with an AUC of 0.96 (bootstrap 95% confidence interval: 94–98%; sensitivity 100% [93–100%], specificity 91% [76–98%], positive predictive value [PPV] 96% [87–99%], negative predictive value [NPV] 100% [87–100%], balanced accuracy 95.7%, **Table 14 & 15, Figure 30**) and an accuracy of 80% after 10-fold cross-validation [73–85%]. This ECGI biomarker panel was able to identify HCM patients at greater risk of SCD (because of prior NSVT or intermediate/high ESC SCD risk status) compared to low-risk patients, with an AUC of 0.97 (bootstrap 95% CI: 96–98%; sensitivity 94% [71–99%], specificity 100% [95–

100%], PPV 100% [77–100%], NPV [99–93%], balanced accuracy 97.2%, **Table 14 & 16**) and an accuracy of 82% after 10-fold cross-validation [78–86%].

	HV (n=26)	G+LVH- (n=70)	G+LVH+ (n=51)	G-LVH+ (n=53)	*p*-value G+LVH- vs HV	G+LVH+ vs G+LVH-	G-LVH+ vs G+LVH+
Demographics							
Age, years	35(25-38)	36(25-41)	52(37-59)	59(50-66)	0.85	**<0.001**	**0.005**
Female, n(%)	14(54%)	41(59%)	17(33%)	8(15%)	0.68	**0.003**	0.09
White, n(%)	21(81%)	57(81%)	43(84%)	36(68%)	0.94	0.68	0.051
BSA, m^2	1.8±0.2	1.9±0.2	1.9±0.2	2.0±0.2	0.45	0.21	0.42
BMI, kg/m^2	24(22-27)	25(22-28)	25(24-28)	26(24-28)	0.24	0.65	0.5
Hypertension, n(%)	0	4(6%)	9(18%)	19(36%)	0.29	**0.029**	**0.035**
Diabetes, n(%)	0	0	2(4%)	0	>0.9	0.17	0.15
On lipid lowering, n(%)	0	0	6(12%)	16(30%)	>0.9	**0.005**	**0.021**
On anti-arrhythmic, n(%)	0	3(4%)	21(41%)	25(47%)	0.56	**<0.001**	0.54
Volumes & Mass							
LVEDV index, ml/m^2	89.3(74-109)	81.4(70-94)	71.0(63-80)	77.7(68-85)	0.07	**<0.001**	0.087
LVEF, %	65.9(63-69)	70.9(66-75)	77.7(73-83)	78.6(75-82)	**0.001**	**<0.001**	0.79
MWT, mm	9.3(8-11)	9.8(9-11)	17.0(15-21)	17.5(16-22)	0.24	**<0.001**	0.24
LV mass index, g/m^2	56.1(47-61)	51.5(43-62)	77.2(67-92)	101.6(82-127)	0.47	**<0.001**	**<0.001**
Tissue Characterization							
ECV, %	26.9(24-29)	27.1(25-30)	29.4(27-34)	26.8(25-30)	0.79	**<0.001**	**0.009**
LGE present, n(%)	0	7(10%)	47(92%)	51(96%)	0.09	**<0.001**	0.43
LGE mass, g	0	0(range:0-4)	8.4(3-15)	5.9(3-14)	0.1	**<0.001**	0.52
LGE mass %	0	0(range: 0-5)	4.9(2-11)	3.5(1-7)	0.12	**<0.001**	0.13
12-lead ECG: measures							
HR, bpm	67(60-75)	65(57-76)	66(56-72)	63(57-73)	0.52	0.59	0.59

QRS, ms	90(87-101)	86(80-94)	96(86-104)	98(92-108)	**0.005**	**<0.001**	**0.029**
PR, ms	160(138-175)	154(140-170)	165(147-181)	172(152-196)	0.58	0.065	0.13
QTc, ms	409±19	397±22	423±29	437±25	0.22	**<0.001**	**0.011**
QT dispersion, ms	48(24-62)	43(20-62)	58(38-77)	52(36-68)	0.62	**0.006**	0.35
Amp-Sokolow, mV	2.0(1.5-2.2)	2.0(1.6-2.7)	2.2(1.8-3.1)	3.0(2.3-4.5)	0.25	0.17	**<0.001**
Amp-Cornell, mV	1.2(0.9-1.5)	1.2(1.0-1.6)	2.1(1.3-2.7)	2.7(1.9-3.1)	0.55	**<0.001**	**0.001**
12-lead ECG: qualitative							
Abnormal ECG, n(%)	1(4%)	21(30%)	39(76%)	48(91%)	**0.014**	**<0.001**	0.052
Q waves, n(%)	1(4%)	14(20%)	14(27%)	14(26%)	0.07	0.36	0.91
TWI, n(%)	0	5(7%)	34(67%)	40(75%)	0.33	**<0.001**	0.32
LVH Voltage criteria, n(%)	0	6(9%)	19(37%)	34(64%)	0.33	**<0.001**	**0.006**
ST Depression, n(%)	0	0	20(39%)	30(57%)	>0.9	**<0.001**	0.076
RBBB, n(%)	0	0	1(2%)	3(6%)	>0.9	0.42	0.62
LBBB, n(%)	0	0	0	5(9%)	>0.9	>0.9	0.06

Table 8. Demographics, CMR and 12-lead ECG variables in healthy volunteers (HV), subclinical HCM (G+LVH-), gene variant positive HCM (G+LVH+) and gene variant negative HCM (G-LVH+).

Values are reported as median(interquartile range), mean±standard deviation or n(%). Amp, amplitude; BMI, body mass index; BSA, body surface area; ECV, extracellular volume; HR, heart rate; LVEDV, left ventricular end-diastolic volume; LGE, late gadolinium enhancement; LVH, left ventricular hypertrophy; MWT, maximal wall thickness; RBBB/LBBB, right/left bundle branch block; QTc, corrected QT; TWI, T-wave inversion

	HV (n=26)	G+LVH- (n=70)	G+LVH+ (n=51)	G-LVH+ (n=53)	p values G+LVH- vs HV	G+LVH+ vs G+LVH-	G-LVH+ vs G+LVH+
Conduction							
Amplitude, mV	1.4(1.1-1.6)	1.4(1.2-1.7)	1.6(1.2-1.9)	1.9(1.4-2.6)	0.4	0.42	0.12
Fractionation (n/1000)	8(0-22)	8(1-20)	13(2-27)	2(0-10)	0.99	0.13	**0.002**
Mean AT, ms	35(31-41)	39(35-45)	41(37-45)	42(38-47)	**0.008**	0.23	0.27
ΔAT, ms	174(153-196)	177(154-196)	183(162-208)	188(159-205)	0.89	0.25	0.76
mean G_{AT}, ms/mm	0.42(0.37-0.47)	0.40(0.31-0.49)	0.40(0.35-0.46)	0.44(0.30-0.56)	0.38	0.82	0.33
max G_{AT}, ms/mm	4.7(4.2-6.0)	4.9(4.2-5.6)	5.1(4.2-5.8)	5.1(4.3-6.4)	0.74	0.54	0.27
Repolarization							
Mean ARIc, ms	247±18	245±26	276±29	281±24	0.78	**<0.001**	0.29
ΔARIc, ms	180(159-197)	181(161-202)	183(162-208)	193(162-213)	0.62	0.62	0.63
Mean RTc, ms	285(274-297)	283(273-292)	322(296-340)	327(305-345)	0.55	**<0.001**	0.21
ΔRTc, ms	160(145-179)	164(147-183)	165(150-178)	170(149-193)	0.48	0.73	0.47
mean G_{RTc}, ms/mm	1.0±0.2	1.1±0.3	1.0±0.3	1.0±0.3	**0.042**	0.13	0.79
max G_{RTc}, ms/mm	9.5(9.0-11)	11.2(10-12.9)	11.3(9.9-12.7)	11.1(9.3-14.0)	**0.005**	0.79	0.92

Table 9. ECGI parameters in HV, subclinical HCM, G+LVH+ and G-LVH+.

Values are median(interquartile range) or mean±standard deviation. Amp, amplitude; AT, activation time; Δ, dispersion; max, maximum; RTc, repolarization time corrected for heart rate; ARIc, activation recovery interval corrected; G, gradient. Other abbreviations as in Table 1.

	HV (n=23)	G+LVH+ (n=51)	*p* value
Amp, mV	1.7(1.1-1.8)	1.6(1.2-1.9)	0.96
Fractionation (n/1000)	0(0-21)	13(2-27)	**0.003**
Mean AT, ms	39(34-43)	41(37-45)	0.28
ΔAT, ms	136(61-188)	183(162-208)	**<0.001**
Mean RTc, ms	272(261-281)	322(296-340)	**<0.001**
ΔRTc, ms	150(119-170)	165(150-178)	**0.023**
Mean ARIc, ms	232±21	276±29	**<0.001**
ΔARIc, ms	161(141-194)	183(162-208)	0.053
mean G_{AT}, ms/mm	0.39(0.25-0.46)	0.40(0.35-0.46)	0.07
max G_{AT}, ms/mm	4.7(3.9-5.9)	5.1(4.2-5.8)	0.37
mean G_{RTc}, ms/mm	0.9±0.3	1.0±0.3	**0.019**
max G_{RTc}, ms/mm	9.0(7.9-10.5)	11.3(9.9-12.7)	**<0.001**

Table 10. ECGI biomarkers in G+LVH+ vs matched healthy volunteers.

Values are median(interquartile range) or mean±standard deviation.
Amp, amplitude; AT, activation time; Δ, dispersion; G+LVH+, gene variant positive left ventricular hypertrophy positive; HV, healthy volunteer; max, maximum; RTc, repolarization time corrected for heart rate; ARIc, activation recovery interval corrected; G, gradient.

	Healthy Volunteers (n=22)	Drug-Free Overt HCM (n=33)	*p* value
Amp, mV	1.6(1.1-1.8)	1.6(1.2-1.9)	0.57
Fractionation (n/1000)	15(1-30)	7(1-25)	0.22
Mean AT, ms	40(33-43)	41(36-44)	0.36
ΔAT, ms	157(62-193)	180(152-194)	0.08
Mean RTc, ms	267(257-288)	317(298-343)	**<0.001**
ΔRTc, ms	153(126-174)	161(143-185)	0.31
Mean ARIc, ms	232±22	275±27	**<0.001**
ΔARIc, ms	171(153-203)	179(156-196)	0.88
mean G_{AT}, ms/mm	0.39(0.26-0.46)	0.36(0.30-0.41)	0.96
max G_{AT}, ms/mm	4.6(3.9-6.0)	4.7(4.2-5.3)	0.75
mean G_{RTc}, ms/mm	1.0(0.7-1.2)	1.0(0.8-1.2)	0.46
max G_{RTc}, ms/mm	9.1(8.3-10.6)	10.9(9.5-13.7)	**0.008**

Table 11. Drug-Free HCM vs matched healthy volunteers.

Values are median(interquartile range) or mean±standard deviation. Abbreviations as in Table 8.

	Isolated Basal Septal LVH (n=52)	Reverse Septal Curvature (n=37)	Other (Apical/Concentric) (n=15)	ANOVA	*p*-values Isolated basal LVH vs reverse septal curvature	*p*-values Isolated basal LVH vs Other	*p*-values Reverse septal curvature vs Other
Amp, mV	1.5(1.2-1.9)	1.8(1.4-2.4)	2.0 (1.7-2. 6)	**<0.001**	**0.009**	**<0.001**	**0.021**
Fractionation (n/1000)	5(0-22)	1(0-36)	1(0-25)	0.77			
Mean AT, ms	41(36-45)	41(38-45)	49(38-54)	**0.002**	0.203	**0.008**	0.11
ΔAT, ms	181(156-197)	196(162-213)	188(167-214)	0.38			
Mean RTc, ms	314(296-332)	330(314-347)	341(326-347)	**<0.001**	**0.009**	**<0.001**	0.25
ΔRTc, ms	159(145-184)	171(157-194)	171(163-180)	0.21			
Mean ARIc, ms	183±31	199±40	188±29	**0.013**	**0.019**	**0.014**	0.57
ΔARIc, ms	183(158-202)	197(173-225)	188(162-211)	0.093			
mean G_{AT}, ms/mm	0.40(0.30-0.49)	0.42(0.35-0.53)	0.40(0.32-0.56)	0.84			
max G_{AT}, ms/mm	5.1(4.3-5.8)	5.0(4.3-6.0)	5.0(4.2-6.4)	0.96			
mean G_{RTc}, ms/mm	1.01(0.86-1.19)	1.08(0.77-1.25)	1.01(0.82-1.24)	0.89			
max G_{RTc}, ms/mm	10.9(9.3-13.3)	11.5(9.6-13.5)	11.2(9.5-13.0)	0.9			

Table 12. Relationship between LV morphology and ECGI parameters

Values are median(interquartile range) or mean±standard deviation.
*Abbreviations as in **Table 10**, Other is mixed ASH-apical LVH or concentric LVH*

	Diagnostic ECGI cut-off points
Conduction Mean AT, ms	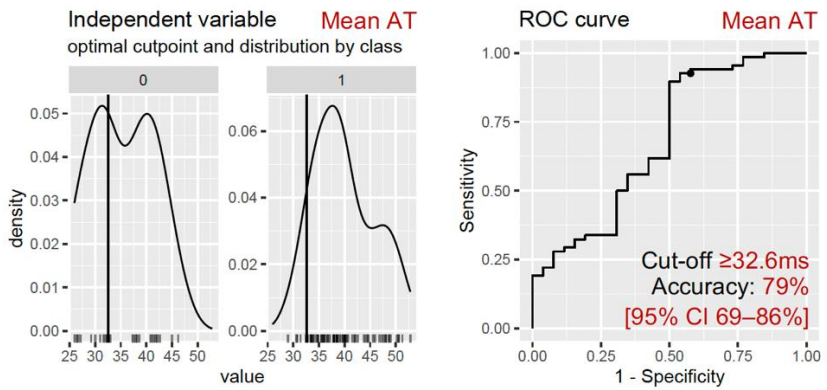
Repolarization Max G_{RTc}, ms/mm	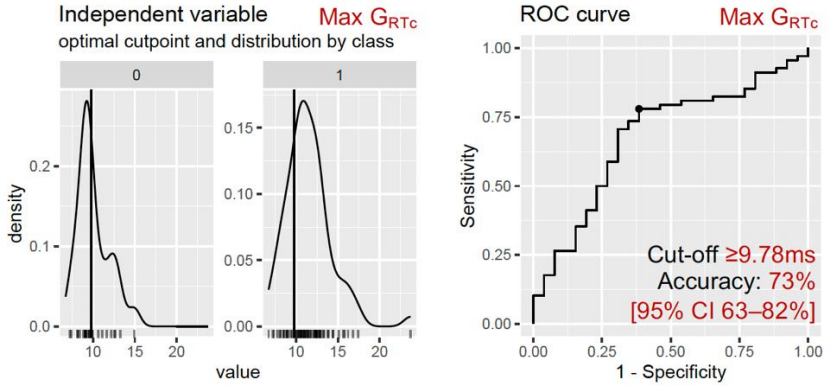

Table 13. ECGI biomarkers in G+LVH+ vs matched healthy volunteers.

Accuracy defined as = True Positive + True Negative / True Positive + True Negative + False Positive + False Negative.
Abbreviations as in Table

SVM model distinguishing subclinical HCM from controls			
	Control	**Subclinical HCM**	**Totals**
Test Positive	3	68	71
Test Negative	32	0	32
Totals	35	68	103
SVM model distinguishing NSVT+ or intermediate/high-risk from low-risk patients			
	Low-risk	**Intermediate/high-risk**	**Totals**
Test Positive	0	17	17
Test Negative	85	1	86
Totals	85	18	103

Table 14. Confusion matrices for the two final SVM models.

Ranked ECGI Parameter	Importance coefficient
Mean AT	0.306
Mean G_{RTc}	0.263
Fractionation	0.167
Max G_{RTc}	0.067
ΔAT	0.062
Max G_{AT}	0.062
Mean RTc	0.038
ΔARIc	0.017
ΔRTc	0.011
Mean Amplitude	0.005
Mean G_{AT}	0.002
Mean ARIc	0.001

Table 15. Contribution of each ECGI determinant to the predictive capacity of the subclinical vs control SVM model.

Ranked ECGI Parameter	Importance coefficient
Max G_{AT}	0.197
ΔAT	0.155
Mean AT	0.127
Mean ARIc	0.086
Mean G_{RTc}	0.077
Fractionation	0.076
ΔARIc	0.074
Mean G_{AT}	0.073
Max G_{RTc}	0.049
Mean Amplitude	0.035
ΔRTc	0.026
Mean RTc	0.025

Table 16. Contribution of each ECGI determinant to the predictive capacity of the low vs intermediate/high-risk HCM SVM model.

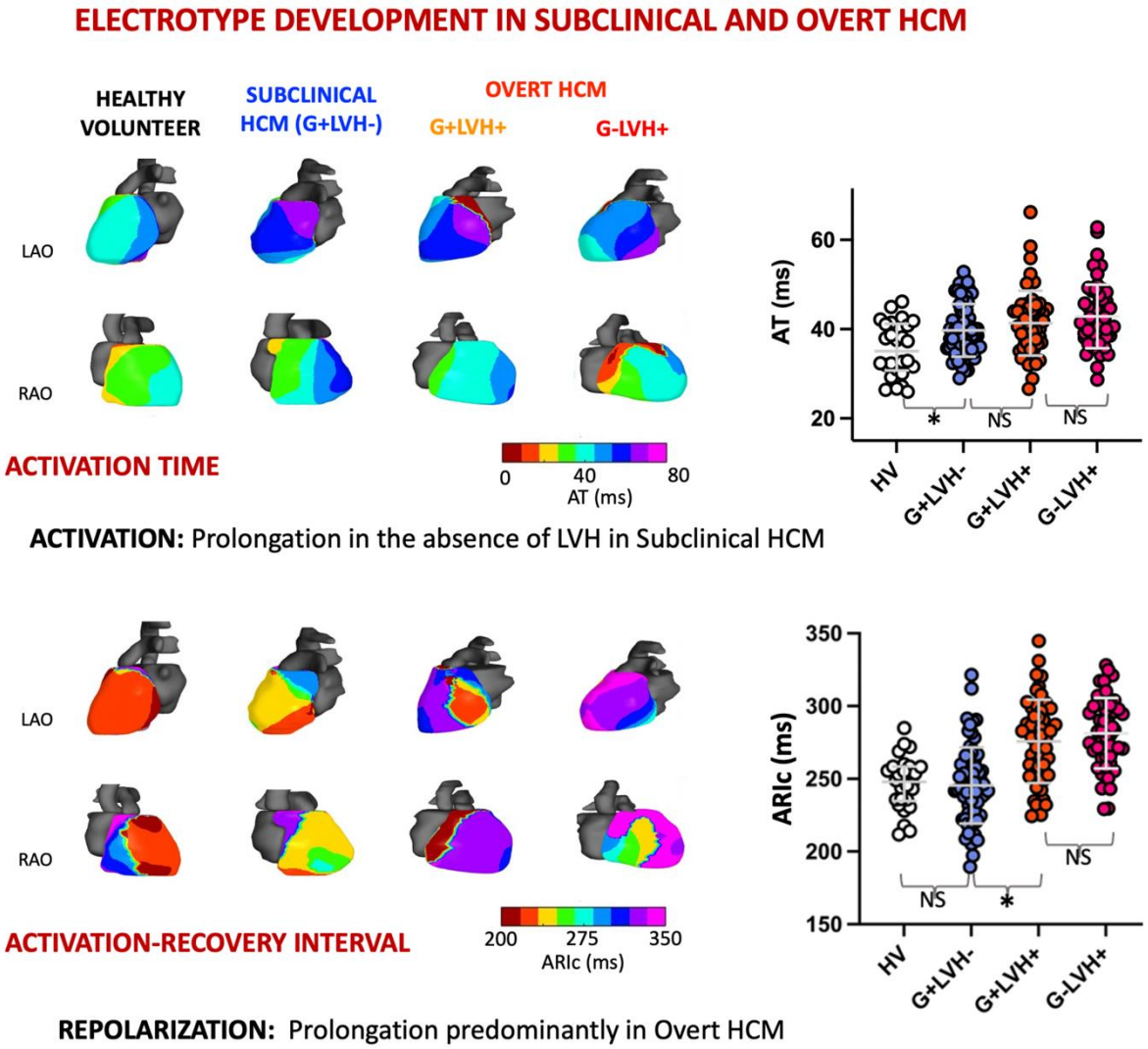

Figure 26. Exemplar AT and ARIc maps.
ECGI detects prolongation of activation even in the absence of LVH in subclinical HCM (G+LVH-). Prolongation of repolarization predominantly occurs in overt HCM (G+LVH+). *, statistically significant $p<0.05$, NS, non-significant.

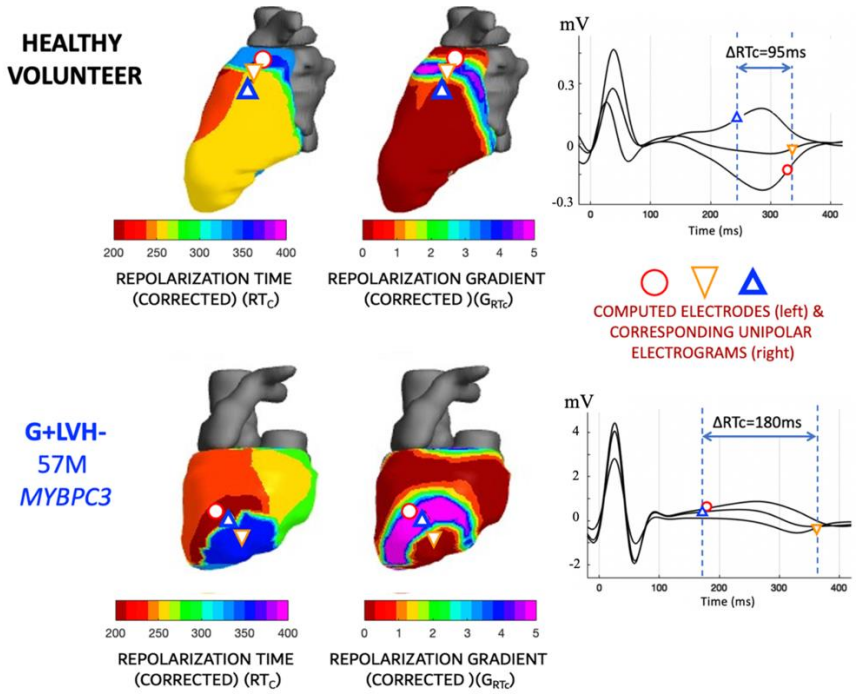

Figure 27. Repolarization Gradient maps.
ECGI identifies concealed repolarization gradients (G_{RT}) occurring in a healthy volunteer and more steeply in subclinical HCM (G+LVH-). **Left:** RTc maps and corresponding G_{RT} gradient maps are shown with superimposed shape labels showing computed electrodes; **Right:** Corresponding unipolar electrograms are shown for each of the three computed unipolar electrodes annotated across the gradient.

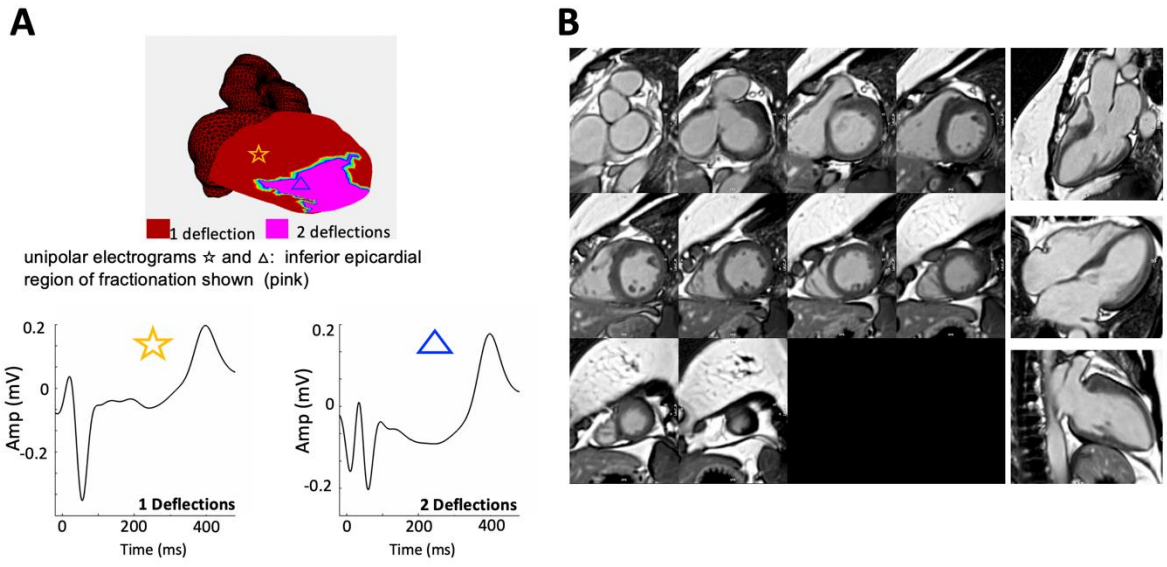

Figure 28. Exemplar fractionation maps in HCM.
(A) G+LVH+ HCM expressing a large region of signal fractionation in spite of no/minimal LGE (and mild LVH) by cardiovascular magnetic resonance imaging (**B**).

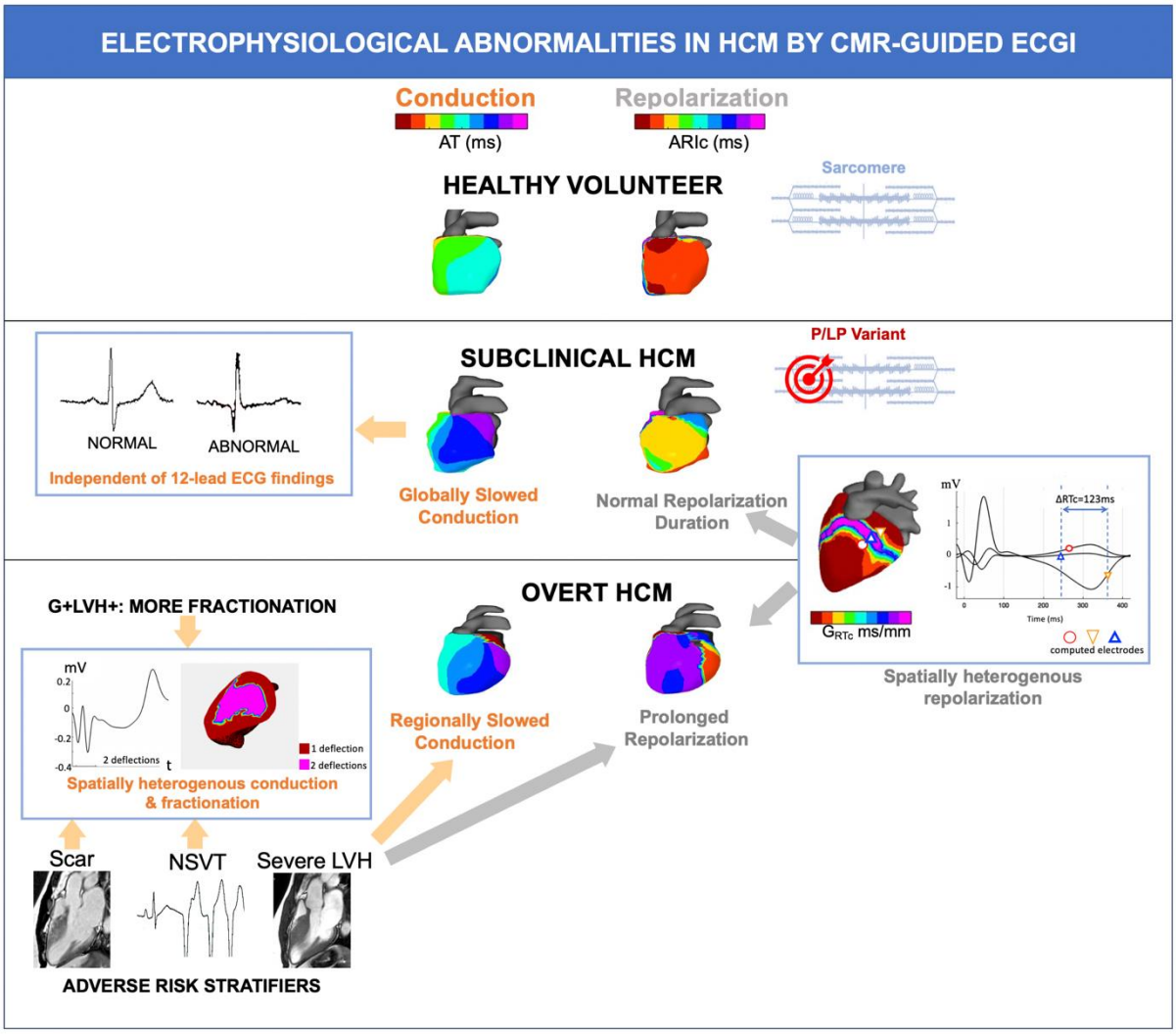

Figure 29. Summary of associations between ECGI and stage of phenotype evolution and associations with conventional markers of risk.

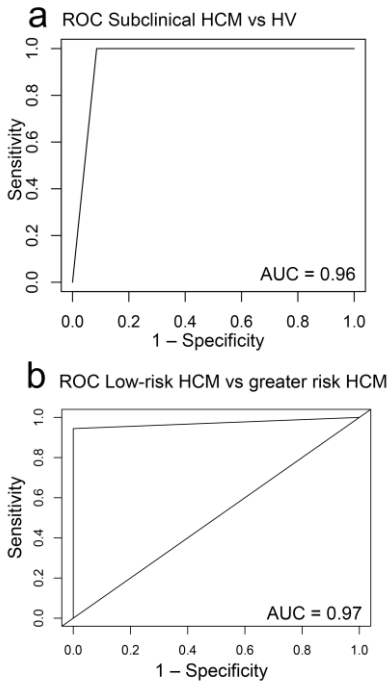

Figure 30. ECGI signature potentially distinguishes subclinical HCM from controls and identifies patients at greater risk of SCD.

ROC curve (**a**) showing the performance of the support vector machine supervised machine learning method applied to all combined ECGI biomarkers in distinguishing patients with subclinical HCM from healthy volunteers (2 subclinical HCM patients and 2 HV were excluded due to missing ECGI parameters). ROC curve (**b**) showing the ability of this ECGI electrotype to identify patients with HCM at intermediate/high risk for SCD or with prior documented NSVT from low-risk patients (1 overt HCM patient excluded due to missing ECGI parameters), with an accuracy of 99% (AUC 0.97, bootstrap 95% CI: 96–98%), which on 10-fold cross validation maintained a mean accuracy across the 10 folds of 82% [78–86%].

CHAPTER 7. RESULTS iv. Identifying sub-phenotypes of HCM using unsupervised learning

HCM is a heterogenous disease with variable expression, LV morphology and clinical outcome. In order to detect whether there are sub-phenotypes within HCM we performed agglomerative hierarchical clustering using advanced phenotyping variables (CMR DTI, quantitative perfusion and ECGI).

Analysis was performed on all HCM participants with complete DTI and ECGI datasets: [n=155: 61 subclinical (G+LVH-) and overt: 49 G+LVH+ / 45 G-LVH+]. Prior to hierarchical clustering of continuous CMR variables, missing data was imputed using the svdimpute function (pcaMethods package). Missing values are therefore imputed using regression with five eigenvectors as predicted. Redundant CMR metrics were eliminated by creating a correlation matrix and eliminating features where r >0.7. Therefore the following features were kept: **ECGI:** Fractionation, mean AT, G_{AT} mean and G_{AT} max, mean ARIc, ARIc dispersion (ARIc range), G_{RTc} mean, G_{RTc} max, MWT, FA, E2A and MPR. The final variables were standardized to mean=0 and standard deviation=1 prior to clustering.

Agglomerative hierarchical clustering was performed using the *hclust* function (stats package). The dissimilarity matrix was calculated using Euclidean distance and clusters were joined using Ward's method, which can separate clusters even in the presence of some noise. The optimal number of clusters was chosen using the NBclust function/package. This method chooses the optimal number of clusters by calculating 27 different cluster validity indices and selecting the final optimal number of clusters using the majority rule. All clustering was performed blinded to clinical data

(demographics, genotype, LVH thresholds, ECG, NSVT) and binary data such as the presence or absence of perfusion defects/ ECG abnormalities.

The amount of missingness of CMR data was 1% across all variables. Cluster validity indices calculated using advanced phenotyping showed that there were three optimal clusters. The dendogram and associated heatmap divided into these clusters are shown in **Figure 31.**

7.1. Deep phenotyping characteristics of clusters

Cluster 1: a benign phenotype without LVH, more preserved microvascular function and microstructure

Compared to other clusters, cluster 1 had lower MWT, preserved MPR, less microstructural alteration, (higher FA, lower E2A). This group had the lowest prevalence of perfusion defects (27% vs cluster 2: 81% and cluster 3 81% both $p<0.001$).

Mean AT was less than cluster 3 but similar to cluster 2. Fractionation was similar to cluster 3 but greater than 2 and conduction was less spatially heterogenous than 3 but similar to 2.

Mean ARIc was less than cluster 2 and 3 but global dispersion (ARIc range) was similar to cluster 3 and greater than 2. Conduction heterogeneity was similar to 3 and less than 2 **(Table 17, Figure 31)**.

Cluster 2: an intermediate phenotype with intermediate microvascular function, microstructural alteration and prolonged repolarization

Cluster 2 had established hypertrophy (high MWT), microvascular impairment (low MPR) and microstructural alteration (lower FA high E2A), and these were intermediate between 1 and 3.

Fractionation was less severe than both cluster 3 and cluster 1. Mean AT was similar to cluster 1 but there was less conduction heterogeneity than clusters 3 and 1. Repolarization was prolonged and similar to Cluster 3, but there was less repolarization dispersion and repolarization heterogeneity **(Table 17, Figure 31)**.

Cluster 3: severe phenotype with severe microvascular impairment, microstructural alteration and severely altered pro-arrhythmic ECGI changes

Cluster 3 had the most adverse microstructural, microvascular and EP phenotype. Compared to the other groups, there was more LVH, more microvascular impairment, more severe microstructural alteration. Activation time was prolonged and more spatially heterogenous, and repolarization was similar in duration to cluster 2 but more spatially heterogenous **(Table 17, Figure 31)**.

7.2. Clinical and demographics differences between clusters.

Cluster 1 were the youngest, more female and had a high prevalence of G+LVH- (only 3 had LVH). These had the lowest incidence of abnormal ECG and no participant with NSVT or a high ESC risk score. Cluster 2 were similar in age to Cluster 3. There was more G+LVH- participants in Cluster 2 compared to Cluster 3. Cluster 2 had a lower prevalence of ECG abnormality than Cluster 3. Cluster 3 had the lowest prevalence of G+LVH-. There was no difference in genotype positive and negative participants between clusters 2 and 3. Cluster 3 had the highest prevalence of ECG abnormality. There was no difference in the prevalence of NSVT or high ESC risk score between groups **(Table 18)**.

7.3. Reclassified subclinical HCM

Subclinical HCM that were reclassified to either Cluster 1 or 3 (n=20, 33%) were not older (p=0.9) and had no difference in MWT (9.5(8.-10.3) vs 10.3(9.0-11.9) p=0.094) but had more impaired MPR (2.6(2.3-3.2) vs 3.2(2.6-3.9) p=0.035), more microstructural alteration (FA: 0.30(0.29-0.31 vs 0.32(0.31-0.33)) p=0.002, E2A: 58.2(48.7-63.6) vs 45.0(41.5-49.9) p<0.001), more prolonged repolarization (ARIc: 250(241-267)ms vs 241(225-254)ms p<0.001) and more spatially heterogenous repolarization (G_{RTc} mean 1.2(1.1-1.3) vs 1.0(0.9-1.3) p=0.008). They did not have a higher prevalence of perfusion defects (40% vs 22% p=0.14) but did have a higher prevalence of abnormal ECG (50% vs 17% p=0.007). There was no difference in the prevalence of MYH7 vs MYBPC3 and thin vs thick filament mutations in those subclinical HCM that were reclassified.

	Cluster 1	Cluster 2	Cluster 3	P values		
	n=44	n=43	n=68	1vs2	2v3	1vs3
MWT	9.7(8.6-10.4)	15.7(11.7-17.2)	17.6(15.1-22.0)	**<0.001**	**<0.001**	**<0.001**
MPR	3.26(2.60-3.86)	2.77(2.31-3.25)	2.21(1.95-2.89)	**0.005**	**0.002**	**<0.001**
FA	0.32(0.31-0.33)	0.29(0.28-0.31)	0.28(0.25-0.29)	**<0.001**	**<0.001**	**<0.001**
E2A	45.2(42.3-49.8)	59.2(54.6-63.8)	62.9(57.3-65.5)	**<0.001**	0.056	**<0.001**
Mean AT	39(35-45)	31(36-44)	41(37-46)	0.53	0.16	**0.031**
Fractionation	12(2-36)	5(0-13)	13(1-36)	**0.013**	**0.008**	0.98
GATmean	0.41(0.33-0.50)	0.38(0.29-0.45)	0.43(0.33-0.57)	0.08	**0.006**	0.23
GATmax	4.8(4.4-5.5)	4.43(4.1-5.2)	5.6(4.6-6.6)	0.14	**<0.001**	**0.007**
Mean ARIc	241(226-254)	280(243-297)	272(253-293)	**<0.001**	0.89	**<0.001**
ARIc Range	188(178-205)	158(144-171)	201(183-218)	**<0.001**	**<0.001**	0.15
GRTcmean	1.2(1.1-1.4)	0.83(0.72-0.99)	1.1(1.0-1.3)	**<0.001**	**<0.001**	0.19
GRTcmax	11.4(10.1-13.3)	9.9(8.8-11.0)	12.4(10.4-14.5)	**<0.001**	**<0.001**	0.2

Table 17 - phenotypic clustering based on hypertrophy, microvascular function, microstructural alteration and ECG Imaging parameters.

MWT, maximum wall thickness, MPR, myocardial perfusion reserve, FA, fractional anisotropy, E2A, second eigenvector angle, AT activation time, G_{AT}, gradient of activation time, ARIc, activation recovery interval corrected, G_{RTc}, gradient of repolarization time corrected.

	Cluster 1	Cluster 2	Cluster 3	P values		
	n=44	n=43	n=68	1vs2	2v3	1vs3
Age	38(24-48)	48(35-57)	55(41-61)	**0.004**	0.06	**<0.001**
Female	25(57%)	15(34%)	17(25%)	**0.04**	**<0.001**	0.26
White	37(84%)	36(84%)	18(74%)	>0.9	0.21	0.19
G+LVH-	41(93%)	12(28%)	8(12%)	**<0.001**	**0.031**	**<0.001**
G+LVH+	2(5%)	17(40%)	30(44%)	**<0.001**	0.63	**<0.001**
G-LVH+	1(2%)	14(33%)	30(44%)	**<0.001**	0.23	**<0.001**
Abnormal ECG	7(15%)	29(67%)	59(87%)	**<0.001**	**0.014**	**<0.001**
NSVT	(0/3)	3/31(10%)	12/60(20%)	>0.9	0.21	0.39
ESC Risk score	(0/3)	2/31(6%)	8/60(13%)	>0.9	0.32	0.5
NSVT + ESC risk score	(0/3)	3/31(10%)	15/60(25%)	>0.9	0.082	0.32

Table 18. Clinical characteristics of each cluster

G+/-, genotype positive/negative, LVH+/-, left ventricular hypertrophy positive/negative, NSVT, non-sustained ventricular tachycardia, ESC, European society of cardiology.

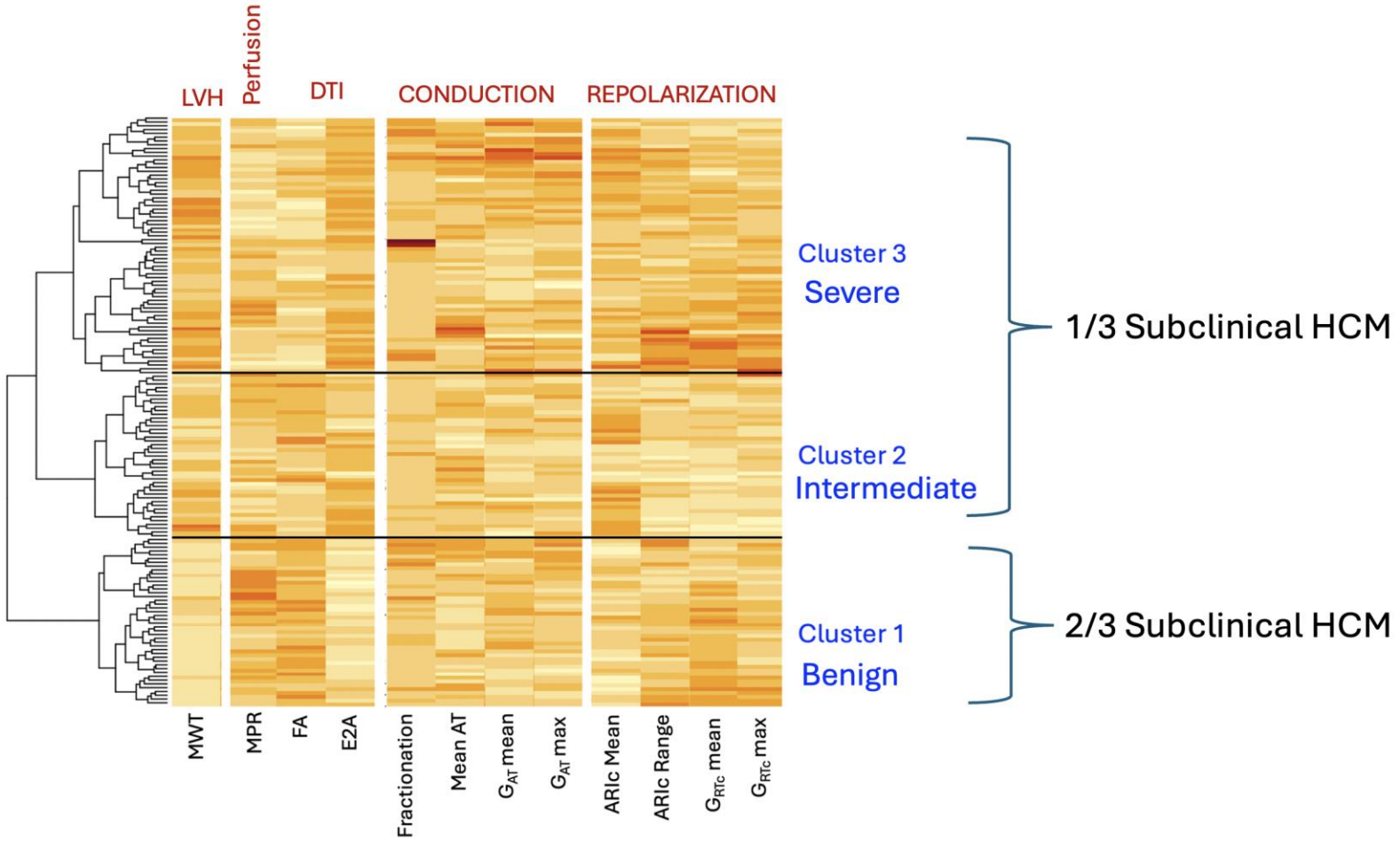

Figure 31. Heat map with dendrogram to show phenotypic clustering based on hypertrophy, microvascular function, microstructural alteration and ECG Imaging parameters

MWT, maximum wall thickness, MPR, myocardial perfusion reserve, FA, fractional anisotropy, E2A, second eigenvector angle, AT activation time, G_{AT}, gradient of activation time, ARIc, activation recovery interval corrected, G_{RTc}, gradient of repolarization time corrected

CHAPTER 8. DISCUSSION i. Microvascular function in physiological and pathological hypertrophy

8.1. Discussion

In this study exploring myocardial perfusion in conditions causing physiological (athletes) and pathological (hypertensives, subclinical HCM) hypertrophy, the main findings were i) hypertensives had more impaired perfusion compared to athletes but similar perfusion compared to controls ii) athletes had a higher myocardial perfusion reserve compared to healthy volunteers but required higher adenosine doses to achieve stress iii) subclinical HCM showed a lower MPR compared to health, comparable myocardial perfusion compared to hypertension and markedly reduced perfusion compared to athletes.

The enhanced microvascular function found in athletes compared to hypertensives and subclinical HCM show that microvascular remodelling likely differs in pathological vs physiological hypertrophy; both athletes, hypertensives and subclinical HCM had higher MWT compared to health. A small proportion of subclinical HCM in this group had perfusion defects, but this was never found in health, hypertensives or athletes. Findings support the hypothesis that microvascular function could potentially be used to discriminate between physiological and pathological myocardial states.

Interestingly extracellular volume did not differ between athletes and hypertensives and were higher than health in both, in contrast with prior work by Swoboda et al showing that athleticism results in lower ECV (135). This could in part reflect the older

(veteran) athletes in our cohort compared to prior published work, suggesting that possibly life-long exercise dose may play a role in fibrosis in athletes.

The findings relating to myocardial perfusion in athletes compared to health are more difficult to interpret. There is some indication that MPR is higher in athletes than non-athletes, however a higher adenosine dose was needed to achieve stress. The result is however maintained when included an unmatched young healthy volunteer cohort receiving high-dose adenosine after statistical corrections for age and adenosine dose. The statistical approach of using multiple regression in a small cohort is supported by the use of limited variables in the model as reported by Austin et al (130). Furthermore, prior work comparing quantitative perfusion in high-dose to standard dose adenosine showed no difference in those with preserved ejection fraction suggesting that adenosine dosing might not have influenced our results (114). Further work is required in external validation cohorts to confirm this finding.

Remodelling findings match prior literature (136). Interestingly mass-volume ratio was elevated in both athletes and subclinical HCM. This likely reflects differing processes with athletes experiencing more eccentric remodelling in response to prolonged exercise, whereas in subclinical HCM this may be more reflective of an asymmetric distribution of LV mass.

8.2. Limitations

Only male athletes have been studied. Adenosine stress does not physiologically reflect myocardial vasodilation during exercise. Those receiving high dose adenosine underwent a perfusion study using the FLASH sequence on a different scanner which could influence perfusion quantification, however these differences are within the variance of repeatability for perfusion (78). Epicardial coronary vasodilation was not assessed. Blood pressure was only measured in athletes and subclinical HCM.

Subclinical HCM were scanned on 3T but other cohorts on 1.5T. Medication use may influence perfusion results.

8.3. Conclusion

Quantitative perfusion is a possible discriminator cases for “grey-zone” pathological versus physiological LVH. Athletes require a higher adenosine dose to achieve physiological stress. Initial exploratory findings suggest athletes have enhanced myocardial vasodilation and pharmacological stress compared to health but further work is needed to confirm this on larger external cohorts.

CHAPTER 9. DISCUSSION ii: Microstructural and microvascular abnormalities in subclinical and overt HCM

9.1. Discussion

In the era of cascade genetic screening and emerging novel therapy, detection of phenotype development in subclinical HCM is an emerging priority. Study findings show that changes in diffusion tensor imaging and quantitative perfusion occur even in the absence of hypertrophy. DTI abnormalities in subclinical disease relate to ECG abnormalities and perfusion defects, showing the likely importance of disarray and microvascular disease in phenotype development.

Recent evidence suggests genotype positive vs genotype negative HCM are different in LV morphology and clinical outcomes (17,31,91). In overt disease with LVH, all genotype positive patients have perfusion defects with 18% of genotype negative having none. DTI abnormalities were unexpectedly more marked if gene negative (more elevated |E2A|). This suggests changes in DTI and quantitative perfusion are sensitive to mutation status.

The study is both the largest *in-vivo* cDTI study performed to date and the largest prospective study of subclinical HCM. The study utilised a validated DTI sequence and consecutive recruitment from genetics databases of three referral cardiomyopathy centres where phenocopies are routinely screened. The exact mechanisms behind how disarray and microvascular disease are present, even without hypertrophy in those with pathogenic sarcomeric mutations are still elusive.

9.1.1. Microstructural changes, MVD and overt HCM

Based on several preclinical models, DTI abnormalities are likely to relate to microstructural alteration (myocyte disarray and abnormal sheetlet orientation) although further human histological validation is needed (46,127,137). In line with other studies, overt disease was characterised by low FA and high MD (12-15,22). While others found an independent association of FA and MD to fibrosis, our study findings also demonstrate an independent relationship to hypertrophy, mirroring prior histological work (52,55)(26). Our study is the first to systematically examine the presence of microstructural abnormalities including disarray in G+LVH+ vs G-LVH+. Genotype negative HCM has been hypothesised to result in part from polygenic inheritance (17). |E2A| elevation reflects a hypercontracted microstructural state in systole with failure to re-orientate in diastole (44,46,52). Whilst G-LVH+ has been associated with less severe outcomes and fibrosis, here unexpectedly related to elevated |E2A|, suggesting a more severe microstructural phenotype. Conversely, whilst both G-LVH+ and G+LVH+ displayed considerable MVD compared to controls, all G+LVH+ had visual perfusion defects compared with 82% of G-LVH+. In overt disease, perfusion defects associate with abnormal blood pressure response to exercise, and in apical HCM, aneurysm formation (80,82). In a previous Positron Emission Tomography (PET-CT) study, global MBF was more impaired in G+LVH+ vs G-LVH+ and although this was not found here, our study does also support the hypothesis of a more direct deleterious impact of sarcomeric mutation on microvascular function (138).

9.1.2. Microstructural changes and subclinical HCM

Subclinical HCM was characterised by LVH and fibrosis parameters similar to health, and despite this, DTI demonstrated lower FA suggestive of more myocyte disarray. While historically disarray has been described in HCM for several decades, its

presence in phenotype evolution was less understood (47). Recent 3-D histological analysis uncovered that disarray is detected *ex-vivo* in fetal murine models without hypertrophy (62). Our prior work and others have modelled early disease by examining DTI parameters of non-hypertrophied myocardium in overt disease, however this has limitations as remote remodelling (in 'non-hypertrophied segments') occurs by the time LVH is detected (55,107,139). Elevated |E2A| in G+LVH- suggests that the hypercontracted microstructural state demonstrated in overt disease is also present before hypertrophy (44,52,53). Elevated |E2A| may have a role in the hyperdynamic function, diastolic dysfunction and impaired myocardial mechanics found in this cohort (107,108). Overall our findings support the hypothesis that altered myocardial microstructure is an early phenomenon in the disease pathophysiology in keeping with animal model work (62).

9.1.3. Microstructural changes and perfusion relationship

Twenty-eight percent of subclinical HCM had perfusion defects and these had evidence of low FA suggestive of more disarray, and more elevated |E2A| than those without perfusion defects. This relationship also persisted into overt disease with markers of MVD being independently associated with markers of microstructural integrity. A unifying explanation for the findings of abnormal microstructure, fibrosis and abnormal microvasculature is the capillary:myocyte coupling hypothesis where microvasculature and the matrix meshwork is abnormal even during organogenesis (61,81). In overt HCM, compressive forces of hypertrophied myocardium and left ventricular outflow tract obstruction also worsen ischaemia (59). An interrelationship of perfusion, disarray and myocardial mechanics could explain the compounding of

perfusion and microstructural changes with LVH and their continued association in overt disease.

9.1.4. MVD, microstructural changes and pathological ECG findings

In line with other studies in subclinical HCM, pathological ECG findings occurred in 34% and were more common in overt disease at 84% (88,140). The study shows for the first time that microstructural alteration (including lower FA suggestive of cardiomyocyte disarray) independently associate with ECG abnormalities in subclinical disease. Prognostically, pathological ECG findings in subclinical HCM associate with a fourfold increased risk of progression to overt disease (88). Mechanisms linking disarray to arrhythmia susceptibility include disruption of gap-junctions, alteration of longitudinal to transverse conduction velocity ratios and provision of different pathways for conduction (47). A pioneering DTI study elicited FA of the thickest LV segment associated with NSVT, however histological studies demonstrate large variations in disarray from segment-to-segment (26). This relationship was not replicated here when using global FA accounting for the low numbers of NSVT in this relatively low risk cohort (implantable devices excluded) (55). Others have hypothesised that ischaemia results in scar which in turn leads to re-entry circuits (141). Whereas we found an independent association of MVD parameters with abnormal ECG, with MPR associating with ECG abnormalities in subclinical HCM, suggesting that the arrhythmogenic potential of MVD could be more complex than scar formation itself (88).

9.2. Limitations

DTI parameters are variably influenced by the presence of fibrosis and other factors, and therefore are not direct measures of disarray. However best available techniques

were used for measurement of important confounders: fibrosis, perfusion and hypertrophy. Myocardial blood flow using adenosine stress is also an indirect measure of MVD and does not represent physiologically exercise. We are unable to fully exclude coronary disease as systematic invasive coronary imaging was not performed. Healthy volunteers did not undergo genotyping or Holter monitoring. Subclinical genotype negative disease was not assessed. As with all contemporaneous cDTI sequences, susceptibility artefact particularly in the inferolateral wall was commonly found and patients with devices were excluded.

9.3. Conclusions

Microstructural alteration and MVD occur in overt HCM and are different in G+ vs G- patients. Both occur even in the absence of hypertrophy in sarcomeric mutation carriers, where changes associate with ECG abnormalities. Microstructural alteration and MVD associate in both subclinical and overt disease suggesting relationships in phenotype development. Measurable changes in myocardial microstructure and microvascular function are early-phenotype biomarkers in in the emerging era of disease-modifying therapy.

CHAPTER 10. DISCUSSION iii: Detection of electrophysiological abnormalities in subclinical and overt HCM

10.1. Discussion

This is the largest clinical ECGI study ever performed and the only one to date to have studied subclinical HCM. This was a multicenter genotyped cohort who underwent 12-lead ECG and comprehensive myocardial tissue characterisation by CMR. Using a non-invasive, high-throughput reusable and fully integrated CMR-ECGI approach, we obtained new insights on electrophysiological substrate aberrations across the spectrum of HCM.

CMR-ECGI detects EP substrate abnormalities in the absence of hypertrophy, including those with normal 12-lead ECGs where there was slower ventricular conduction and more spatially heterogenous repolarization. Those with established LVH (G+LVH+) were similar to G+LVH- but showed prolonged repolarization. The epicardial electrotypes of G+ vs G- HCM were largely overlapping except for epicardial potential fractionation that was more prevalent in G+LVH+ despite similar MWT and scar burden.

As novel HCM therapies shows promise in disease modification, the discovery of sensitive biomarkers for early disease is an emerging priority (11). Structural changes adopted in modern day HCM risk stratification (LA dilation, severe LVH, LVOTO, high LGE burden) tend to occur late. Furthermore NSVT is the only EP marker considered in current risk stratification algorithms and has the highest hazard ratio for SCD; it is however uncommon in early disease (142). Here we show pro-arrhythmic changes occurring in the absence of hypertrophy that track adverse structural features and

differ by genotype in overt disease. The ability to quantify subclinical pro-arrhythmic EP changes before any LVH or 12-lead ECG changes will enhance our ability to risk stratify patients across the full spectrum of HCM and improve precision for more a personalized therapeutic approach including decisions surrounding ICD and exercise. Longitudinal studies relating ECGI changes to events are now possible using this more sustainable, time and cost-effective ECGI methodology.

Ventricular conduction is slower in G+LVH- compared to controls in spite of the absence of scar and LVH and to a similar degree to overt G+ HCM. Importantly this occurred in a cohort predominantly without bundle branch block (2% in G+LVH+, none in G+LVH-). Furthermore, slowed ventricular conduction is missed by the 12-lead ECG occurring in both G+LVH- with normal and abnormal 12-lead ECG (QRS duration perhaps slightly shorter than controls). This finding is consistent with invasive endocardial mapping findings in overt HCM which showed lateral LV activation before the septum, longer action potential durations, prolonged stimulus-to-V times and reduced action potential upstroke velocity on patch-clamp tests of HCM myocardium (87)(85). Mechanisms of ventricular conduction slowing in HCM are likely to include decreased electrical coupling, discontinuous propagation and reduced conduction velocity. Our discovery that these occur in the absence of hypertrophy and fibrosis in subclinical HCM, challenges the LVH-centric view of EP abnormalities and raises the possibility that electrical changes may be more closely related to myocyte disarray, subendocardial ischaemia or electromechanical factors, than actual LVH (143,144). However, a compounding effect of LVH is observed in overt disease as demonstrated by the association of MWT and both activation time and dispersion in overt disease. Slowed discontinuous ventricular conduction and local conduction disturbances are a well-known pre-requisite for ventricular arrhythmia formation. Findings provide a

possible reason behind the increased incidence of ventricular arrhythmia observed with greater degrees of LVH (85) (145). Slower ventricular conduction has been detected by ECGI in other disease states with primary structural substrate changes including arrhythmogenic right ventricular cardiomyopathy (AC) and cardiac amyloidosis, and overlying the right ventricular outflow tract epicardium in Brugada syndrome (while this is primarily a channelopathy, epicardial focal fibrosis has also been observed on autopsy) (146–148). Furthermore, in aborted SCD survivors and Brugada syndrome, ECGI has demonstrated greater conduction heterogeneity post-exercise further demonstrating its ability to detect abnormal pro-arrhythmic rate adaptation (149).

Repolarization in subclinical HCM was more spatially heterogenous (steep repolarization gradients) when detected by ECGI but globally, repolarization was largely normal on ECG (normal QTc, low prevalence of TWI/ no ST depression). While prolonged repolarization was not observed in subclinical HCM, a positive relationship existed between MWT and ARIc in this cohort suggesting prolongation is related to the development of early hypertrophy. In overt disease, prolonged repolarization was established and detected in both ECG (elevated QTc) and ECGI (ARIc, RTc). In HCM mechanisms of repolarization abnormalities are likely related to ionic remodelling which can be heterogenous due to LVH, calcium handling and sensitivity changes, both of which can result in action potential prolongation with early and late afterdepolarization leading to ventricular arrhythmia in structurally remodelled (hypertrophy, fibrosis, disarray) and therefore susceptible myocardium (87) (136,138–140). The exaggerated spatially heterogenous repolarization noted in the absence of hypertrophy could be evidence of cellular and molecular changes occurring in response to sarcomeric mutation or pre-hypertrophic myocardial substrate changes

(143,144). Repolarization gradients as seen in subclinical HCM have been observed in ventricular fibrillation survivors with structurally normal hearts. (96). Spatially heterogenous repolarization supports the conditions for asymmetric excitability and propagation of re-entry. This abnormality has also been demonstrated by ECGI in multiple arrhythmogenic diseases including Brugada, AC, Long QT syndrome and early repolarization, and hypothesized in heart failure . Other ECG techniques quantifying repolarization abnormality in overt HCM include dynamic QTc changes on Holter monitoring, prolonged QTc as a predictor of ICD discharge, and QT dispersion, however none have been especially useful in HCM, limited by lack of spatial information, technical limitations and bias towards more advanced disease (90) (153). With QTc being normal in subclinical disease, it is unlikely to afford benefits as an early disease biomarker.

Scar volume was related to spatial conduction heterogeneity (activation dispersion and fractionation). This demonstrates the ability of ECGI to detect and quantify pre-clinical conduction discontinuities resulting from scar (not detected by LGE CMR). Conduction discontinuities most likely occur due to islands of viable tissue trapped within fibrotic tissue. Indeed, the fact that myocytes are electrotonically uncoupled by this will serve to exaggerate cellular repolarization differences and increase repolarization gradients. This EP phenomenon has potential for arrhythmia formation (154) through asymmetric loading on a propagating wavefront favouring unidirectional block, creating dispersion of repolarization and facilitating re-entry. Both spatial conduction heterogeneity and fractionation are observed in AC scar and fractionation is observed in both infarct and AC scar (97).

Despite similar MWT and LGE burden and a more benign 12-lead ECG phenotype, ECGI-detected fractionation is greater in genotype-positive HCM patients compared

to G-LVH+. Greater fractionation in G+LVH+ could not be accounted for by bundle branch block or Q-waves, suggesting a genuinely greater area of tissue with fractionated UEGs. Exaggerated spatially heterogenous ventricular conduction is another plausible contributor to the greater ventricular arrhythmia seen in G+LVH+ HCM compared to G-LVH+ (91).

Unexpectedly, we found more severe 12-lead ECG abnormalities in G-LVH+ compared to G+LVH+ HCM (longer QRS duration, longer QTc and greater QRS amplitudes). This mirrors data from a prior study showing G-LVH+ was characterised by greater lateral T-wave inversion (155). Overall differences in ECG and ECGI between G- and G+ HCM could be in part related to different LV morphologies (greater LV mass despite similar MWT) and different tissue characterisation (lower ECV) as described by large registry studies (31,91).

10.2. Limitations

ECGI provides epicardial EP mapping data only and does not therefore measure potentially important transmural electrophysiology; it also misses EP phenomena occurring within septum. As expected, the subclinical HCM cohort were 16 years younger than overt disease counterparts and medication use affects electrophysiology and may influence results. However, our sensitivity analyses showed consistent EP changes even when comparing overt HCM and drug-free HCM to age-matched healthy volunteers.

10.3. Conclusion

ECGI detects pro-arrhythmic conduction/repolarization abnormalities in HCM and these relate differently to mutation status and adverse structural change. In subclinical HCM, ECGI detects abnormalities missed by the conventional 12 lead ECG

Chapter 11. Discussion iv. Sub-phenotypes of HCM using unsupervised learning

HCM is a heterogenous disease with variable expressivity, LV morphology and clinical outcome. We performed an agglomerative hierarchical clustering analysis using advanced phenotyping parameters (DTI, ECGI, quantitative perfusion). We found 3 optimal clusters: i) a benign phenotype without LVH, preserved microvascular function and less microstructural alteration ii) an intermediate phenotype with intermediate microvascular function, microstructural alteration and prolonged repolarization iii) severe phenotype with severe microvascular impairment, microstructural alteration and severely altered pro-arrhythmic ECGI changes.

HCM is defined by arbitrary maximum wall thickness cutoffs (15mm/13mm in first degree relatives of patients with HCM). This fails to acknowledge the phenotypic spectrum of disease expression before these wall thickness cutoffs occur. Furthermore defining disease by a singular wall thickness cutoff means adverse changes are not targeted before this stage, where changes might be reversible. In the discovery of first-in-class myosin inhibitor mavacamten, the reversal of disarray occurred only in subclinical HCM treated-mice and not at the overt disease stage (110).

Our findings show that in subclinical HCM, 1 in 3 that have more impaired microvascular function, microstructural alteration and pro-arrhythmic EP changes, predominantly prolonged and heterogenous repolarization. This cohort has a high prevalence of abnormal ECG which itself confers a fourfold increased risk of

progression of overt disease and therefore are expected to carry an increased risk progress; longitudinal follow-up will uncover this further. Importantly this sub-phenotype is not differentiated by a borderline elevated MWT meaning that deep phenotyping techniques are the only method of identifying this cohort and incremental to the 12-lead ECG.

In overt disease, there was virtually no ‘benign’ phenotype (only 3 overt LVH in the benign cluster) suggesting that once LVH has developed the other domains are frequently adversely affected. There was no enrichment of either phenotype with genotype positive vs negative suggesting that these two phenotypes overlap significantly. The severe phenotype had worse LVH, microvascular disease, microstructural alteration (steeper sheetlet orientation). Almost all ECGI parameters were more adverse in the severe phenotype except for ARIc suggesting this prolongs early with LVH with other abnormalities occurring later. While some ECGI parameters were more severe in the benign phenotype than intermediate, it is difficult to ascertain the significance as the benign phenotype was much younger and ECGI parameters are expected to relate closely to age. Interestingly, the presence of high ESC risk score and NSVT were not weighted towards either group which could in part explain the limited accuracy markers in external validation cohorts.

CHAPTER 12: Overall Discussion and Conclusion

12.1. Background

The aim of this study was to understand the microstructural, microvascular and electrophysiological changes occurring in early (pre-hypertrophy) and overt HCM. Investigations were advanced imaging modalities that are yet to fully integrate into mainstream of clinical care: diffusion tensor imaging (DTI), quantitative perfusion and electrocardiographic imaging (ECGI). Relationships in overt disease were explored between genotype (genotype positive vs negative HCM), adverse structural change (scar, diffuse fibrosis) and conventional markers of risk (NSVT, ESC risk score). The work builds on studies by our group and others showing macroscopic changes occurring pre-hypertrophy in HCM (abnormal trabeculation, crypts, mitral valve abnormalities) and later microvascular changes detected by advanced imaging. The overarching aims from this PhD were to ascertain whether these early changes could be used for early phenotype detection, monitoring of phenotype development and potentially risk. The work was timely due to the emergence of potential disease modifying agents and gene therapy during the course of the PhD. As HCM is characterised by left ventricular hypertrophy, an initial exploratory study was performed examining microvascular changes occurring with physiological LVH (due to athleticism) and pathological LVH caused by excessive afterload (hypertension). This study would explore any discriminatory value of quantitative perfusion to aid the diagnosis in cases of ‘grey-zone’ LVH.

12.2. Key findings, limitations and clinical implications

Quantitative perfusion mapping in physiological (athleticism) and pathological (hypertension) left ventricular hypertrophy: The main finding of this study was that there were differences in microvascular function as measured by quantitative perfusion between LVH caused by athleticism, excessive afterload in hypertension and subclinical HCM. Athletes, hypertensives and subclinical HCM were matched in terms of extent of fibrosis (ECV) and maximum wall thickness although athletes and hypertensives had elevated LV mass. Relative to athletes, subclinical HCM and hypertensives had impaired myocardial perfusion supporting the potential of quantitative perfusion as a disease discriminator. The findings comparing athleticism to health were more difficult to interpret due to the higher adenosine requirements in athleticism. While an enhanced perfusion reserve was detected in athletes compared to health even after adjusting for higher adenosine dose, further prospective work comparing dose-matched healthy volunteers would be needed to confirm this finding. However, collaborators have found no significant difference in higher doses of adenosine compared to standard dosing of adenosine. Prior work predominantly using PET-CT in this area has been conflicting. In this initially exploratory study, findings would suggest that further work ascertaining the discriminatory value of quantitative perfusion in grey-zone LVH is worthwhile. This work would need to account for known influencing factors in perfusion – age, sex, ethnicity, medication and comorbidities – in order for robust cut-points to be determined.

Microstructural and microvascular phenotype of sarcomere mutation carriers and overt hypertrophic cardiomyopathy. In this study we showed that abnormalities in diffusion tensor imaging and quantitative perfusion occur in the absence of

hypertrophy in hypertrophic cardiomyopathy. This showed that potentially these advanced CMR techniques could be used for early disease detection due to their sensitivity to early myocardial changes. As disease modification is possible and has been proven from studies on the first-in-class myosin inhibitor mavacamten, advanced imaging techniques may play a role in facilitating early therapy – even before hypertrophy. Further longitudinal work would ascertain whether DTI/perfusion detects positive microstructural changes with myosin inhibitors, and whether these changes are predictive of LVH. Mechanistically our findings of DTI abnormalities in the absence of hypertrophy reflects pre-clinical work showing that myocyte disarray occurs in the absence LVH in *mybpc3* knock-out mice. Another mechanistic finding was that diffusion tensor changes and quantitative perfusion were associated in both subclinical and overt disease. Others have hypothesised that abnormalities in the myocyte matrix (expanded ECV, disarray) and microvasculature are not explainable solely by sarcomeric mutations and suggest developmental origins. Our imaging findings support this hypothesis however there are limitations to macroscopic imaging in forming histological impressions, mainly the resolution (1 voxel contains over ~50,000 myocytes) and there lack of specificity for disarray (DTI is influenced by fibrosis and likely also myocyte size). In overt disease, genotype associated with both microstructure (genotype negative HCM had more adverse DTI findings – steeper sheetlet orientation) and microvascular function (genotype positive HCM was characterized by a 100% prevalence of perfusion defects). This could be important as genotype in overt disease clinically associates with differing outcomes (genotype positive have a higher prevalence of ventricular arrhythmia, sudden cardiac death) and differing LV morphology (genotype negative – more LVOTO, more apical LVH).

Overall this chapter has shifted attention towards early disease microstructural changes and defining HCM by its non-LVH characteristics. Observing these earliest changes occurring *in-vivo* may redefine hypertrophy and fibrosis as late markers.

Detection of electrophysiological abnormalities in subclinical and overt HCM. In this study we showed that electrocardiographic imaging could detect EP changes in subclinical disease – namely slowing of ventricular conduction, and spatial heterogeneity of repolarization. This finding is important as it shows the earliest electrical changes in adults occurring with sarcomeric mutation. The possible mechanisms behind this are multiple, ranging from ionic remodelling to microstructure or electromechanical factors. Importantly changes occurred in the absence of LVH and 12-lead ECG changes. Clinical implications include the earlier detection of phenotype development and possibly with further longitudinal work, enhanced accuracy of which individuals will go on to develop LVH and ventricular arrhythmia. Current models of care include imaging surveillance, of which inefficiencies are coupled with an increasing identification of sarcomeric mutation carriers year-on-year through cascade screening. Importantly, current conventional markers of risk – presence of a sarcomeric mutation, LVH, scar – had associations with ECGI changes.

The main limitation to this work was the lack of longitudinal follow-up for subclinical HCM; almost half of these individuals are expected to develop overt disease over 15 years. At 5 years, penetrance is closer to 20%. The detection of SCD equivalent events in overt disease was much more challenging due to low-event rates in this low-risk cohort (implantable devices were excluded). Even the 5-year follow-up of HCMR, one of the largest prospective registries of HCM (over 2000 patients) are low on

events, limiting the ability of HCMR to find imaging and genetic predictors of sudden cardiac death (105)

As part of the PhD I assisted Dr Captur in co-inventing the washable and re-useable ECGI vest – patent approved. The streamlined workflow of this vest (10 minutes for body surface electrogram acquisition, 5 minutes for heart-torso geometry acquisition) far surpasses current clinical solutions – often 2 hours in total. This technical improvement may facilitate the longitudinal work that is required to relate ECGI findings to clinical outcome.

Identifying sub-phenotypes of HCM using unsupervised learning: HCM is a heterogenous disease with variable expressivity, LV morphology and clinical outcome. We performed an agglomerative hierarchical clustering analysis using advanced phenotyping parameters (DTI, ECGI, quantitative perfusion). We found 3 optimal clusters: i) a benign phenotype without LVH, preserved microvascular function and less microstructural alteration ii) an intermediate phenotype with intermediate microvascular function, microstructural alteration and prolonged repolarization iii) severe phenotype with severe microvascular impairment, microstructural alteration and severely altered pro-arrhythmic ECGI changes.

Subclinical HCM was therefore reclassified; the benign phenotype comprised mostly of subclinical HCM (only three in this phenotype had LVH), and one third of subclinical HCM was reclassified into the severe phenotype. This cohort had a higher prevalence of abnormal ECG (50%) suggesting they were the most likely to progress to overt disease. The intermediate and severe phenotypes were equally balanced between genotype positive and negative overt HCM suggesting large overlaps in deep phenotype or potentially differences are more difficult to discriminate once LVH is

present. The work highlights that using arbitrary maximum wall thickness to define HCM fails to detect the adverse phenotypic spectrum of gene expression occurring before the MWT cutoffs are reached.

12.3. Ongoing Future Work/ Collaborations

1. *Human histological validation of diffusion tensor imaging* – following on from the diffusion tensor work, I have collaborated with the surgeons at Barts Heart Centre to collect myectomy samples for further *ex-vivo* synchrotron based imaging (in collaboration with Prof Andrew Cook, UCL). We will scan eligible patients pre-operatively using diffusion tensor imaging and compare findings to *ex-vivo* findings to ascertain whether DTI changes are consistent with disarray.
2. *ECGI in subclinical HCM* – work from Imperial College has shown that ECGI abnormalities are more prevalent in susceptible individuals (Brugada syndrome, idiopathic VF survivors) on exercise. An interesting enquiry will be whether the exercise-ECGI has increased sensitivity in detecting the abnormalities described from my PhD work.

12.4. Conclusion

Findings. **In left ventricular hypertrophy**, quantitative perfusion may supplement current techniques for discrimination of pathological vs physiological LVH. **In HCM,** abnormalities in myocardial microstructure, microvasculature and electrophysiology occur in the absence of LVH. In overt disease, abnormalities associate with important clinical characteristics (adverse structural changes, genotype). One third of subclinical HCM form a more severe microstructural, microvascular and EP phenotype with comparable adverse changes to overt disease.

Potential Clinical Application. I have optimised new techniques to visualize *in-vivo* early histological and EP changes occurring in HCM. Whilst we have integrated LVH and scar in cardiac MRI for clinical care, my work has made the measurement of disarray and microvascular disease robust in HCM for future clinical and trial utility. Furthermore early electrophysiological abnormalities can now be detected through integration of ECGI with CMR. We found remarkable microstructural, microvascular and EP changes occurring in subclinical disease in the absence of LVH. Curious insights into genotype negative vs positive disease show both overlapping and distinctive phenotypes. These biomarkers may now be tested in longitudinal studies to track whether abnormalities relate to disease progression and ventricular arrhythmia formation. Overall findings suggest clinical techniques could supplement current care, especially for the detection of early disease but also potentially risk stratification and disease discrimination.

ACADEMIC OUTPUTS

Awards

International

1. Evidence for microstructural and microvascular alteration in subclinical and overt hypertrophic cardiomyopathy, **EACVI 2023 Young Investigator Award Runner up**

2. Redefining HCM using deep phenotyping of mutation carriers, **SCMR 2022, Early Career Award Runner-up**

3. Prospective Case-Control Study of Cardiovascular Abnormalities 6 Months Following Mild COVID-19 in Healthcare Workers, **EuroCMR2021, Young Investigator Award Runner-up**

National

1. Non-invasive detection of microstructural and microvascular abnormalities in subclinical and overt hypertrophic cardiomyopathy, **RSM President's Prize 2023 - Silver Medal Winner**

2. Microstructural and microvascular phenotype of subclinical and overt HCM, **RSM 2022, Silvia Pica Young Investigator Award Runner-up**

First Author Publications

1. **Joy G,** Moon JC, Lopes LR. Detection of subclinical hypertrophic cardiomyopathy, **Nat Rev Cardiol 2023**
2. **Joy G,** … Moon JC, Lopes LR. Microstructural and Microvascular Phenotype of Sarcomere Mutation Carriers and Overt Hypertrophic Cardiomyopathy, **Circulation 2023**
3. **Joy G**, Lopes LR…Captur G. Detection of electrophysiological abnormalities in subclinical and overt HCM; insights from ECG Imaging, **JACC 2024**

Inventions:

Co-inventor capturECGI vest [US Patent Approved Application No. US 18/194 235].

Media Relating To PhD

New scanning methods can detect deadly heart condition before symptoms appear

19 July 2023 Joe Cousins

Category: Research

Combining two types of heart scan could help doctors to detect the deadly heart condition hypertrophic cardiomyopathy (HCM) before symptoms and signs on conventional tests appear, according to research funded by us. The team behind the study, published today in the journal Circulation, say it offers an unprecedented opportunity to improve treatment for the condition at the earliest stages.

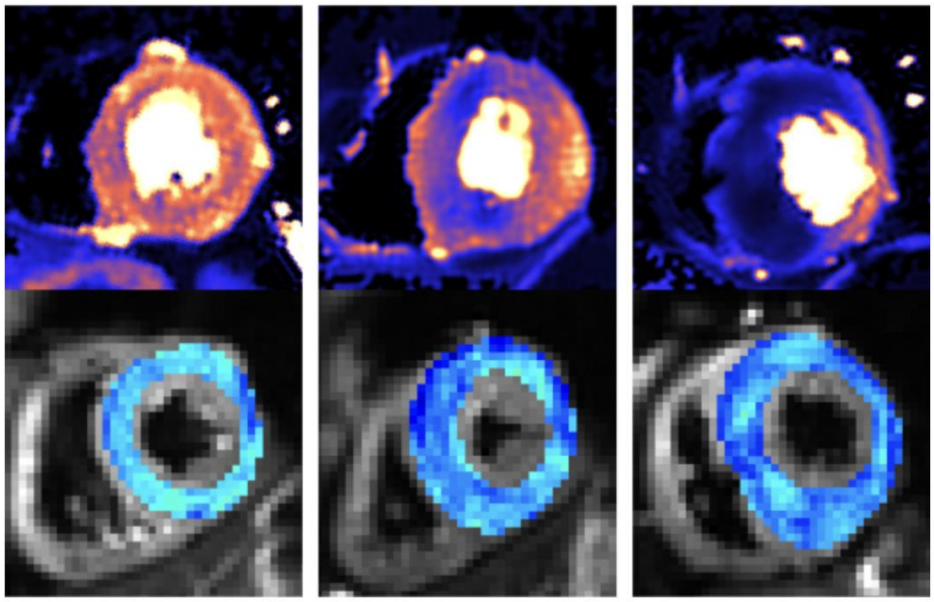

https://www.bhf.org.uk/what-we-do/news-from-the-bhf/news-archive/2023/july/new-scanning-methods-detect-hcm-before-symptoms-appear

Cardiology Section President announces winner of UK research contest

Published 27 September 2023

The Royal Society of Medicine

The second prize of £500 went to Dr George Joy, Clinical Research Fellow at Barts Heart Centre and UCL, for 'Non-invasive detection of microstructural and electrophysiological abnormalities in subclinical and overt hypertrophic cardiomyopathy'.

https://www.rsm.ac.uk/latest-news/2023/cardiology-section-president-announces-winner-of-uk-research-contest/

The Standard

Wearable vest that detects electrical impulses can help spot early signs of heart disease

UCL scientists say screening tool could prevent most common cause of sudd death for young people

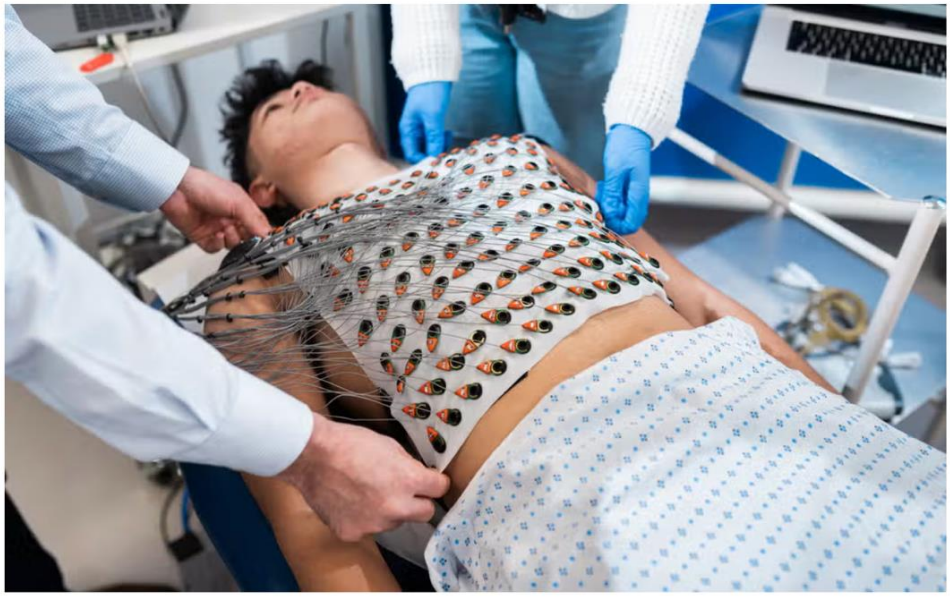

A PATIENT AT UCL UNDERGOES A SCAN USING THE ECGI HEART VEST

https://www.standard.co.uk/news/health/wearable-vest-ucl-help-detect-early-signs-heart-disease-b1140548.html

Co-Author publications relating to PhD

1. Webber M, **Joy G**…Captur G. Technical development and feasibility of a reusable vest to integrate cardiovascular magnetic resonance with electrocardiographic imaging. **J Cardiovasc Magn Reson 2023**

2. Hughes RK…**Joy G**…Moon JC. Apical Ischemia Is a Universal Feature of Apical Hypertrophic Cardiomyopathy. **Circ Cardiovasc Imaging 2023**

3. Hughes RK…**Joy G**…Moon JC. Improved Diagnostic Criteria for Apical Hypertrophic Cardiomyopathy. **JACC Cardiovasc Imaging 2023**

4. Das A…**Joy G**…Dall'Armellina E. Phenotyping hypertrophic cardiomyopathy using cardiac diffusion magnetic resonance imaging: the relationship between microvascular dysfunction and microstructural changes, **Eur Heart J Cardiovasc Imaging 2022**

5. Patel KP…**Joy G…**Moon JC. Impact of afterload and infiltration on coexisting aortic stenosis and transthyretin amyloidosis, **Heart 2022**

6. Webber M…**Joy G**…Captur G. Study protocol: MyoFit46-the cardiac sub-study of the MRC National Survey of Health and Development. **BMC Cardiovasc Disord 2022**

7. Seraphim A…**Joy G**…Kellman P. Prognostic Value of Pulmonary Transit Time and Pulmonary Blood Volume Estimation Using Myocardial Perfusion CMR. **JACC Cardiovasc Imaging. 2021**

8. Hughes RK…**Joy G…Lopes, LR,** Moon JC. Myocardial Perfusion Defects in Hypertrophic Cardiomyopathy Mutation Carriers. **J Am Heart Assoc. 2021**

9. Seraphim A**…Joy G…**Manisty C. Use of quantitative cardiovascular magnetic resonance myocardial perfusion mapping for characterization of ischemia in patients with left internal mammary coronary artery bypass grafts. **J Cardiovasc Magn Reson 2021**

Presentations

1. Electrophysiological abnormalities in subclinical and overt HCM, **CMR 2024**
2. AI left ventricular segmentation outperforms humans for the prediction of all-cause mortality in known or suspected coronary disease, **CMR 2024**
3. CMR-ECGI detects electrophysiological abnormalities before hypertrophy or ECG changes in subclinical HCM, **AHA 2023**
4. Advanced microstructural substrate detection in pre-hypertrophic HCM and its relationship to arrhythmogenesis, **ESC Congress 2022**

5. Microvascular and mechanical improvements following bariatric surgery in the obese; mechanistic insights from advanced & automated quantitative perfusion cardiac MRI, **Oral Presentation EACVI Best of Imaging 2020**
6. Reversibility of distal aortic stiffness in people with obesity after bariatric surgery, **SCMR 2021**
7. Impact of obesity on myocardial microvasculature assessed using fully-automated inline myocardial perfusion mapping CMR, Poster Presentation, **EACVI Best of Imaging 2020**
8.

Teaching

Secondary Supervisor: intercalated BsC UCL: Alessandra Ardissino, Distinction

Examiner: intercalated BsC final year presentations: UCL 2023

Examiner: intercalated BsC manuscript, UCL 2023

Supervisor for ongoing research projects: UCL Medstudent: Tuguldur Gantur, IMT Papworth Hospital: Zaid Abdullelah, Barts FY2: Karan Punjabi

Lead Fellow for CMR Teaching: Barts Heart Centre & UCL

Bibliography

1. Maron BJ., Rowin EJ., Maron MS. Global Burden of Hypertrophic Cardiomyopathy. JACC Heart Fail. 2018 May 1;6(5):376–8.
2. Finocchiaro G, Papadakis M, Tanzarella G, et al. Sudden Death Can Be the First Manifestation of Hypertrophic Cardiomyopathy. JACC Clin Electrophysiol. 2019 Feb 1;5(2):252–4.
3. Weissler-Snir A, Allan K, Cunningham K, Connelly KA, Lee DS, Spears DA, et al. Hypertrophic Cardiomyopathy–Related Sudden Cardiac Death in Young People in Ontario. Circulation. 2019 Nov 19;140(21):1706–16.
4. Ommen SR, Mital S, Burke MA, Day SM, Deswal A, et al. 2020 AHA/ACC Guideline for the Diagnosis and Treatment of Patients With Hypertrophic Cardiomyopathy. Circulation. 2020 Dec 22;142(25):e558–631.
5. Maron BJ, Rowin EJ, Udelson JE, Maron MS. Clinical Spectrum and Management of Heart Failure in Hypertrophic Cardiomyopathy. JACC Heart Fail. 2018 May 1;6(5):353–63.
6. Lorenzini M, Anastasiou Z, O'Mahony C, Guttman OP, Gimeno JR, Monserrat L, et al. Mortality Among Referral Patients With Hypertrophic Cardiomyopathy vs the General European Population. JAMA Cardiol. 2020 Jan 1;5(1):73–80.
7. Ommen SR, Mital S, Burke MA, Day SM, Deswal A, et al. 2020 AHA/ACC Guideline for the Diagnosis and Treatment of Patients With Hypertrophic Cardiomyopathy. Circulation. 2020 Dec 22;142(25):e558–631.
8. Finocchiaro G, Sheikh N, Biagini E, Papadakis M, Maurizi N, Sinagra G, et al. The electrocardiogram in the diagnosis and management of patients with hypertrophic cardiomyopathy. Heart Rhythm. 2020 Jan 1;17(1):142–51.
9. Olivotto I, Oreziak A, Barriales-Villa R, Abraham TP, Masri A, Garcia-Pavia P, et al. Mavacamten for treatment of symptomatic obstructive hypertrophic cardiomyopathy (EXPLORER-HCM): a randomised, double-blind, placebo-controlled, phase 3 trial. The Lancet. 2020 Sep 12;396(10253):759–69.
10. Desai Milind Y., Owens Anjali, Geske Jeffrey B., Wolski Kathy, Naidu Srihari S., Smedira Nicholas G., et al. Myosin Inhibition in Patients With Obstructive Hypertrophic Cardiomyopathy Referred for Septal Reduction Therapy. J Am Coll Cardiol. 2022 Jul 12;80(2):95–108.
11. Ho Carolyn Y., Mealiffe Matthew E., Bach Richard G., Bhattacharya Mondira, Choudhury Lubna, Edelberg Jay M., et al. Evaluation of Mavacamten in Symptomatic Patients With Nonobstructive Hypertrophic Cardiomyopathy. J Am Coll Cardiol. 2020 Jun 2;75(21):2649–60.
12. Saberi S, Cardim N, Yamani M, Schulz-Menger J, Li W, Florea V, et al. Mavacamten Favorably Impacts Cardiac Structure in Obstructive Hypertrophic Cardiomyopathy. Circulation. 2021 Feb 9;143(6):606–8.
13. https://www.nice.org.uk/guidance/ta913/chapter/1-Recommendations.
14. https://ir.cytokinetics.com/news-releases/news-release-details/cytokinetics-announces-positive-results-sequoia-hcm-pivotal.
15. Marian AJ. Molecular Genetic Basis of Hypertrophic Cardiomyopathy. Circ Res. 2021 May 14;128(10):1533–53.
16. Hoss S, Habib M, Silver J, Care M, Chan RH, Hanneman K, et al. Genetic Testing for Diagnosis of Hypertrophic Cardiomyopathy Mimics. Circ Genomic Precis Med. 2020 Jan 1;13(2):e002748.
17. Watkins H. Time to Think Differently About Sarcomere-Negative Hypertrophic Cardiomyopathy. Circulation. 2021 Jun 22;143(25):2415–7.
18. Roberts R, Sigwart U. Current Concepts of the Pathogenesis and Treatment of Hypertrophic Cardiomyopathy. Circulation. 2005 Jul 12;112(2):293–6.
19. Frangogiannis NG. The inflammatory response in myocardial injury, repair, and remodelling. Nat Rev Cardiol. 2014 May 1;11(5):255–65.
20. Kaul S, Jayaweera AR. Myocardial Capillaries and Coronary Flow Reserve**Editorials published in the Journal of the American College of Cardiology reflect the views of the authors and do not necessarily represent the views of JACC or the American College of Cardiology. J Am Coll Cardiol. 2008 Oct 21;52(17):1399–401.
21. Schelbert EB, Wong TC, Gheorghiade M. Think Small and Examine the Constituents of Left Ventricular Hypertrophy and Heart Failure: Cardiomyocytes Versus Fibroblasts, Collagen, and Capillaries in the Interstitium. J Am Heart Assoc. 4(9):e002491.

22. Mahmood SS, Levy D, Vasan RS, Wang TJ. The Framingham Heart Study and the epidemiology of cardiovascular disease: a historical perspective. The Lancet. 2014 Mar 15;383(9921):999–1008.
23. Seliger SL, de Lemos J, Neeland IJ, Christenson R, Gottdiener J, Drazner MH, et al. Older Adults, "Malignant" Left Ventricular Hypertrophy, and Associated Cardiac-Specific Biomarker Phenotypes to Identify the Differential Risk of New-Onset Reduced Versus Preserved Ejection Fraction Heart Failure: CHS (Cardiovascular Health Study). JACC Heart Fail. 2015 Jun 1;3(6):445–55.
24. Teare D. ASYMMETRICAL HYPERTROPHY OF THE HEART IN YOUNG ADULTS. Br Heart J. 1958 Jan 1;20(1):1.
25. Hughes RK, Augusto JB, Knott K, Davies R, Shiwani H, Seraphim A, et al. Apical Ischemia Is a Universal Feature of Apical Hypertrophic Cardiomyopathy. Circ Cardiovasc Imaging. 2023 Mar 1;16(3):e014907.
26. Varnava AM, Elliott PM, Sharma S, McKenna WJ, Davies MJ. Hypertrophic cardiomyopathy: the interrelation of disarray, fibrosis, and small vessel disease. Heart. 2000 Nov 1;84(5):476.
27. Ferrans VJ, Morrow AG, Roberts WC. Myocardial ultrastructure in idiopathic hypertrophic subaortic stenosis. A study of operatively excised left ventricular outflow tract muscle in 14 patients. Circulation. 1972;45(4):769–92.
28. Noorden SV, Olsen EGJ, Pearse AGE. Hypertrophic obstructive cardiomyopathy, a histological, histochemical, and ultrastructural study of biopsy material1. Cardiovasc Res. 1971 Jan 1;5(1):118–31.
29. Cui H, Schaff HV, Lentz Carvalho J, Nishimura RA, Geske JB, Dearani JA, et al. Myocardial Histopathology in Patients With Obstructive Hypertrophic Cardiomyopathy. J Am Coll Cardiol. 2021 May 4;77(17):2159–70.
30. Treibel TA, López B, González A, Menacho K, Schofield RS, Ravassa S, et al. Reappraising myocardial fibrosis in severe aortic stenosis: an invasive and non-invasive study in 133 patients. Eur Heart J. 2018 Feb 21;39(8):699–709.
31. Neubauer S, Kolm P, Ho CY, Kwong RY, Desai MY, Dolman SF, et al. Distinct Subgroups in Hypertrophic Cardiomyopathy in the NHLBI HCM Registry. J Am Coll Cardiol. 2019 Nov 12;74(19):2333–45.
32. Nordin S, Kozor R, Vijapurapu R, Augusto JB, Knott KD, Captur G, et al. Myocardial Storage, Inflammation, and Cardiac Phenotype in Fabry Disease After One Year of Enzyme Replacement Therapy. Circ Cardiovasc Imaging. 2019 Dec 1;12(12):e009430.
33. Ho CY, López B, Coelho-Filho OR, Lakdawala NK, Cirino AL, Jarolim P, et al. Myocardial Fibrosis as an Early Manifestation of Hypertrophic Cardiomyopathy. N Engl J Med. 2010 Aug 5;363(6):552–63.
34. Chan RH, Maron BJ, Olivotto I, Assenza GE, Haas TS, Lesser JR, et al. Significance of Late Gadolinium Enhancement at Right Ventricular Attachment to Ventricular Septum in Patients With Hypertrophic Cardiomyopathy. Am J Cardiol. 2015 Aug 1;116(3):436–41.
35. Ismail TF, Prasad SK, Pennell DJ. Prognostic importance of late gadolinium enhancement cardiovascular magnetic resonance in cardiomyopathy. Heart. 2012 Mar 15;98(6):438.
36. Galati G, Leone O, Pasquale F, Olivotto I, Biagini E, Grigioni F, et al. Histological and Histometric Characterization of Myocardial Fibrosis in End-Stage Hypertrophic Cardiomyopathy. Circ Heart Fail. 2016 Sep 1;9(9):e003090.
37. Chan RH, Maron BJ, Olivotto I, Pencina MJ, Assenza GE, Haas T, et al. Prognostic Value of Quantitative Contrast-Enhanced Cardiovascular Magnetic Resonance for the Evaluation of Sudden Death Risk in Patients With Hypertrophic Cardiomyopathy. Circulation. 2014 Aug 5;130(6):484–95.
38. Rodrigues T, Raposo SC, Brito D, Lopes LR. Prognostic relevance of exercise testing in hypertrophic cardiomyopathy. A systematic review. Int J Cardiol. 2021 Sep 15;339:83–92.
39. Patel P, Dhillon A, Popovic ZB, Smedira NG, Rizzo J, Thamilarasan M, et al. Left Ventricular Outflow Tract Obstruction in Hypertrophic Cardiomyopathy Patients Without Severe Septal Hypertrophy. Circ Cardiovasc Imaging. 2015 Jul 1;8(7):e003132.
40. Anish Bhuva, Geoff Charles-Edwards, Jonathan Ashmore, Alexandra Lipton, Matthew Benbow, David Grainger, et al. Joint British Society consensus recommendations for magnetic resonance imaging for patients with cardiac implantable electronic devices. Heart. 2022 Sep 13;heartjnl-2022-320810.
41. Moon JCC, Reed E, Sheppard MN, Elkington AG, Ho S, Burke M, et al. The histologic basis of late gadolinium enhancement cardiovascular magnetic resonance in hypertrophic cardiomyopathy. J Am Coll Cardiol. 2004 Jun 16;43(12):2260–4.

42. Habib Manhal, Adler Arnon, Fardfini Kimia, Hoss Sara, Hanneman Kate, Rowin Ethan J., et al. Progression of Myocardial Fibrosis in Hypertrophic Cardiomyopathy. JACC Cardiovasc Imaging. 2021 May 1;14(5):947–58.
43. Raman B, Ariga R, Spartera M, Sivalokanathan S, Chan K, Dass S, et al. Progression of myocardial fibrosis in hypertrophic cardiomyopathy: mechanisms and clinical implications. Eur Heart J - Cardiovasc Imaging. 2019 Feb 1;20(2):157–67.
44. Ferreira PF, Kilner PJ, McGill LA, Nielles-Vallespin S, Scott AD, Ho SY, et al. In vivo cardiovascular magnetic resonance diffusion tensor imaging shows evidence of abnormal myocardial laminar orientations and mobility in hypertrophic cardiomyopathy. J Cardiovasc Magn Reson. 2014 Nov 12;16(1):87.
45. Khalique Z, Ferreira PF, Scott AD, Nielles-Vallespin S, Firmin DN, Pennell DJ. Diffusion Tensor Cardiovascular Magnetic Resonance Imaging: A Clinical Perspective. JACC Cardiovasc Imaging. 2020 May 1;13(5):1235–55.
46. Nielles-Vallespin S, Khalique Z, Ferreira PF, de Silva R, Scott AD, Kilner P, et al. Assessment of Myocardial Microstructural Dynamics by In Vivo Diffusion Tensor Cardiac Magnetic Resonance. J Am Coll Cardiol. 2017 Feb 14;69(6):661–76.
47. Finocchiaro G, Sheikh N, Leone O, Westaby J, Mazzarotto F, Pantazis A, et al. Arrhythmogenic potential of myocardial disarray in hypertrophic cardiomyopathy: genetic basis, functional consequences and relation to sudden cardiac death. EP Eur. 2021 Jul 1;23(7):985–95.
48. Khalique Z, Ferreira PF, Scott AD, Nielles-Vallespin S, Firmin DN, Pennell DJ. Diffusion Tensor Cardiovascular Magnetic Resonance Imaging: A Clinical Perspective. JACC Cardiovasc Imaging. 2020 May 1;13(5):1235–55.
49. McKenna WJ, Stewart JT, Nihoyannopoulos P, McGinty F, Davies MJ. Hypertrophic cardiomyopathy without hypertrophy: two families with myocardial disarray in the absence of increased myocardial mass. Br Heart J. 1990 May 1;63(5):287.
50. Nguyen C, Fan Z, Sharif B, He Y, Dharmakumar R, Berman DS, et al. In vivo three-dimensional high resolution cardiac diffusion-weighted MRI: A motion compensated diffusion-prepared balanced steady-state free precession approach. Magn Reson Med. 2014 Nov 1;72(5):1257–67.
51. Das A, Kelly C, Teh I, Stoeck CT, Kozerke S, Chowdhary A, et al. Acute Microstructural Changes after ST-Segment Elevation Myocardial Infarction Assessed with Diffusion Tensor Imaging. Radiology. 2021 Apr 1;299(1):86–96.
52. Das A, Kelly C, Teh I, Nguyen C, Brown LAE, Chowdhary A, et al. Phenotyping hypertrophic cardiomyopathy using cardiac diffusion magnetic resonance imaging: the relationship between microvascular dysfunction and microstructural changes. Eur Heart J - Cardiovasc Imaging. 2022 Mar 1;23(3):352–62.
53. Das A, Chowdhary A, Kelly C, Teh I, Stoeck CT, Kozerke S, et al. Insight Into Myocardial Microstructure of Athletes and Hypertrophic Cardiomyopathy Patients Using Diffusion Tensor Imaging. J Magn Reson Imaging. 2021 Jan 1;53(1):73–82.
54. Khalique Z, Scott AD, Ferreira PF, Nielles-Vallespin S, Firmin DN, Pennell DJ. Diffusion tensor cardiovascular magnetic resonance in hypertrophic cardiomyopathy: a comparison of motion-compensated spin echo and stimulated echo techniques. Magn Reson Mater Phys Biol Med. 2020 Jun 1;33(3):331–42.
55. Ariga Rina, Tunnicliffe Elizabeth M., Manohar Sanjay G., Mahmod Masliza, Raman Betty, Piechnik Stefan K., et al. Identification of Myocardial Disarray in Patients With Hypertrophic Cardiomyopathy and Ventricular Arrhythmias. J Am Coll Cardiol. 2019 May 28;73(20):2493–502.
56. Gotschy A, von Deuster C, Weber L, Gastl M, Schmiady MO, van Gorkum RJH, et al. CMR Diffusion Tensor Imaging Provides Novel Imaging Markers of Adverse Myocardial Remodeling in Aortic Stenosis. JACC Cardiovasc Imaging. 2021 Jul 1;14(7):1472–4.
57. Gotschy A, von Deuster C, van Gorkum RJH, Gastl M, Vintschger E, Schwotzer R, et al. Characterizing cardiac involvement in amyloidosis using cardiovascular magnetic resonance diffusion tensor imaging. J Cardiovasc Magn Reson. 2019 Sep 5;21(1):56.
58. Das A, Kelly C, Teh I, Stoeck CT, Kozerke S, Sharrack N, et al. Pathophysiology of LV Remodeling Following STEMI: A Longitudinal Diffusion Tensor CMR Study. JACC Cardiovasc Imaging. 2023 Feb 1;16(2):159–71.
59. Raphael CE, Cooper R, Parker KH, Collinson J, Vassiliou V, Pennell DJ, et al. Mechanisms of Myocardial Ischemia in Hypertrophic Cardiomyopathy: Insights From Wave Intensity Analysis and Magnetic Resonance. J Am Coll Cardiol. 2016 Oct 11;68(15):1651–60.

60. Basso C, Thiene G, Corrado D, Buja G, Melacini P, Nava A. Hypertrophic cardiomyopathy and sudden death in the young: Pathologic evidence of myocardial ischemia. Hum Pathol. 2000 Aug 1;31(8):988–98.
61. Olivotto I, Cecchi F, Poggesi C, Yacoub MH. Developmental origins of hypertrophic cardiomyopathy phenotypes: a unifying hypothesis. Nat Rev Cardiol. 2009 Apr 1;6(4):317–21.
62. Garcia-Canadilla P, Cook AC, Mohun TJ, Oji O, Schlossarek S, Carrier L, et al. Myoarchitectural disarray of hypertrophic cardiomyopathy begins pre-birth. J Anat. 2019 Nov 1;235(5):962–76.
63. Captur G, Ho CY, Schlossarek S, Kerwin J, Mirabel M, Wilson R, et al. The embryological basis of subclinical hypertrophic cardiomyopathy. Sci Rep. 2016 Jun 21;6(1):27714.
64. Sharma S, Merghani A, Mont L. Exercise and the heart: the good, the bad, and the ugly. Eur Heart J. 2015 Jun 14;36(23):1445–53.
65. Petersen SE, Jerosch-Herold M, Hudsmith LE, Robson MD, Francis JM, Doll HA, et al. Evidence for Microvascular Dysfunction in Hypertrophic Cardiomyopathy. Circulation. 2007 May 8;115(18):2418–25.
66. Camaioni C, Knott KD, Augusto JB, Seraphim A, Rosmini S, Ricci F, et al. Inline perfusion mapping provides insights into the disease mechanism in hypertrophic cardiomyopathy. Heart. 2020 Jun 1;106(11):824.
67. Bhuva AN, D'Silva A, Torlasco C, Jones S, Nadarajan N, Van Zalen J, et al. Training for a First-Time Marathon Reverses Age-Related Aortic Stiffening. J Am Coll Cardiol. 2020 Jan 7;75(1):60–71.
68. Karamitsos TD, Dass S, Suttie J, Sever E, Birks J, Holloway CJ, et al. Blunted Myocardial Oxygenation Response During Vasodilator Stress in Patients With Hypertrophic Cardiomyopathy. J Am Coll Cardiol. 2013 Mar 19;61(11):1169–76.
69. Heinonen I, Kudomi N, Kemppainen J, Kiviniemi A, Noponen T, Luotolahti M, et al. Myocardial blood flow and its transit time, oxygen utilization, and efficiency of highly endurance-trained human heart. Basic Res Cardiol. 2014 May 28;109(4):413.
70. Rahman H, Scannell CM, Demir OM, Ryan M, McConkey H, Ellis H, et al. High-Resolution Cardiac Magnetic Resonance Imaging Techniques for the Identification of Coronary Microvascular Dysfunction. JACC Cardiovasc Imaging. 2021 May 1;14(5):978–86.
71. Laaksonen MS, Kalliokoski KK, Luotolahti M, Kemppainen J, Teräs M, Kyröläinen H, et al. Myocardial perfusion during exercise in endurance-trained and untrained humans. Am J Physiol-Regul Integr Comp Physiol. 2007 Aug 1;293(2):R837–43.
72. Sun JP, Xu TY, Ni XD, Yang XS, Hu JL, Wang SC, et al. Echocardiographic strain in hypertrophic cardiomyopathy and hypertensive left ventricular hypertrophy. Echocardiography. 2019 Feb 1;36(2):257–65.
73. Rodrigues JCL, Amadu AM, Dastidar AG, Hassan N, Lyen SM, Lawton CB, et al. Prevalence and predictors of asymmetric hypertensive heart disease: insights from cardiac and aortic function with cardiovascular magnetic resonance. Eur Heart J - Cardiovasc Imaging. 2016 Dec 1;17(12):1405–13.
74. Authors/Task Force members, Elliott PM, Anastasakis A, Borger MA, Borggrefe M, Cecchi F, et al. 2014 ESC Guidelines on diagnosis and management of hypertrophic cardiomyopathy: The Task Force for the Diagnosis and Management of Hypertrophic Cardiomyopathy of the European Society of Cardiology (ESC). Eur Heart J. 2014 Oct 14;35(39):2733–79.
75. Keteepe-Arachi T, Malhotra A, Basu J, Parry-Williams G, Ensam B, Miles C, et al. P3839Hypertension or hypertrophic cardiomyopathy? Using cardiovascular magnetic resonance imaging to unmask the great imitator. Eur Heart J. 2019 Oct 1;40(Supplement_1):ehz745.0680.
76. Maceira AM, Joshi J, Prasad SK, Moon JC, Perugini E, Harding I, et al. Cardiovascular Magnetic Resonance in Cardiac Amyloidosis. Circulation. 2005 Jan 18;111(2):186–93.
77. Kellman P, Hansen MS, Nielles-Vallespin S, Nickander J, Themudo R, Ugander M, et al. Myocardial perfusion cardiovascular magnetic resonance: optimized dual sequence and reconstruction for quantification. J Cardiovasc Magn Reson. 2017 Apr 7;19(1):43.
78. Brown LAE, Onciul SC, Broadbent DA, Johnson K, Fent GJ, Foley JRJ, et al. Fully automated, inline quantification of myocardial blood flow with cardiovascular magnetic resonance: repeatability of measurements in healthy subjects. J Cardiovasc Magn Reson. 2018 Jul 9;20(1):48.
79. Cecchi F, Olivotto I, Gistri R, Lorenzoni R, Chiriatti G, Camici PG. Coronary Microvascular Dysfunction and Prognosis in Hypertrophic Cardiomyopathy. N Engl J Med. 2003 Sep 11;349(11):1027–35.

80. Yoshida Noriko, Ikeda Hisao, Wada Toyofumi, Matsumoto Akira, Maki Sanae, Muro Aiko, et al. Exercise-induced abnormal blood pressure responses are related to subendocardial ischemia in hypertrophic cardiomyopathy. J Am Coll Cardiol. 1998 Dec 1;32(7):1938–42.
81. Hughes RK, Camaioni C, Augusto JB, Knott K, Quinn E, Captur G, et al. Myocardial Perfusion Defects in Hypertrophic Cardiomyopathy Mutation Carriers. J Am Heart Assoc. 2021 Aug 3;10(15):e020227.
82. Kim EK, Lee SC, Chang SA, Jang SY, Kim SM, Park SJ, et al. Prevalence and clinical significance of cardiovascular magnetic resonance adenosine stress-induced myocardial perfusion defect in hypertrophic cardiomyopathy. J Cardiovasc Magn Reson. 2020 May 4;22(1):30.
83. Raman B, Tunnicliffe EM, Chan K, Ariga R, Hundertmark M, Ohuma EO, et al. Association Between Sarcomeric Variants in Hypertrophic Cardiomyopathy and Myocardial Oxygenation: Insights From a Novel Oxygen-Sensitive Cardiovascular Magnetic Resonance Approach. Circulation. 2021 Nov 16;144(20):1656–8.
84. Crilley JG, Boehm EA, Blair E, Rajagopalan B, Blamire AM, Styles P, et al. Hypertrophic cardiomyopathy due to sarcomeric gene mutations is characterized by impaired energy metabolism irrespective of the degree of hypertrophy. J Am Coll Cardiol. 2003 May 21;41(10):1776–82.
85. Schumacher B, Gietzen FH, Neuser H, Schümmelfeder J, Schneider M, Kerber S, et al. Electrophysiological Characteristics of Septal Hypertrophy in Patients With Hypertrophic Obstructive Cardiomyopathy and Moderate to Severe Symptoms. Circulation. 2005 Oct 4;112(14):2096–101.
86. Saumarez RC, Pytkowski M, Sterlinski M, Bourke JP, Clague JR, Cobbe SM, et al. Paced ventricular electrogram fractionation predicts sudden cardiac death in hypertrophic cardiomyopathy. Eur Heart J. 2008 Jul 1;29(13):1653–61.
87. Coppini R, Ferrantini C, Yao L, Fan P, Del Lungo M, Stillitano F, et al. Late Sodium Current Inhibition Reverses Electromechanical Dysfunction in Human Hypertrophic Cardiomyopathy. Circulation. 2013 Feb 5;127(5):575–84.
88. Lorenzini M, Norrish G, Field E, et al. Penetrance of Hypertrophic Cardiomyopathy in Sarcomere Protein Mutation Carriers. J Am Coll Cardiol. 2020 Aug 4;76(5):550–9.
89. Gray B, Ingles J, Medi C, Semsarian C. Prolongation of the QTc Interval Predicts Appropriate Implantable Cardioverter-Defibrillator Therapies in Hypertrophic Cardiomyopathy. JACC Heart Fail. 2013 Apr 1;1(2):149–55.
90. Jalanko M, Väänänen H, Tarkiainen M, Sipola P, Jääskeläinen P, Lauerma K, et al. Fibrosis and wall thickness affect ventricular repolarization dynamics in hypertrophic cardiomyopathy. Ann Noninvasive Electrocardiol Off J Int Soc Holter Noninvasive Electrocardiol Inc. 2018/07/04 ed. 2018 Nov;23(6):e12582–e12582.
91. Ho CY, Day SM, Ashley EA, Michels M, Pereira AC, Jacoby D, et al. Genotype and Lifetime Burden of Disease in Hypertrophic Cardiomyopathy. Circulation. 2018 Oct 2;138(14):1387–98.
92. Rudy Y. Noninvasive Mapping of Repolarization With Electrocardiographic Imaging. J Am Heart Assoc. 2021 May 4;10(9):e021396.
93. Oster HS, Taccardi B, Lux RL, Ershler PR, Rudy Y. Electrocardiographic Imaging. Circulation. 1998 Apr 21;97(15):1496–507.
94. Ramanathan C, Ghanem RN, Jia P, Ryu K, Rudy Y. Noninvasive electrocardiographic imaging for cardiac electrophysiology and arrhythmia. Nat Med. 2004 Apr 1;10(4):422–8.
95. Ramanathan C, Jia P, Ghanem R, Ryu K, Rudy Y. Activation and repolarization of the normal human heart under complete physiological conditions. Proc Natl Acad Sci. 2006 Apr 18;103(16):6309–14.
96. Cluitmans MJM, Bear LR, Nguyên UC, van Rees B, Stoks J, ter Bekke RMA, et al. Noninvasive detection of spatiotemporal activation-repolarization interactions that prime idiopathic ventricular fibrillation. Sci Transl Med. 13(620):eabi9317.
97. Cuculich PS, Zhang J, Wang Y, Desouza KA, Vijayakumar R, Woodard PK, et al. The Electrophysiological Cardiac Ventricular Substrate in Patients After Myocardial Infarction: Noninvasive Characterization With Electrocardiographic Imaging. J Am Coll Cardiol. 2011 Oct 25;58(18):1893–902.
98. Andrews CM, Srinivasan NT, Rosmini S, Bulluck H, Orini M, Jenkins S, et al. Electrical and Structural Substrate of Arrhythmogenic Right Ventricular Cardiomyopathy Determined Using Noninvasive Electrocardiographic Imaging and Late Gadolinium Magnetic Resonance Imaging. Circ Arrhythm Electrophysiol. 2017 Jul 1;10(7):e005105.

99. Perez-Alday EA, Haq KT, German DM, Hamilton C, Johnson K, Phan F, et al. Mechanisms of Arrhythmogenicity in Hypertrophic Cardiomyopathy: Insight From Non-invasive Electrocardiographic Imaging. Front Physiol [Internet]. 2020;11. Available from: https://www.frontiersin.org/articles/10.3389/fphys.2020.00344
100. Graham AJ, Orini M, Zacur E, Dhillon G, Daw H, Srinivasan NT, et al. Simultaneous Comparison of Electrocardiographic Imaging and Epicardial Contact Mapping in Structural Heart Disease. Circ Arrhythm Electrophysiol. 2019 Apr 1;12(4):e007120.
101. Graham AJ, Orini M, Zacur E, Dhillon G, Daw H, Srinivasan NT, et al. Evaluation of ECG Imaging to Map Hemodynamically Stable and Unstable Ventricular Arrhythmias. Circ Arrhythm Electrophysiol. 2020 Feb 1;13(2):e007377.
102. Duchateau J, Sacher F, Pambrun T, Derval N, Chamorro-Servent J, Denis A, et al. Performance and limitations of noninvasive cardiac activation mapping. Heart Rhythm. 2019 Mar 1;16(3):435–42.
103. Cuculich PS, Schill MR, Kashani R, Mutic S, Lang A, Cooper D, et al. Noninvasive Cardiac Radiation for Ablation of Ventricular Tachycardia. N Engl J Med. 2017 Dec 14;377(24):2325–36.
104. Maron BJ, Casey SA, Chan RH, Garberich RF, Rowin EJ, Maron MS. Independent Assessment of the European Society of Cardiology Sudden Death Risk Model for Hypertrophic Cardiomyopathy. Am J Cardiol. 2015 Sep 1;116(5):757–64.
105. Sherrid Mark V., Massera Daniele. Risk Stratification and Hypertrophic Cardiomyopathy Subtypes∗. J Am Coll Cardiol. 2019 Nov 12;74(19):2346–9.
106. Maron MS, Olivotto I, Harrigan C, Appelbaum E, Gibson CM, Lesser JR, et al. Mitral Valve Abnormalities Identified by Cardiovascular Magnetic Resonance Represent a Primary Phenotypic Expression of Hypertrophic Cardiomyopathy. Circulation. 2011 Jul 5;124(1):40–7.
107. Captur G, Lopes LR, Mohun TJ, Patel V, Li C, Bassett P, et al. Prediction of Sarcomere Mutations in Subclinical Hypertrophic Cardiomyopathy. Circ Cardiovasc Imaging. 2014 Nov 1;7(6):863–71.
108. Ho CY, Sweitzer NK, McDonough B, Maron BJ, Casey SA, Seidman JG, et al. Assessment of Diastolic Function With Doppler Tissue Imaging to Predict Genotype in Preclinical Hypertrophic Cardiomyopathy. Circulation. 2002 Jun 25;105(25):2992–7.
109. Seitler S, De Zoysa Anthony S, Obianyo CCC, Syrris P, Patel V, Sado DM, et al. Systolic anterior motion of the anterior mitral valve leaflet begins in subclinical hypertrophic cardiomyopathy. Eur Heart J - Cardiovasc Imaging. 2024 Jan 1;25(1):86–94.
110. Green EM, Wakimoto H, Anderson RL, Evanchik MJ, Gorham JM, Harrison BC, et al. A small-molecule inhibitor of sarcomere contractility suppresses hypertrophic cardiomyopathy in mice. Science. 2016 Feb 5;351(6273):617–21.
111. Ho CY, Cirino AL, Lakdawala NK, Groarke J, Valente AM, Semsarian C, et al. Evolution of hypertrophic cardiomyopathy in sarcomere mutation carriers. Heart. 2016 Nov 15;102(22):1805.
112. Webber M, Joy G, Bennett J, Chan F, Falconer D, Shiwani H, et al. Technical development and feasibility of a reusable vest to integrate cardiovascular magnetic resonance with electrocardiographic imaging. J Cardiovasc Magn Reson. 2023 Dec 4;25(1):73.
113. Webber M, Falconer D, AlFarih M, Joy G, Chan F, Davie C, et al. Study protocol: MyoFit46—the cardiac sub-study of the MRC National Survey of Health and Development. BMC Cardiovasc Disord. 2022 Apr 1;22(1):140.
114. Brown LAE, Saunderson CED, Das A, Craven T, Levelt E, Knott KD, et al. A comparison of standard and high dose adenosine protocols in routine vasodilator stress cardiovascular magnetic resonance: dosage affects hyperaemic myocardial blood flow in patients with severe left ventricular systolic impairment. J Cardiovasc Magn Reson. 2021 Mar 18;23(1):37.
115. Richards S, Aziz N, Bale S, Bick D, Das S, Gastier-Foster J, et al. Standards and guidelines for the interpretation of sequence variants: a joint consensus recommendation of the American College of Medical Genetics and Genomics and the Association for Molecular Pathology. Genet Med. 2015 May 1;17(5):405–24.
116. O'Mahony C, Jichi F, Pavlou M, Monserrat L, Anastasakis A, Rapezzi C, et al. A novel clinical risk prediction model for sudden cardiac death in hypertrophic cardiomyopathy (HCM Risk-SCD). Eur Heart J. 2014 Aug 7;35(30):2010–20.
117. P. W. Macfarlane, B. Devine, E. Clark. The university of glasgow (Uni-G) ECG analysis program. In: Computers in Cardiology, 2005. 2005. p. 451–4.
118. Macfarlane PW, McLaughlin SC, Rodger JC. Influence of Lead Selection and Population on Automated Measurement of QT Dispersion. Circulation. 1998 Nov 17;98(20):2160–7.
119. Carolyn Y Ho, Allison L Cirino, Neal K Lakdawala, John Groarke, Anne Marie Valente, Christopher Semsarian, et al. Evolution of hypertrophic cardiomyopathy in sarcomere mutation carriers. Heart. 2016 Nov 15;102(22):1805.

120. Davies RH, Augusto JB, Bhuva A, Xue H, Treibel TA, Ye Y, et al. Precision measurement of cardiac structure and function in cardiovascular magnetic resonance using machine learning. J Cardiovasc Magn Reson. 2022 Mar 10;24(1):16.
121. Augusto JB, Davies RH, Bhuva AN, Knott KD, Seraphim A, Alfarih M, et al. Diagnosis and risk stratification in hypertrophic cardiomyopathy using machine learning wall thickness measurement: a comparison with human test-retest performance. Lancet Digit Health. 2021 Jan 1;3(1):e20–8.
122. Flett AS, Hasleton J, Cook C, Hausenloy D, Quarta G, Ariti C, et al. Evaluation of Techniques for the Quantification of Myocardial Scar of Differing Etiology Using Cardiac Magnetic Resonance. JACC Cardiovasc Imaging. 2011 Feb 1;4(2):150–6.
123. Messroghli DR, Moon JC, Ferreira VM, Grosse-Wortmann L, He T, Kellman P, et al. Clinical recommendations for cardiovascular magnetic resonance mapping of T1, T2, T2* and extracellular volume: A consensus statement by the Society for Cardiovascular Magnetic Resonance (SCMR) endorsed by the European Association for Cardiovascular Imaging (EACVI). J Cardiovasc Magn Reson. 2017 Oct 9;19(1):75.
124. Xue H, Davies RH, Brown LAE, Knott KD, Kotecha T, Fontana M, et al. Automated Inline Analysis of Myocardial Perfusion MRI with Deep Learning. Radiol Artif Intell. 2020 Nov 1;2(6):e200009.
125. Kotecha T, Monteagudo JM, Martinez-Naharro A, Chacko L, Brown J, Knight D, et al. Quantitative cardiovascular magnetic resonance myocardial perfusion mapping to assess hyperaemic response to adenosine stress. Eur Heart J - Cardiovasc Imaging. 2021 Mar 1;22(3):273–81.
126. Schulz-Menger J, Bluemke DA, Bremerich J, Flamm SD, Fogel MA, Friedrich MG, et al. Standardized image interpretation and post-processing in cardiovascular magnetic resonance - 2020 update. J Cardiovasc Magn Reson. 2020 Mar 12;22(1):19.
127. Teh I, McClymont D, Burton RAB, Maguire ML, Whittington HJ, Lygate CA, et al. Resolving Fine Cardiac Structures in Rats with High-Resolution Diffusion Tensor Imaging. Sci Rep. 2016 Jul 28;6(1):30573.
128. Orini M, Srinivasan N, Graham AJ, Taggart P, Lambiase PD. Further Evidence on How to Measure Local Repolarization Time Using Intracardiac Unipolar Electrograms in the Intact Human Heart. Circ Arrhythm Electrophysiol. 2019 Nov 1;12(11):e007733.
129. Andršová I, Hnatkova K, Šišáková M, Toman O, Smetana P, Huster KM, et al. Influence of heart rate correction formulas on QTc interval stability. Sci Rep. 2021 Jul 12;11(1):14269.
130. Austin PC, Steyerberg EW. The number of subjects per variable required in linear regression analyses. J Clin Epidemiol. 2015 Jun 1;68(6):627–36.
131. Hollander Z, Dai DLY, Putko BN, Yogasundaram H, Wilson-McManus JE, Thompson RB, et al. Gender-specific plasma proteomic biomarkers in patients with Anderson–Fabry disease. Eur J Heart Fail. 2015 Mar 1;17(3):291–300.
132. Liu HX, Zhang RS, Luan F, Yao XJ, Liu MC, Hu ZD, et al. Diagnosing Breast Cancer Based on Support Vector Machines. J Chem Inf Comput Sci. 2003 May 1;43(3):900–7.
133. Swan AL, Mobasheri A, Allaway D, Liddell S, Bacardit J. Application of Machine Learning to Proteomics Data: Classification and Biomarker Identification in Postgenomics Biology. OMICS J Integr Biol. 2013 Dec 1;17(12):595–610.
134. Cawley G, Talbot N. Preventing Over-Fitting during Model Selection via Bayesian Regularisation of the Hyper-Parameters. J Mach Learn Res. 2007 Apr 1;8:841–61.
135. Swoboda PP, McDiarmid AK, Erhayiem B, Broadbent DA, Dobson LE, Garg P, et al. Assessing Myocardial Extracellular Volume by T1 Mapping to Distinguish Hypertrophic Cardiomyopathy From Athlete's Heart. J Am Coll Cardiol. 2016 May 10;67(18):2189–90.
136. Lovic D, Narayan P, Pittaras A, Faselis C, Doumas M, Kokkinos P. Left ventricular hypertrophy in athletes and hypertensive patients. J Clin Hypertens. 2017 Apr 1;19(4):413–7.
137. Nguyen C, Fan Z, Xie Y, Dawkins J, Tseliou E, Bi X, et al. In vivo contrast free chronic myocardial infarction characterization using diffusion-weighted cardiovascular magnetic resonance. J Cardiovasc Magn Reson. 2014 Sep 17;16(1):68.
138. Olivotto I, Girolami F, Sciagrà R, Ackerman MJ, Sotgia B, Bos JM, et al. Microvascular Function Is Selectively Impaired in Patients With Hypertrophic Cardiomyopathy and Sarcomere Myofilament Gene Mutations. J Am Coll Cardiol. 2011 Aug 16;58(8):839–48.
139. Castelletti S, Menacho K, Davies RH, Maestrini V, Treibel TA, Rosmini S, et al. Hypertrophic cardiomyopathy: insights from extracellular volume mapping. Eur J Prev Cardiol. 2021 Dec 1;28(18):e39–41.

140. Lakdawala NK, Thune JJ, Maron BJ, Cirino AL, Havndrup O, Bundgaard H, et al. Electrocardiographic Features of Sarcomere Mutation Carriers With and Without Clinically Overt Hypertrophic Cardiomyopathy. Am J Cardiol. 2011 Dec 1;108(11):1606–13.
141. Maron MS, Olivotto I, Maron BJ, Prasad SK, Cecchi F, Udelson JE, et al. The Case for Myocardial Ischemia in Hypertrophic Cardiomyopathy. J Am Coll Cardiol. 2009 Aug 25;54(9):866–75.
142. O'Mahony C, Jichi F, Pavlou M, Monserrat L, Anastasakis A, Rapezzi C, et al. A novel clinical risk prediction model for sudden cardiac death in hypertrophic cardiomyopathy (HCM Risk-SCD). Eur Heart J. 2014 Aug 7;35(30):2010–20.
143. Joy G, Moon JC, Lopes LR. Detection of subclinical hypertrophic cardiomyopathy. Nat Rev Cardiol. 2023 Jun 1;20(6):369–70.
144. Joy G, Kelly CI, Webber M, Pierce I, Teh I, McGrath L, et al. Microstructural and Microvascular Phenotype of Sarcomere Mutation Carriers and Overt Hypertrophic Cardiomyopathy. Circulation [Internet]. [cited 2023 Aug 2];0(0). Available from: https://doi.org/10.1161/CIRCULATIONAHA.123.063835
145. Monserrat L, Elliott PM, Gimeno JR, Sharma S, Penas-Lado M, McKenna WJ. Non-sustained ventricular tachycardia in hypertrophic cardiomyopathy: an independent marker of sudden death risk in young patients. J Am Coll Cardiol. 2003 Sep 3;42(5):873–9.
146. Orini M, Graham AJ, Martinez-Naharro A, Andrews CM, de Marvao A, Statton B, et al. Noninvasive Mapping of the Electrophysiological Substrate in Cardiac Amyloidosis and Its Relationship to Structural Abnormalities. J Am Heart Assoc. 2019 Sep 17;8(18):e012097.
147. Andrews CM, Srinivasan NT, Rosmini S, Bulluck H, Orini M, Jenkins S, et al. Electrical and Structural Substrate of Arrhythmogenic Right Ventricular Cardiomyopathy Determined Using Noninvasive Electrocardiographic Imaging and Late Gadolinium Magnetic Resonance Imaging. Circ Arrhythm Electrophysiol. 2017 Jul 1;10(7):e005105.
148. Zhang J, Sacher F, Hoffmayer K, O'Hara T, Strom M, Cuculich P, et al. Cardiac Electrophysiological Substrate Underlying the ECG Phenotype and Electrogram Abnormalities in Brugada Syndrome Patients. Circulation. 2015 Jun 2;131(22):1950–9.
149. Shun-Shin MJ, Leong KMW, Ng FS, Linton NWF, Whinnett ZI, Koa-Wing M, et al. Ventricular conduction stability test: a method to identify and quantify changes in whole heart activation patterns during physiological stress. EP Eur. 2019 Sep 1;21(9):1422–31.
150. Zhang J, Hocini M, Strom M, Cuculich PS, Cooper DH, Sacher F, et al. The Electrophysiological Substrate of Early Repolarization Syndrome: Noninvasive Mapping in Patients. JACC Clin Electrophysiol. 2017 Aug 1;3(8):894–904.
151. Vijayakumar R, Silva JNA, Desouza KA, Abraham RL, Strom M, Sacher F, et al. Electrophysiologic Substrate in Congenital Long QT Syndrome. Circulation. 2014 Nov 25;130(22):1936–43.
152. Tomaselli GF, Beuckelmann DJ, Calkins HG, Berger RD, Kessler PD, Lawrence JH, et al. Sudden cardiac death in heart failure. The role of abnormal repolarization. Circulation. 1994 Nov 1;90(5):2534–9.
153. Maron BJ, Leyhe MJ III, Casey SA, Gohman TE, Lawler CM, Crow RS, et al. Assessment of QT dispersion as a prognostic marker for sudden death in a regional nonreferred hypertrophic cardiomyopathy cohort. Am J Cardiol. 2001 Jan 1;87(1):114–5.
154. Gardner PI, Ursell PC, Fenoglio JJ, Wit AL. Electrophysiologic and anatomic basis for fractionated electrograms recorded from healed myocardial infarcts. Circulation. 1985 Sep 1;72(3):596–611.
155. Robyns T, Breckpot J, Nuyens D, Vandenberk B, Corveleyn A, Kuiperi C, et al. Clinical and ECG variables to predict the outcome of genetic testing in hypertrophic cardiomyopathy. Eur J Med Genet. 2020 Mar 1;63(3):103754.